Review

Shaoni Kar, Nur Fadilah Jamaludin, Natalia Yantara, Subodh G. Mhaisalkar* and Wei Lin Leong*

Recent advancements and perspectives on light management and high performance in perovskite light-emitting diodes

https://doi.org/10.1515/nanoph-2021-0033
Received January 26, 2021; accepted March 9, 2021; published online March 30, 2021

Abstract: Perovskite semiconductors have experienced meteoric rise in a variety of optoelectronic applications. With a strong foothold on photovoltaics, much focus now lies on their light emission applications. Rapid progress in materials engineering have led to the demonstration of external quantum efficiencies that surpass the previously established theoretical limits. However, there remains much scope to further optimize the light propagation inside the device stack through careful tailoring of the optical processes that take place at the bulk and interface levels. Photon recycling in the emitter material followed by efficient outcoupling can result in boosting external efficiencies up to 100%. In addition, the poor ambient and operational stability of these materials and devices restrict further commercialization efforts. With best operational lifetimes of only a few hours reported, there is a long way to go before perovskite LEDs can be perceived as reliable alternatives to more established technologies like organic or quantum dot-based LED devices. This review article starts with the discussions of the mechanism of luminescence in these perovskite materials and factors impacting it. It then looks at the possible routes to achieve efficient outcoupling through nanostructuring of the emitter and the substrate. Next, we analyse the instability issues of perovskite-based LEDs from a photophysical standpoint, taking into consideration the underlying phenomena pertaining to defects, and summarize recent advances in mitigating the same. Finally, we provide an outlook on the possible routes forward for the field and propose new avenues to maximally exploit the excellent light-emitting capabilities of this family of semiconductors.

Keywords: light emission; light-emitting diode; light outcoupling; perovskite.

1 Introduction

Hybrid organic–inorganic metal halide perovskites have completely revolutionized the field of optoelectronics in the last decade, with exponential growth in efficiency observed for both photovoltaic and light emission applications. Since the pioneering work by Miyasaka et al. [1], perovskite solar cell efficiencies have surpassed 25% in single junction configuration [2]. The arrival of perovskite-based light-emitting diodes (PeLEDs) in the scene in 2014 [3] has presented a breakthrough for low-cost, high-performance emitters. PeLED efficiency trajectory has experienced a remarkable surge with a pace hitherto unseen for other mature LED technologies, such as organic LEDs (OLEDs) and quantum dot LEDs (QLEDs) (Figure 1). This can be attributed to the wide range of unique optoelectronic properties exhibited by

Shaoni Kar and Nur Fadilah Jamaludin have contributed equally.

***Corresponding authors: Subodh G. Mhaisalkar**, Energy Research Institute at Nanyang Technological University (ERI@N), Research Techno Plaza, X-Frontier Block, Level 5, 50 Nanyang Drive, Singapore 637553, Singapore; and School of Materials Science and Engineering, Nanyang Technological University, Nanyang Avenue, 639798, Singapore, Singapore, E-mail: subodh@ntu.edu.sg; and **Wei Lin Leong**, Energy Research Institute at Nanyang Technological University (ERI@N), Research Techno Plaza, X-Frontier Block, Level 5, 50 Nanyang Drive, Singapore 637553, Singapore; and School of Electrical and Electronic Engineering, Nanyang Technological University, 50 Nanyang Avenue, Singapore 639798, Singapore, E-mail: wlleong@ntu.edu.sg. https://orcid.org/0000-0002-1402-0083
Shaoni Kar, Energy Research Institute at Nanyang Technological University (ERI@N), Research Techno Plaza, X-Frontier Block, Level 5, 50 Nanyang Drive, Singapore 637553, Singapore; School of Electrical and Electronic Engineering, Nanyang Technological University, 50 Nanyang Avenue, Singapore 639798, Singapore; and Interdisciplinary Graduate School, Nanyang Technological University, 639798, Singapore, Singapore. https://orcid.org/0000-0002-7325-1527
Nur Fadilah Jamaludin and Natalia Yantara, Energy Research Institute at Nanyang Technological University (ERI@N), Research Techno Plaza, X-Frontier Block, Level 5, 50 Nanyang Drive, Singapore 637553, Singapore

perovskites such as direct bandgap [93], high defect tolerance [94] and extremely high colour purity [95].

On the processing front, perovskites too present an advantage over other conventional emitters. Their optoelectronic properties, in particular, the emission wavelength, can be easily tuned via solution-based compositional and structural engineering to achieve application-specific characteristics. It is thus unsurprising that rapid performance enhancement in PeLEDs, where maximum efficiency exceeding 20% for green, red and near infrared (NIR) emissions, as well as the uptick in blue emissive PeLED efficiency, has been observed in recent years. The external quantum efficiency (EQE) of LED can be defined as the product of carrier injection efficiency (η_{inj}), photoluminescence quantum yield (PLQY) and light outcoupling efficiency (η_{out}). With device and materials engineering pushing state-of-the-art PeLEDs close to their maximum theoretical efficiency in a planar bottom-emitting device configuration ($\eta_{out} \approx 20\%$) [4], the only way to further the efficiency is by investing in structures promoting higher light outcoupling efficiency. The relatively less expansive reports on incorporating outcoupling structures in PeLEDs, both internally and externally, highlight the loss in efficiency potential for PeLEDs. More effort should thus be directed towards improving light management in current PeLEDs to push the boundaries of efficiency further.

In addition, beyond the efficiency race, PeLED commercialization is still hampered by its operational stability which is inferior to industrial standards. In fact, the longest lifetime reported to date for initial luminance (L_0) of 100 cd m^{-2} to drop by 50% (T_{50}) is in hundreds of hours, which is still far from the thousands of hours reported for commercial OLEDs (at initial L_0 = 1000 cd m^{-2}) as shown in Table 1. Therefore, improving stability will be a key step towards bringing PeLEDs closer towards real-world applications. In general, the degradation of LED performance can be induced by both external (environmental) and internal factors. While external factors that accelerate degradation can be eliminated by using matured OLED or QLED encapsulation techniques, internal factors such as materials or interface instability under device operation, are challenges which still need to be addressed.

One of the key advantages of this class of materials is the ease of tuning emission wavelength (bandgap) by modifying one or all of its constituent elements in the precursor solution. Low-temperature, solution-based processing of lead halide perovskites is possible due to their ionic nature, allowing for rapid crystallization to occur even at ambient temperatures [107]. While the ionic bonding nature and the antibonding characteristics of the band extrema translates to relatively shallow defects (lead and halide vacancies: V_{Pb} and V_X respectively) which do not significantly contribute to non-radiative recombination of charge carriers [108], their low formation energy highlights the need to suppress their occurrence due to their propensity as initiation sites for degradation process. It has been reported that migration of both negatively and positively charged ions can occur in the presence of point defects [109–111], with the process becoming more dominant at the surfaces and grain boundaries [112]. Aside from ion migration, these defects also facilitate the ingress of moisture and oxygen, thus increasing perovskite susceptibility to degradation by lowering the ion migration activation energy [113]. While ion migration may originate from the perovskite layer, the proliferation in the adjacent layers

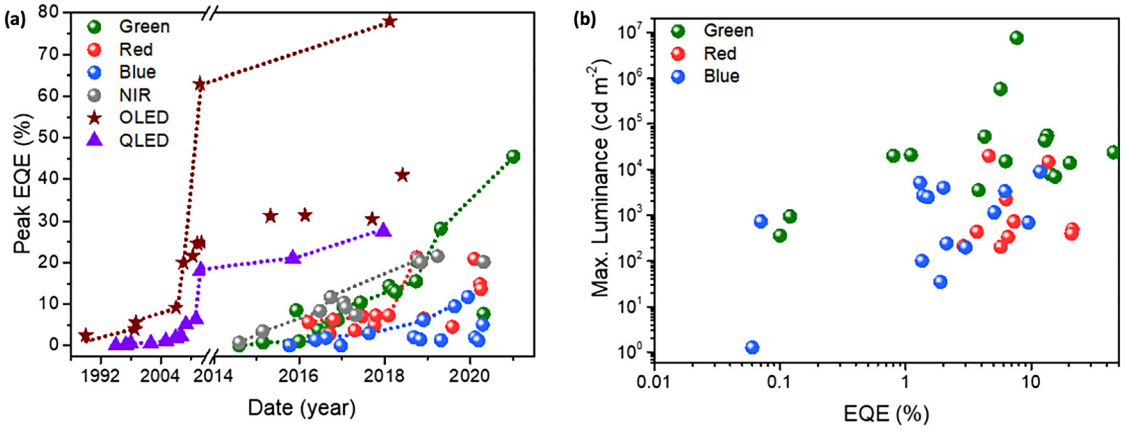

Figure 1: (a) Yearly peak external quantum efficiency (EQE) growth and (b) maximum luminance as a function of EQE for red, green and blue perovskite-based light-emitting diodes (PeLEDs) and as well as those of current lighting technologies (OLED and QLED). The data are collected from previous studies [3–93] and are tabulated in Table 1.

Table 1: Summary of recent advances in red, blue, green and near-IR LEDs based on organic emitters, quantum dots and perovskites.

Lighting technology	Colour	Year	EQE (%)	Max. luminance (Cd. m^{-2})	Ref.
OLED		1989	2.5	5062	[96]
		1998	4	–	[97]
		1999	5.6	–	[19]
		2007	9.2	–	[86]
		2008	20	–	[17]
		2010	21.6	207,839	[55]
		2011	24.6	–	[23]
		2011	63		[89]
		2012	24.8	–	[81]
		2013	30.2	–	[11]
		2015	31.2	–	[98]
		2016	31.4	–	[52]
		2017	30.5	–	[54]
		2018	41	–	[99]
		2018	78		[82]
QLED		1995	0.0333	–	[100]
		1997	0.2254	578.126	
		1998	0.5413	–	
		2002	0.5484	2045.537	
		2005	1.1193	–	
		2007	1.9402	8947.301	
		2008	2.3502	–	
		2009	5.1492	12,340	
		2011	6.3467	31,710	
		2012	18.1648	–	
		2015	21	–	[78]
		2017	27.6	–	[38]
Perovskite	Blue	2015	0.07	742	[5]
		2016	1.38	2673	[71]
		2016	1.9	35	[24]
		2016	0.06	1.26	[62]
		2017	3	200	[36]
		2018	2.12	245	[41]
		2018	1.5	2480	[72]
		2018	6.2	3340	[33]
		2019	1.35	100.6	[101]
		2019	9.5	700	[74]
		2019	11	9040	[85]
		2020	5.08	1151	[44]
		2020	2.01	4015	[57]
		2020	1.3	5141	[84]
	Green	2014	0.1	364	[3]
		2015	0.8	20,000	[14]
		2015	1.1	21,014	[61]
		2015	8.53	–	[87]
		2015	0.12	946	[5]
		2016	3.8	3515	[30]
		2016	3	330	[24]
		2016	6.27	15,185	[58]
		2016	4.26	53,525	[88]
		2016	5.7	591,197	[92]
		2017	9.3	–	[39]
		2017	10.4	91,000	[102]
		2018	14.36	9120	[40]

Table 1: (continued)

Lighting technology	Colour	Year	EQE (%)	Max. luminance (Cd. m^{-2})	Ref.
		2018	15.5	7000	[59]
		2018	20.31	14,000	[4]
		2018	13.4	34,480	[69]
		2018	12.9	43,400	[22]
		2019	28.2	–	[70]
		2020	7.7	7.65E+06	[48]
		2021	45.5	24,000	[103]
	Red	2016	5.7	206	[25]
		2016	2.9	214	[67]
		2016	6.3	2216	[46]
		2017	3.7	440	[77]
		2017	0.071	–	[75]
		2017	5	–	[79]
		2017	7.3	–	[42]
		2018	7.3	732	[73]
		2018	21.3	500	[104]
		2018	6.55	338	[6]
		2019	4.6	20,000	[9]
		2020	20.9	400	[68]
		2020	18.6	–	[43]
		2020	13.7	14,725	[49]
	Near-IR	2014	0.76	–	[3]
		2015	3.5		[14]
		2016	8.8	–	[8]
		2016	11.7	–	[83]
		2017	10.4	–	[39]
		2017	9.23	–	[29]
		2017	7.4	–	[65]
		2018	20.7	–	[105]
		2018	20.1	–	[76]
		2019	21.6	–	[91]
		2020	20.2	–	[106]

OLED, organic LED; QLED, quantum dot-based LED.

during prolonged device operation [114], contributes towards PeLED degradation.

The presence of these defects and thus dominance of monomolecular recombination also has implications on radiative recombination efficacy, where high charge carrier densities are required for high PLQY to be achieved. However, the low carrier injection regime in which PeLEDs operate in, presents a challenge to the development of high performing devices [115], underscoring the need to effectively concentrate and confine carriers through both physical (band alignment), and/or dielectric means [69, 116–118]. In practice, two kinds of charge carrier confinement approaches have been successfully deployed viz., creation of quasi two-dimensional (2D) perovskite or nanocrystals [118, 119]. The first approach revolves around introducing bulky ammonium-functionalized cation (L) to break the three-dimensional (3D) perovskite [BX_6] octahedral network and form layered [BX_6] octahedral framework in between single or bilayer L cations. Known as Ruddlesden-Popper (RP) perovskites with a general formula of $L_2A_{m-1}B_mX_{3m+1}$, the bandgap (E_g) of the resulting material can be raised by increasing the proportion of L cation (m) [120]. While the creation of phase-pure RP perovskite film is challenging due to small differences in the thermodynamic stability of the compound with increasing m values [121], the formation of multi-domain films with various E_g values can form a pseudo-quantum well landscape, which promotes energy transfer and charge carrier confinement to the smallest E_g domain [118]. Aside from RP perovskite series, other quasi-2D perovskite types may also be templated depending on the cations used. When the mono-ammonium functionalized ligand, typical of RP perovskite, is substituted with a bi-functionalized alternative, Dion–Jacobson (DJ) [122] perovskites may crystallize. The difference in stacking motif and

symmetry offered by DJ molecules has been shown to impart greater rigidity in perovskites [123–125] enabling higher spectral stability to be achieved under prolonged device operation. However, care needs to be taken in the design of DJ molecules to ensure that the dual binding offered does not inadvertently result in formation of lattice defects. Alternating cations in interlayer space (ACI) type of perovskite achieved from the use of two different types of small A-site cations, has previously been reported for solar cell application [126]. However, their use for light emission applications has been less extensively explored. The second approach of employing nanocrystal emitters also offers charge carrier confinement effects within the crystals as nanocrystal surfaces are capped with less conducting ligands. Moreover, the adoption of such synthesis routes has resulted in reports of sufficiently high brightness/luminance levels, bringing PeLEDs one step closer towards display and lighting applications.

In this review article, we aim to highlight the efforts made towards improving the light outcoupling efficiency for high-performance PeLEDs. There are several excellent reviews and perspectives written recently on active PeLED materials and nanostructuring of perovskites [127–134]. This article, instead, aims to provide a comprehensive review on the design and management of light outcoupling in PeLED, analyses the defects issues and approaches to mitigate them. We hope to provide the readers with a roadmap of general guidelines to maximally exploit the excellent light-emitting capabilities of this family of semiconductors, serving as a guide to expedite future developments in the field.

2 The luminescence mechanism and underlying photophysics

Absorption spectra of perovskite thin films show low Urbach energies (~15–25 meV) [135, 136], comparable to commercially established systems such as GaAs and c-Si (respectively, ~7.5 and ~10 meV) [137, 138]. In spite of having considerably high defect density [139], low energetic disorder has also been shown to be present, thus enabling their use in various light emission applications [140]. Although many studies have probed and standardized the recombination mechanisms underlying luminescence in these systems [141], it is yet to be completely understood how charge injection affects perovskite in an LED device stack. The charge carrier recombination dynamics of 3D perovskites can be quantitatively described by the rate equation [141]:

$$\frac{dn}{dt} = G - k_1 n - k_2 n^2 - k_3 n^3 \quad (1)$$

where n refers to the carrier density, G denotes the rate of generation of charge carriers, and k_1, k_2 and k_3 are the coefficients of the first-order monomolecular recombination, second-order bimolecular recombination and third-order Auger recombination respectively. These occur at different excitation fluence regimes; exhibiting linear, quadratic and cubic dependencies on n. Initial studies using optical-pump-terahertz-probe (OPTP) photoconductivity spectroscopy and photoluminescence (PL) measurements have shown clear origins of these recombination events [141, 142]. Monomolecular recombination is a direct consequence of the trapping of charges in defect states and can be seen to occur at low fluences of $<10^{15}$ cm^{-3}. Accordingly, k_1 dominates in this regime with typical rates of ~10^7 s^{-1}. Radiative bimolecular recombination on the other hand, typically occurs at fluences of 10^{15}–10^{17} cm^{-3} with k_2 rates of ~10^{-10} cm^3 s^{-1} and is usually attributed to non-Langevin direct band-to-band recombination in the continuum states of the conduction and valence band. However, other studies note the influence of Rashba spin–orbit coupling [143], mixture of bandgap states [144] and other relativistic effects [145] on recombination process. Finally, Auger recombination which takes place at very high fluences $>10^{17}$ cm^{-3}, is considered to be intrinsically linked with the electronic band structure of the system and is a phenomenon mandated by the requirement for energy and momentum conservation for all charge carriers involved [140]. Typical rates for k_3 are of the order of 10^{-28} cm^6 s^{-1} [146]. It is important to note that these coefficients directly determine the photoluminescence quantum yield (PLQY) of a perovskite system, which is essentially the ratio of the radiative to total recombination rates [145]. It is expressed as,

$$\eta = \frac{nk_2}{k_1 + nk_2 + n^2 k_3} \quad (2)$$

This function dictates the correlation discussed above with different recombination regimes getting activated with increasing fluence. Moving along from monomolecular to bimolecular regimes with increasing excitation density, η increases concomitantly before peaking with $n = (k_1/k_3)^{0.5}$. Furthermore, at very high carrier densities where Auger events dominate, η undergoes a decrease [147, 148].

There is a discrepancy of a few orders of magnitude between n, at which η is maximum, (~10^{17} cm^{-3}) and operationally feasible n values in LEDs (~10^{15} cm^{-3}) [22]. To bridge this gap, it is hence desirable to reduce trap densities in the system (mainly affecting k_1). On the other hand, although it is important to enhance radiative recombination (higher k_2), there is an associated broadening of the PL

peak [149]. The routes to mitigate these in a bid to move towards higher PLQY at reasonable fluences, are twofold. The first approach is dimensional reduction of the lattice structure to create quantum (and/or dielectric) spatial confinement such that luminescence emission can originate from both excitons and free carriers. The energy landscape is built in a way to induce higher binding energy and create local recombination centres to promote excitonic recombination. Thus, several quasi-2D (2D-3D) perovskites (such as $(PEA)_2PbBr_4$ [150], $PEA_2Cs_{n-1}Pb_n(Br/Cl)_{3n+1}$ [151] etc.), 1D (such as $C_4N_2H_{14}PbBr_4$) [152] and 0D systems (such as $Cs_3Cu_2I_5$) [153] have been investigated for light emission. With highly efficient exciton self-trapping yielding below-gap broadband luminescence [154, 155], these lower-dimensional systems are extremely promising as emitter materials. In addition, improved environmental and operational stability lend them reliability for deployment in device application [156, 157].

The second method is geometrical reduction of the emitter in order to obtain tuneable, colour-pure emission. To this avail, nanocrystals, quantum dots, nanowire arrays and several other nanostructures offering precise diameters, have been fabricated. These show luminous efficiencies which are not only superior to their greater-dimensional counterparts but are also almost on par with organic emitters [133]. Facile chemical and morphological tuneability resulting in a wide colour gamut have made these the staple emitter materials for very highly efficient PeLEDs recently [117, 151].

In light emission application, EQE serves as the key figure of merit under consideration that requires maximization. A quantitative picture of the dependence of EQE on several parameters can be expressed as [134]:

$$\mathrm{EQE} = f_{\mathrm{balance}} \times f_{\mathrm{e-h}} \times \eta_{\mathrm{radiative}} \times \eta_{\mathrm{out}} \tag{3}$$

where f_{balance} denotes the probability of charge injection balance, $f_{\mathrm{e-h}}$ is the probability of exciton formation per injected carrier (an indicator of leakage current), $\eta_{\mathrm{radiative}}$ is the radiative recombination probability for each e–h pair (a.k.a PLQY of emitter material) and η_{out} is the light outcoupling efficiency. Approaches to ensure high PLQY of the materials such as complete control of film morphology [158] and chemical composition of the emitter [136, 159] as well as suitable interface engineering aimed at defect reduction at interfaces and grain boundaries [135] has led to the attainment of almost-unity internal PLQY in perovskites [160]. Furthermore, energy funnelling strategies introduced by employing multi-domain RP perovskite to create natural multi-quantum well (MQW) structures lead to higher $\eta_{\mathrm{radiative}}$ especially at lower carrier injection rate [161]. This in turn, has resulted in the plateauing of further enhancement in EQEs of PeLEDs from an emitter material quality perspective.

After ensuring near unity $\eta_{\mathrm{radiative}}$ of the perovskite emitter itself, maximizing both f_{balance} and $f_{\mathrm{e-h}}$ via rigorous device engineering is essential to further enhance the EQE. In general, the choice of electron or hole injection layers are adopted from the well-studied solution-processed OLEDs or conventional quantum dot-based (QD) LEDs. Indeed, with internal quantum efficiency (IQE, defined as product of f_{balance}, $f_{\mathrm{e-h}}$ and $\eta_{\mathrm{radiative}}$) almost reaching the limits, efficient light outcoupling management strategies will play a major role in the future to amplify the EQE. Strategies to enhance η_{out} include modifications to the design of materials and interfaces from optics point of view as well as external light outcouplers.

From materials and interfaces perspectives, while PeLEDs have adopted similar emitter and device configuration as OLEDs, the difference between the light emission process occurring in an OLED as compared to that in a PeLED highlights the advantage of photon recycling (PR) in the latter (Figure 2a). The dominance of PR in PeLED is attributed to the relatively smaller Stokes shift for perovskite emitters as compared to organic emitters [139]. In addition, organic emitters generally possess high exciton binding energies that limits the PLQY severely due to the non-emissive nature of spin-triplet excitons in compliance with spin statistics [163]. Accumulation of triplet excitons at high carrier densities leads to optical losses within the system [164]. Several techniques such as employing triplet quenchers [148, 165], singlet-triplet exciton annihilation (STA) [166], inducing delayed fluorescence by reverse intersystem crossing, rapid intersystem crossing etc. [147], have been extensively used to bypass this obstacle. However, in perovskites, such limitations do not exist due to reduced excitonic interactions. In addition, owing to smaller emission linewidths and facile bandgap tuneability, perovskite materials seem to enjoy a clear advantage in devices over OLEDs. The strategies to exploit PR to boost the η_{out} and overall device performances will be discussed further in the next chapter (Section 2.1).

Materials engineering on perovskite to boost the η_{out} within the emitter itself can be carried out by manipulating the transient dipole moments (TDM) of the materials [162]. By using a formalism for quantum efficiency specified for organic emitters, a new figure of merit, the alignment constant (ζ) is defined with consideration of the position and orientation of the emissive TDM of the emitter along with their refractive indices. A concept adapted from the field of OLEDs, the TDM method allows complete mapping of the energy distribution into the different optical modes as well as affords close insight into the influence of other

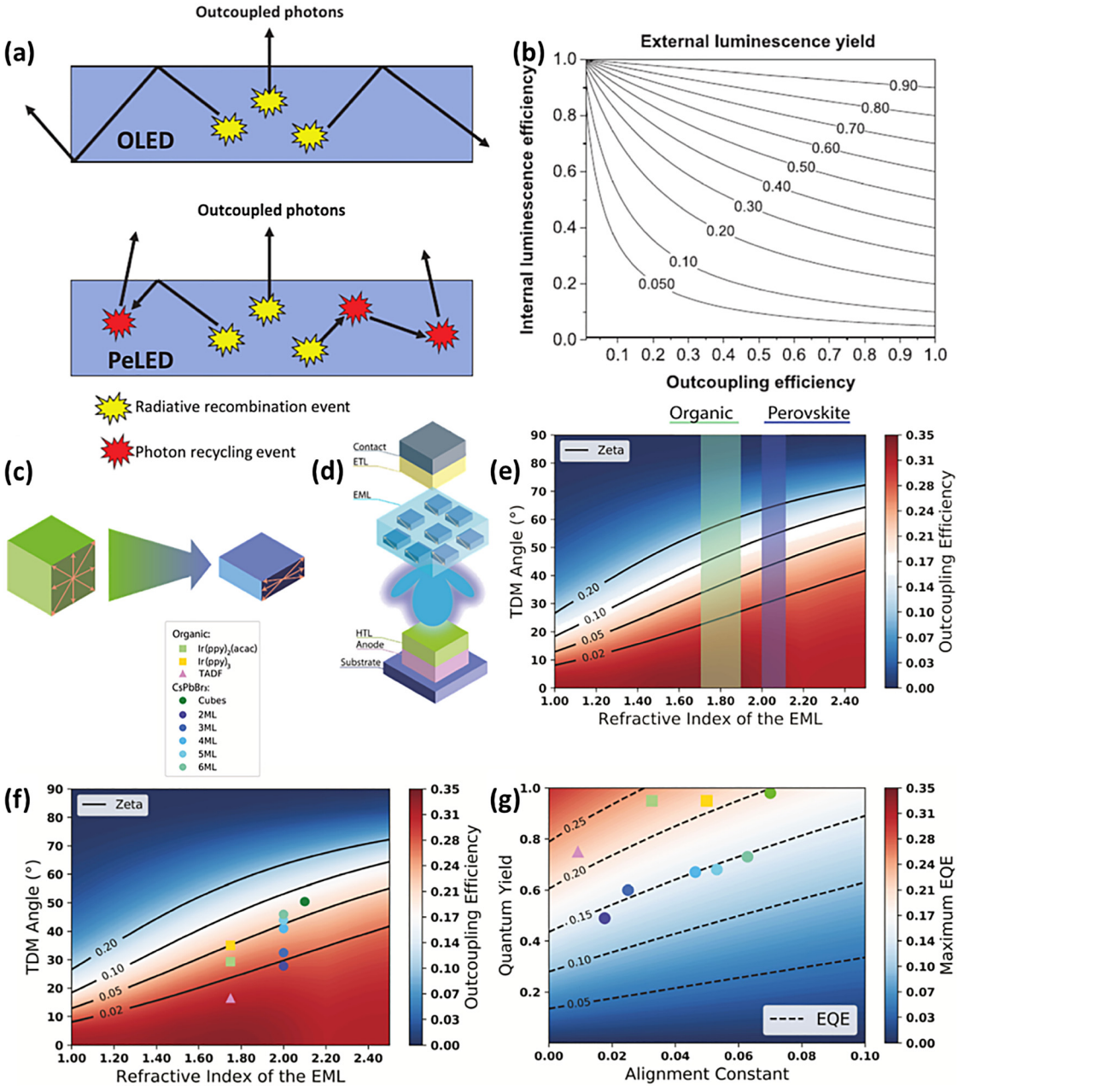

Figure 2: (a) Schematic to compare the light outcoupling in an organic LEDs (OLED) (top) and perovskite-based light-emitting diodes (PeLED) (bottom), with the arrows denoting photon trajectories. Large Stokes shifts in OLEDs mostly prevent reabsorption and hence minimal PR occurs, in contrast to PeLEDs. Thus, a larger fraction of the waveguided photons are re-emitted and outcoupled in the forward direction. (b) External luminescence yields as a function of outcoupling efficiency and internal luminescence yield calculated by considering PR processes. TDM affecting light outcoupling in perovskite nanocrystal LEDs. Reproduced with permission from [139]. (c) Schematic of the possible orientations of the TDM in perovskite nanocrystals. (d) Depiction of an exemplary stack design used to simulate the outcoupling efficiency of perovskite LEDs. (e) The outcoupling efficiency dependence on the angle of the emissive TDM and the refractive index of the EML. Samples with the same alignment constant yield identical light outcoupling efficiency, as indicated by the contour lines. Outcoupling efficiency and EQE limits of PeLEDs. (f) The outcoupling efficiency dependence on the TDM angle and the refractive index of the EML for perovskite nanocrystals and some prototypical organic emitters. (g) Performance of the investigated exemplary PeLED stack for different quantum yields and alignment constants of the emissive nanocrystals. Reproduced with permission from [162].

optical effects within/around the emitter material that can affect the η_{out} (Figure 2b–g). The parameter ζ not only specifies the final η_{out} in a more holistic approach but also contains information about the angular distribution of emitted power. It is given by,

$$\zeta = \frac{\sin^2\varphi_{TDM}}{n_{EML}^4 - \sin^2\varphi_{TDM}\left(n_{EML}^4 - 1\right)} \quad (4)$$

where, η_{EML} is the refractive index of the emitter perovskite layer and ΦTDM is the angle of the emissive TDM with respect to the film surface. Thus, ζ can assume values between 0 and 1, corresponding to perfectly horizontal and vertical TDMs respectively. Tuning these variables can result in further boosting η_{out} and device performance. In addition, light outcoupling management strategies via materials or interfaces engineering aim to reduce parasitic absorption loss (A_{para}) and enhance light extraction are pursued and will be elaborated further in Section 2.2. Furthermore, recent progress on the use of external light outcoupler in PeLEDs as well as other potential light outcoupler candidates will be summarized in Section 2.3.

2.1 Photon recycling: theoretical and experimental considerations

Akin to commercially available luminescent semiconductor systems such as GaAs [167], metal halide perovskites have also been reported to show excellent PR capabilities. The phenomenon of PR in perovskites was first reported by Deschler et al. where it was shown that in perovskite solar cells, a single photoexcited state may undergo repeated absorption–diffusion–emission events before final energy loss by non-radiative decay [168]. Unexpectedly long spatial decays and contradictorily high recombination rates with long diffusion lengths can only be accounted for through such recycling events. In general, the sharp absorption onsets at the optical band edge of such material systems [169] along with long charge-carrier lifetimes [170] and minimum non-radiative recombination losses [171] are indicative of conditions conducive for PR.

PeLEDs success in surpassing the 20% EQE limit specified by classical optical models [4] in spite of the significantly thick (~200 nm) emissive layer with uncontrolled positions and orientations of the dipole emitters, is attributed to the vital role played by PR in such systems. For an emitter with adequately high $\eta_{radiative}$, PR has been shown to enable better η_{out} by converting photons from trapped to outcoupled modes through randomization of propagation direction [127]. It has been reported to contribute to upwards of 70% of the overall light emission [174]. Theoretical models predict up to 100% emission efficiency with PR taken into consideration. Although such values are prevented by non-ideal thermodynamic losses in a device, PR is a key parameter that can drive up EQEs further. However, for $\eta_{radiative}$, it can also prove to be a primary loss mechanism. Thus, it is crucial to optimize device design to achieve PR-assisted η_{out}. Recent reports hint towards deployment of nanophotonic designs along with high PLQY perovskite emitters as a viable approach to achieve enhanced emission.

Quantification of PR for both photovoltaic and light-emitting devices was shown by Bowman et al. [172] using a generalized formulation for number of PR events per initial excitation, N, valid for all excitation and emission in these systems. This is of the form,

$$N = \sum_{i=0}^{\infty} i p_i (1-p) = \frac{p}{(1-p)} = \mathrm{PLQE}_{ext}\left(\frac{1}{\eta_{out}} - 1\right) \quad (5)$$

where p is the probability of a photon reabsorption event occurring. Hence, denoting the total number of PR process probabilities as p_i and the emitted photon escape probability as η_{out}, plots for N as a function of several important parameters can be plotted. This was used to quantify the PR using appropriate emittance models to show that the number of PR events in PeLEDs is high (up to 8) per initial excitation as compared to solar cells (~1). In addition, PR dependence on film thickness, charge trapping rates and front and back reflection coefficients (Figure 3a–f) among other controllable parameters, was studied. Hence, the critical importance of PR in light management in LEDs is undeniable.

In an effort to further improve this quantification, another significant work by Fassl et al. has recently attempted to establish a more accurate curve-fitting model for the precise determination of the η_{out} and in turn, the IQE of perovskite films [175]. It attributes the varied PL spectral shapes reported in literature for the same system simply to light scattering events occurring before reabsorption. It takes into account the initial trapped PL before outcoupled modes emerge and show that η_{out} is underestimated by more than 10% without this consideration. Through application of this theory to highly luminescent $MAPbI_3$ thin films, EQE of up to 47.4% and IQE of ~78% emerge, which confirms a scope for minimization of non-radiative decay channels by a factor of two or more.

Time-resolved spectroscopy of these systems have led to the consensus that out of the mono-, bi- and tri-molecular recombination regimes, mostly the bimolecular one is radiative and linearly dependent on excitation fluence. This has made it mandatory for PR to account for the large discrepancy between the internally and externally obtained

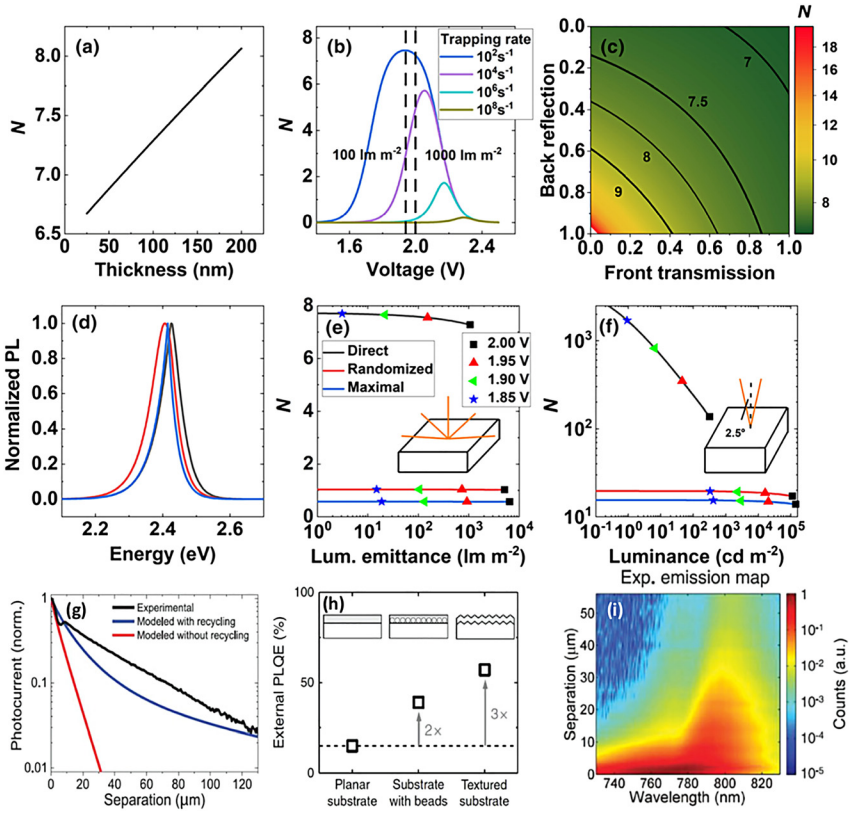

Figure 3: Number of PR events N in a $CsPbBr_3$-based PeLED as a function of (a) film thickness (for an applied voltage giving 1000 lm m^{-2} with no charge trapping), (b) voltage for different charge trapping rates. (c) (N on log scale) as a function of front transmission and back reflection coefficients. (d) Normalized photoluminescence spectra for direct, randomized and maximal emittance models. (e) N and luminous emittance as functions of applied voltage for the three models for emission into a full 2π hemisphere and (f) into a 2.5° cone about the surface normal. Reproduced with permission from [172]. (g) Predicted spatial photocurrent decay for perovskite thin film with and without PR. (h) External PLQYs for $MAPbI_{3-x}Cl_x$ for different substrates. (i) Experimentally measured light emission map for different separation distances between collection and excitation. Reproduced with permission from [168] and [173].

PLQY. By correlating data from transient absorption (TA) and PLQY, the monomolecular non-radiative recombination has been traditionally attributed to trap-mediated SRH pathways whereas the radiative bimolecular recombination was shown to originate from band-to-band transitions [176]. With the three-particle non-radiative Auger processes forming the other major loss mechanism, the carrier recombination landscape in such systems has been well-explored. PR affects the radiative bimolecular constant as apparent through the higher internal recombination constant being up to 8 times higher than the externally observed constant [173]. Richter et al. show that, with an escape probability of ~12.5%, 7 out of 8 photons in a $MAPbX_3$ (X = I, Br)-based LEDs will undergo recycling to produce a 20% external PLQE. Without re-emission processes, this value would have been a mere ~9%.

Several works on these lines have ventured to experimentally materialize such theoretical predictions. By modifying critical experimental parameters, the maximum EQE limit can be escalated to lie between 30 and 50% [177]. Overall, the common aim is to fabricate devices with optimally low perovskite refractive index, increased PR events and suppressed parasitic absorption through judicious selection of proximal transport layers and conductive electrodes. A recent, notable report in this direction is one by Cho and co-workers, where highly luminescent thin films of 2D-3D $PEA_2Cs_{n-1}Pb_nBr_{3n+1}$ perovskite are used to distinctly trace scattered photons versus recycled photons at a finite distance from the excitation point by marking the corresponding redshifts [151]. Through this, PR was shown to account for 55% of the total luminance intensity. Localized excitation giving rise to light output at a distance was also observed when further applied to a PeLED, which reinforces the proposed dependence of PR on device geometry (lateral and vertical). On a slightly different note, optically thick $MAPbX_3$ bulk single crystals were studied, and their significant PL redshift as compared to their thin-film counterparts was attributed to PR events [178]. It was also shown that the dependence of PL peak energy on the grain size in polycrystalline thin films is explainable by considering intra- and inter-grain PR events along with the spatial distribution of excited carriers.

In summarizing these various findings, some key points emerge that are seen to be valid for all cases. First, maximizing the emittance seems to be the key route to achieving high-performing LEDs. This is irrespective of the amount of PR events in the system. Second, it is critical to account for all optical events in the system including scattering, total internal reflections, reabsorption, emission and all other unregulated propagation modes before and after PR events that arise due to the optical and morphological properties of the perovskite emitter as well

as the device configuration. This would also include accurate attribution of the observed Stokes shift to PR or other phenomena as well as the ability to spatially and angularly resolve emission dependencies. Third, attaining EQEs approaching almost 100% appears well within reach via careful device engineering, as proposed by recent reports [174]. This mainly involves removing parasitic absorption pathways through techniques such as reduction of effective injection area and reduction of emissive area in contact with substrate. Also, as evident from applying the Moss relation [179], perovskite materials show dependence of bandgap on refractive index (RI) which results in a large mismatch while outcoupled to far-field modes in air, thus inhibiting emission efficiency. This can be tackled either through introduction of an index gradient to increase the light escape angle or by nanostructuring. For the purpose of better optical management, commonly used approaches are texturing or patterning of the substrate (Figure 4a–b), emitter film surface and electrodes, addition of back-reflectors [182], and use of nanostructures such as microlens arrays [183] to suppress stray internal reflection, among others (as reinforced by the simulation results in Figure 3g–i). Further, it is possible to tune emission spectrally and angularly by using photonic cavities and nanostructures in conjunction with the rest of the device architecture [184], which will be discussed in subsequent sections.

2.2 Photon management through materials and interfaces engineering

In PeLEDs, taking PR into consideration and assuming near unity value of EQE, the EQE can be described as [174]:

$$EQE_{PR,\,max} = LEE_0 / (LEE_0 + A_{para}) \quad (6)$$

where LEE_0 is direct light outcoupling and A_{para} is parasitic absorption loss. Hence, it establishes the non-negligible role played by parasitic absorption in device performance. Furthermore, the interplay between refractive index (RI) of emitter and its surrounding too play an important role. Depending on the refractive index of the material sets, wave-guiding effect can occur, in which light is trapped inside the emitter due to the large difference in refractive index between the active layer and its surroundings [185]. Since contacts and interfaces facilitate such losses, careful selection of electron-transporting layer (ETL) and hole-transporting layer (HTL) are needed from both electronic and optical point of view. While efficiency and balance of carrier injection to the emitter are considered from an electronic perspective, ETL/HTL pairs with optimum refractive index to reduce both parasitic absorption loss and wave-guiding effect are needed. By scanning a range of possible ETL/HTL materials (with appropriately chosen RI) such as ZnO/NPD, TPBi/PVK and ZnO/TFB, it was proposed that the most optimum device structure for best η_{out} would consist of the following architecture: transparent electrode/high RI transport layer/perovskite/low RI transport layer/reflective electrode [181].

In addition, optical nanostructures can be deployed to improve the η_{out}. Theoretical studies by Meng et al. correlated key parameters such as refractive indices (RI), layer thicknesses and emitter dipole orientation of materials with the η_{out} (Figure 4c–h) [181]. The value of perovskite refractive index varies depending on the choice of cations and halide anions as well as emission wavelength. Hence, optical simulation is needed to design nanostructures with optimal $\eta_{out.}$ The optical losses arising from this RI mismatch affecting the η_{out} can be modelled through various approaches, such as transfer matrices, Monte Carlo and finite difference time domain methods (enabled by commercial software packages like MATLAB, Lumerical or open-source platforms like Python MEEP). Meng et al. proposed that substrates patterned with moth-eye nanostructures with horizontal orientation of the perovskite's transition dipole moment would be the most optimum for maximizing η_{out}.

The same report also contains another simulation study done for perovskite emitters in the vicinity of optical nanostructures affected by resonance enhancement phenomena such as Purcell effect and other wave-guiding routes [181]. It was shown that patterned LEDs can achieve η_{out} values of 17.9, 24.8 and 38.3% respectively for blue, green and red, well over 1.75 times that of their planar counterparts. Apart from this, there has been a steady rise in the number of theoretical reports in this area [186], firmly establishing the benefit of employing such nanostructures for synergistic manipulation in PeLED device stacks. Recently, Zhang and co-workers provided a comprehensive review on extending the η_{out} maximization strategies used in related disciplines such as organic LEDs or other conventional semiconductors to perovskites [134].

Several nanophotonic schemes including nanostructuring the interface as well as precise nanofabrication, which have been employed for traditional semiconductors, e.g. III-nitride-based LEDs [187, 188] can be transferred to PeLEDs as well. A broad overview of these approaches is illustrated in Figure 5. From bottom-up materials approach (for fabrication of nanorods, nanowires, etc.) to application of advanced lithographic nanofabrication techniques, much progress has been made to achieve complete control over light propagation within the device. Taking cues from

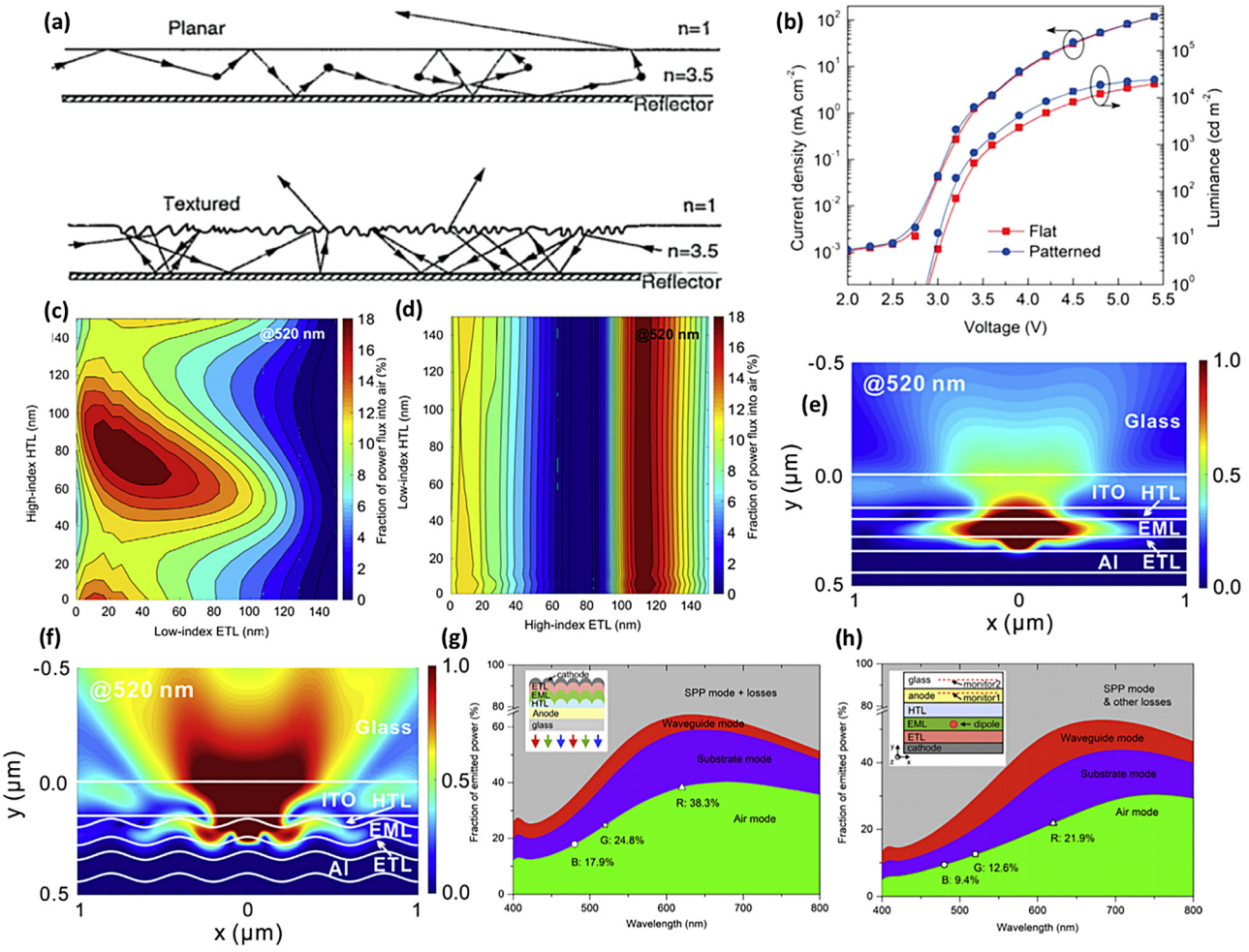

Figure 4: (a) Comparative study of outcoupling efficiency for planar and patterned devices: schematic of light extraction in typical planar and textured active layers. Reproduced with permission from [180]. (b) Current density–voltage (J–V) and luminance–voltage (L–V) characteristics for $CsPbBr_3$ PeLEDs. Reproduced with permission from [70]. Simulated η_{out} of planar PeLEDs emitting at 520 nm vs. the layer thickness of ETL and HTL with (c) low-index ETL and high-index HTL and (d) high-index ETL and low-index HTL, high-index and low-index refer to the values of 2.5 and 1.5 respectively. Normalized cross-section near-field intensity distributions of PeLEDs without and with the moth-eye nanopatterns for light extraction in (e) planar and (f) patterned device structures emitting at 620 nm. Fractions of mode powers of (g) planar and (h) patterned PeLEDs with an isotropic dipole orientation as a function of dipole-emitting wavelength calculated by the FDTD method. The theoretical maximums of red (620 nm, circle), green (520 nm, star) and blue (480 nm, triangle) emitted powers into air are marked. Reproduced with permission from [181].

these related domains, PeLEDs have also been coupled with such structures with promising results. A study using vertical $MAPbI_3$ NW arrays fabricated on porous alumina membranes (PAMs) reported 45% PLQY and 130 times increase in EQE by tuning the NW diameter [189]. About 56-fold enhancement in IQE enabled by 2–3 times increase in light-outcoupling was observed when NW dimensions were shrunk to the quantum confined regime (~6 nm across).

Apart from this, there have been instances of resonant nanostructures incorporation into the emitter layer, transport layer or emitter–transport interface to maximize efficiency [190]. This is done by making use of plasmon enhancement [191] and core–shell-like effects on the emitter [192]. One such recent work involving the incorporation of Au nanospheres in the HTL of a $MAPbBr_3$-based perovskite reported relative EQE enhancement of over 50% [193]. Similarly, Ag nanorods, when introduced into the perovskite–HTL interface of a $CsPbBr_3$ system-based LED enabled a 43.3% improvement in EQE [194]. Yet another approach has focused on nanocrystal heterostructures with core–shell, nanocomposite, nanohybrid and other configurations. To this avail, systems such as $CsPbI_3$-PbSe nanocomposite [195], $CsPbBr_3$/amorphous

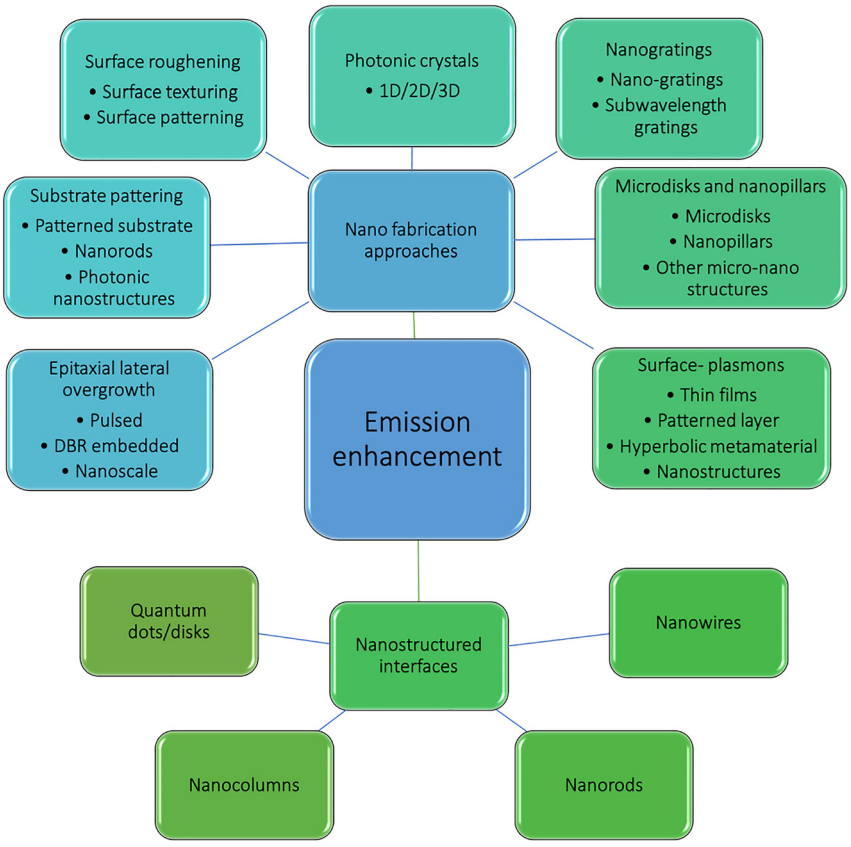

Figure 5: Overview of approaches to nanostructuring the perovskite, interface or substrate to boost emission efficiency beyond material limits.

$CsPbBr_x$ core-shell [196], $CsPbX_3$-ZnS heterodimers [197] and $CsPbBr_3$–$Ti_3C_2T_x$ MXene nanocomposites [198] have been successfully demonstrated to be effective.

2.3 Deploying external outcouplers

The resonant light recycling in external photonic cavities such as Bragg mirrors and gratings has already been shown to be useful for light extraction in several perovskite optoelectronic applications including photovoltaics and lasing. Shen and co-workers fabricated PeLEDs by embedding a moth-eye nanostructure (MEN) at the front electrode/perovskite interface via soft imprinting [70]. The MEN-modified $CsPbBr_3$ emitter showed massive improvement in EQE up to 20.3% and current efficiency of 61.9 cdA^{-1}, both ~1.5 times higher from the non-nanostructured reference device. Further, they showed that by employing a half-ball lens to outcoupled substrate-trapped photonic modes, EQE can be boosted to 28.2% and CE to 88.7 cd A^{-1}, both record values for PeLEDs emitting in this wavelength range. Deschler et al. proposed improvised device architectures to maximize PR effect in PeLEDs [174]. Reduced contact area of nanostructured electrodes (<30 nm across) coupled with an appropriate back reflector was pitched as a possible device design to achieve near 100% EQE. This is owing to the inherent scattering and plasmonic effects of such structures coupled with heightened PR events due to nanostructuring. Apart from this, device stacks fitted with 1D metallic nanogrids (as polarizers), angle-resolving microstructures (for directional emission) and distributed Bragg reflectors (DBRs) (for narrow emission profile), were shown to serve different purposes. These are all feasible integrable designs for PeLEDs in the imminent future.

Tang et al. employed a moth-eye nanostructured ZnO layer in a PeLED stack to serve the dual purpose of a hole injection layer as well as for enhanced outcoupling [70]. Lova and co-workers tuned the spontaneous broadband emission of 2D (EDBE)$PbCl_4$ perovskite by embedding it in flexible polymer DBRs [199]. This allowed directional and spectral redistribution of the PL for promising application in low-cost, large-area, lightweight flexible LEDs. Zhang chose the $MAPbBr_3$ perovskite system in conjugation with anodic alumina membranes (AAM) with different nanostructure geometries for PeLEDs (Figure 6a–d) [200]. The AAMs served as three-dimensional nanophotonic substrates with a layer of alumina nanodome array light outcouplers and a layer of TiO_2 nanowire array optical antennae. This enabled an EQE enhancement from 8.19 to 17.5% for the champion device of this configuration (Figure 6d–f). Through optical simulations and experimental investigation, it was established that

extraction efficiencies reach ~73.6% in these device architectures due to both enhancement of emission and its spatial confinement within the photonic structure. Along similar lines, the aforementioned abrupt difference in refractive index between perovskite and air was bridged by another report that demonstrated a 14.6% EQE in $MAPbI_3$-based red/NIR LEDs employing a randomly distributed nanohole array embedded in a SiN layer between the anode and substrate [201]. The SiN layer and the nanohole array with RI values of 2.02 and 1.0 respectively, enable much higher light extraction, up to 1.64 times the planar control device.

In a novel approach to combine the abovementioned techniques, Geng et al. demonstrated a hybrid plasmonic-photonic architecture to amplify the emission and create directionality through a hybrid metal-dielectric system [202]. One-dimensional DBRs fabricated by alternate layers of SiO_2 and ZrO_2 were used in conjunction with $GdVO_4$:Eu^{3+} nanophosphor emitters to generate field enhancement through Tamm plasmons. The hybrid character of this stack was shown to exhibit reduced dissipative modes and efficient outcoupling of trapped electromagnetic energy to free-space radiative modes. Such approaches seem to be extremely promising for application in PeLEDs as well in the near future. On similar lines, Chen and co-workers used highly reflective HfO_2/SiO_2 planar dielectric layers forming DBRs as the optical resonator for a vertical cavity surface-emitting laser (VCSEL) with a perovskite emitter [203]. A high cavity Q-factor was attained in this configuration which was later extended to flexible polymer substrates. With significant stability and lasing lifetime, such nanostructured DBR stacks are also promising candidates for PeLEDs. Finally, it is essential to note that technological transfer from the domain of organic, inorganic and polymer-based conventional semiconductor LEDs that heavily employ nanostructures, would be extremely beneficial for PeLEDs.

Yet another exciting application of halide perovskites has been seen in the field of active metadevices [190, 204]. Moving away from traditional plasmonics or photonics-enabled spatial confinement at the nanoscale, metaoptics seeks to solely utilize optically resonant dielectric nanostructures for this purpose. To overcome low quantum yields and fabrication-related challenges in traditional semiconductors, halide perovskites seem to offer a promising alternative. It has been shown in several theoretical studies that strong light confinement in such nanostructures result in better light–matter interaction and in turn, enhances light emission from the emitter material

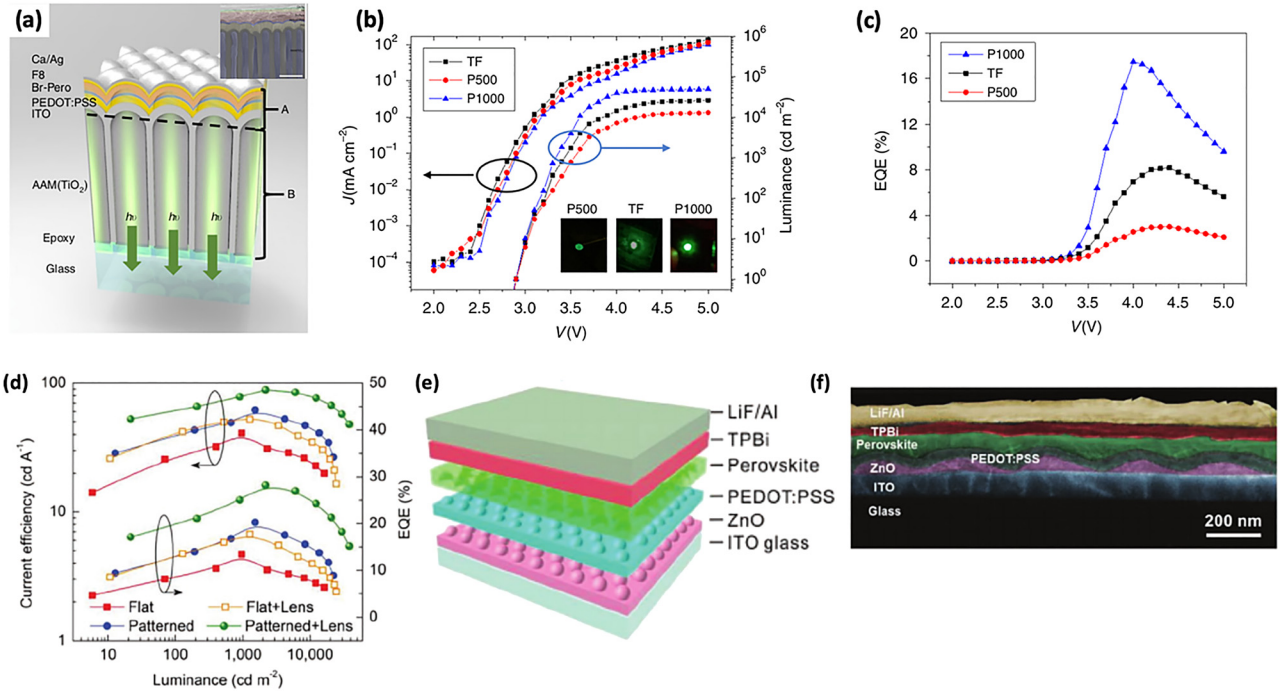

Figure 6: Devices on nanophotonic substrate (a) Device schematic. The materials from top to bottom are: Ca/Ag electrode, F8, $CH_3NH_3PbBr_3$ (Br-Pero), PEDOT: PSS, ITO and anodic alumina membrane (AAM). AAM channels are filled with TiO_2. Device performance. (b) J–V curve, luminance and (c) external quantum efficiency (EQE) of the thin film (TF) and AAM samples. Reproduced with permission from [200]. (d) EQE and CE vs. luminance for device with and without patterning for comparison. (e) Schematic of device with patterned substrate of configuration glass/ITO/ZnO/PEDOT:PSS/$CsPbBr_3$/TPBi/LiF/Al and (f) cross-sectional SEM. Reproduced with permission from [70].

[205]. These devices are inspired by high RI, dielectric metamaterials, where the electromagnetic response is attributed to the magnetic dipole resonances and optical magnetism, arising from resonant dielectric nanostructures. The fundamental idea is to use sub-micrometre Mie atoms (Mie-resonant nanoparticles) to create optical metasurfaces with tuneable functionalities [204]. As applied to perovskite materials, high RI and facile geometric tuneability enable strong geometric resonances and electromagnetic interferences between the multipolar modes corresponding to the constituent elements of the structure. Such metaoptical structures in the form of spheroids, disks, cuboids (for instance, as nanocrystals) have been realized and used for many successful applications [132].

Beyond PeLED, perovskites have also been demonstrated to be superior gain mediums for lasing applications owing to their lower amplified stimulated emission (ASE) threshold (an order of magnitude lower than commercially established systems such as ZnSe, CdS, organic semiconductors etc.) [206]. Nanostructured optical cavities, when used as high-quality feedback resonators, provide a promising route to achieve lasing in these material systems. With careful tuning of key parameters such as the spectral linewidth, efficiency of outcoupling for generated light, cavity Q-factor, gain coefficient and lasing threshold, efficient perovskite lasers can be attained. Along with nanoengineering the feedback structure, many reports also point towards the advantage of nanostructuring the gain medium itself [207].

For cavity effects, periodic optical nanostructures such as gratings and mirrors have been frequently used. To attain strong photon confinement, high reflectivity, unidirectionality and low-loss wave-guiding of propagating modes, several architectures such as distributed Bragg reflectors [202], Fabry–Perot resonators, periodic gratings, whispering gallery mode (WGM) cavities [209] etc. have been reported to exploit optical phenomena such as Purcell effect, multiple reflections, wavelength-specific scattering, polaritonic behaviour etc. for amplification of emission (Figure 7). Recently, optically pumped lasing has been shown to be possible in an LED device architecture with embedded resonator [210]. Such advancements appear to be extremely promising for imminently possible deployment of perovskite systems in lasing applications.

It is important to note that the primary impediments to further advancement are several fundamental challenges that demand extensive investigation into the material system itself. These include poor operational stabilities at high injection density, substantial Joule heating, imbalanced charge injection, local electric fields in the gain medium, and unwanted Auger recombination losses etc. that commonly occur in perovskite-based devices. Most of these obstacles have been outlined in detail recently by Rand et al. [211] and Gao et al. [212]. It is thus imperative to probe further into improving the thermodynamic stability of such systems. In the next section, we will discuss the origin, underlying photophysics and possible solutions to stability challenges that plague PeLEDs currently.

3 Defects and their effect on perovskite stability

3.1 Defects and spatial heterogeneities in perovskites

Fabrication of films from solution-based processing, though ideal for implementation in low-cost, large-scale manufacturing (roll-to-roll processing), often suffer from rapid formation of defects during their preparation [213] (Figure 8a). According to previous calculation and experimental results [108, 217–219], the nature and density of defect states in perovskites is highly sensitive to the film deposition conditions [220]. Point defects, which include vacancies, interstitials and antisites, dominate in perovskites, with the propensity of their formation highly dependent on the formation energy—where lower formation energy translates to these defects forming more readily (Figure 8b). Thankfully, for perovskites, the low formation energy of shallow defects means that these are more thermodynamically favoured [108, 218] as compared to the deep defects, which are more detrimental to its intrinsic properties. Though less destructive in nature, shallow defects are not only sites for non-radiative recombination, but also present a pathway for degradation such as vacancy-mediated ion migration and/or environment stressor-facilitated degradation (Figure 8c). The susceptibility of perovskite to ambient related degradation during film preparation and device operation calls attention to the need to address these defects in order to mitigate issues in perovskite stability. Comprehensive reviews on defect formation mechanisms in perovskites and their impact on optoelectronic devices have previously been published by Chen et al. [221]. These localized degradation regions act as points for initialization of device failure, with the dead regions becoming paths of least resistance, leading to consequences such as spectral intermittency or blinking in emission [222]. Single nanoemitters with strong quantum confinement such as semiconductor quantum dots, on the other hand, have traditionally been shown to exhibit

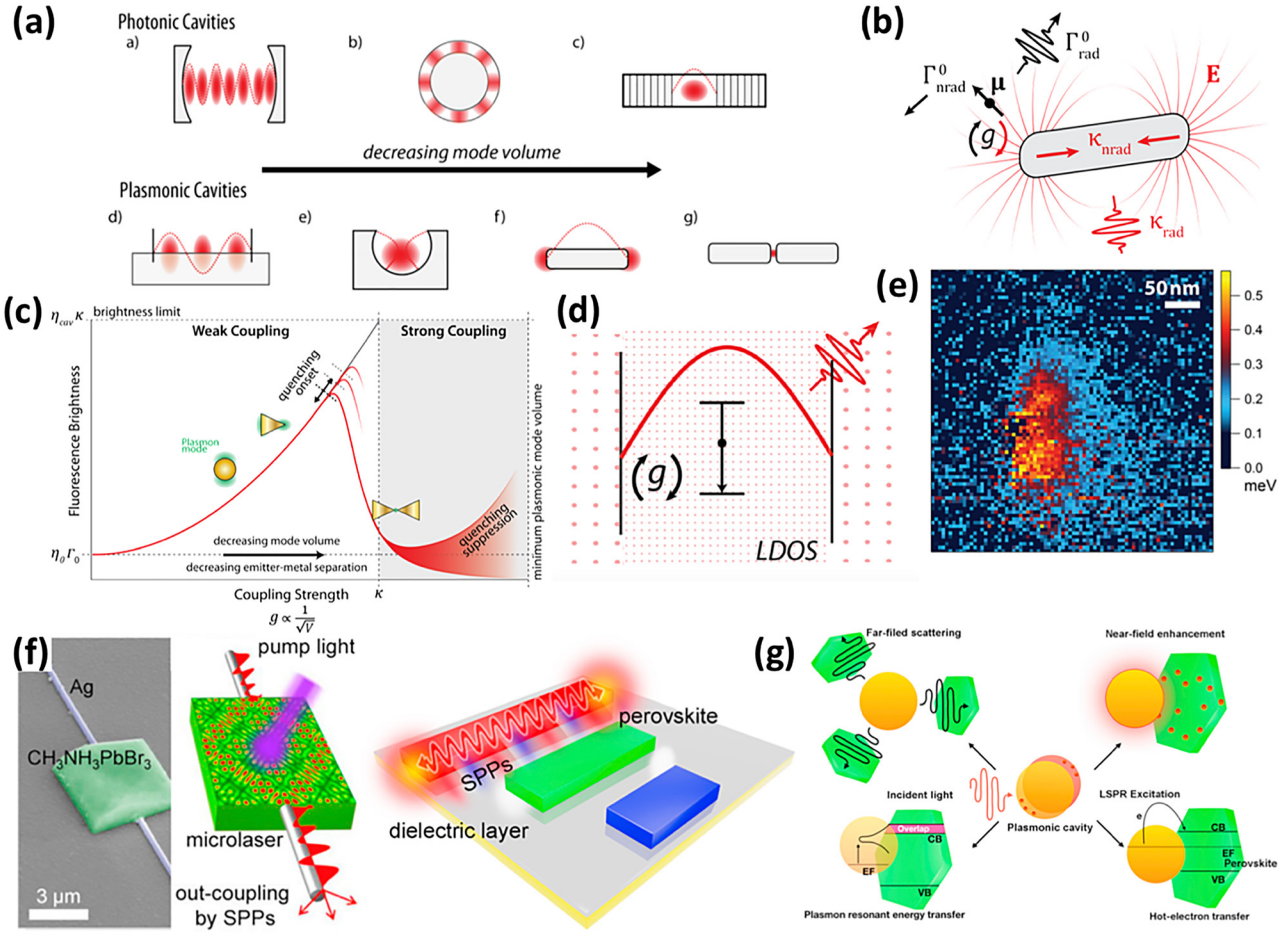

Figure 7: (a) Different forms of photonic cavities (mirrors, microresonators, micro-Bragg stacks, photonic crystals) and plasmonic cavities (trapped standing wave-type SPP cavities, collapsed structures with localized modes, dipole nanoantenna and coupled gap plasmon system respectively). (b) Schematic indicating the various energy dissipation pathways for an excited emitter with dipole moment (μ) in a plasmonic cavity mode (E). (c) Graphic illustrating the increase of brightness of a quantum emitter from the uncoupled free-space value to the theoretical maximum when coupled to a plasmonic nanocavity, given a saturated pumping regime. Here, η_0 is the emitter quantum efficiency, η_{cav} is the radiation efficiency of the cavity, Γ_0 the spontaneous emission rate of the uncoupled molecule, and κ the total cavity decay rate. (d) A cavity provides a frequency-specific way to locally increase the density of states. By placing an emitter in a cavity resonant to its emission, the rate, with which it emits can be considerably enhanced. (e) Map showing coupling strength as a nanoantenna is scanned over an excited single fluorescent molecule at a particular height separation extracted using lifetime values recorded at each point using time-correlated single photon counting. Reprinted with permission from [208]. Copyright (2018) American Chemical Society. (f) SEM image and schematic illustration of an embedded dielectric/metal heterostructure for the plasmonic output of a dielectric laser. (g) Schematic illustration of localized surface plasmon resonance (LSPR) enhancement mechanisms in metal-halide perovskites utilizing a plasmonic cavity: far-field scattering, near-field coupling, hot-electron transfer and plasmon resonant energy transfer. Reproduced with permission from [132].

spatially heterogeneous blinking [223]. In perovskite nanocrystals (NCs), this has been attributed to long-lived carrier trapping in surface defects or intermittent Auger recombination processes leading to charging–discharging cycles of the emissive NC [224]. More interestingly, this behaviour which was previously perceived to be valid only for nanoscale emitters, has recently been shown for microcrystals beyond the diffraction limit [221]. In general, constituent emitters spread over distant domains, are spatiotemporally uncorrelated and average out over the ensemble. Therefore, for emitters with dimensions greater than the quantum confinement range, homogeneous intensity of PL is observed under moderate excitation fluences. The only instances where spectral correlation between individual emitters in an extended system have been observed are in CdSe quantum wires and individually stacked monolayers of $MoSe_2/WS_2$ (transition metal dichalcogenides), both of which are attributed to delocalized excitons facilitating unprecedented charge transport [225, 226]. However, in a recent work, Pathoor et al.

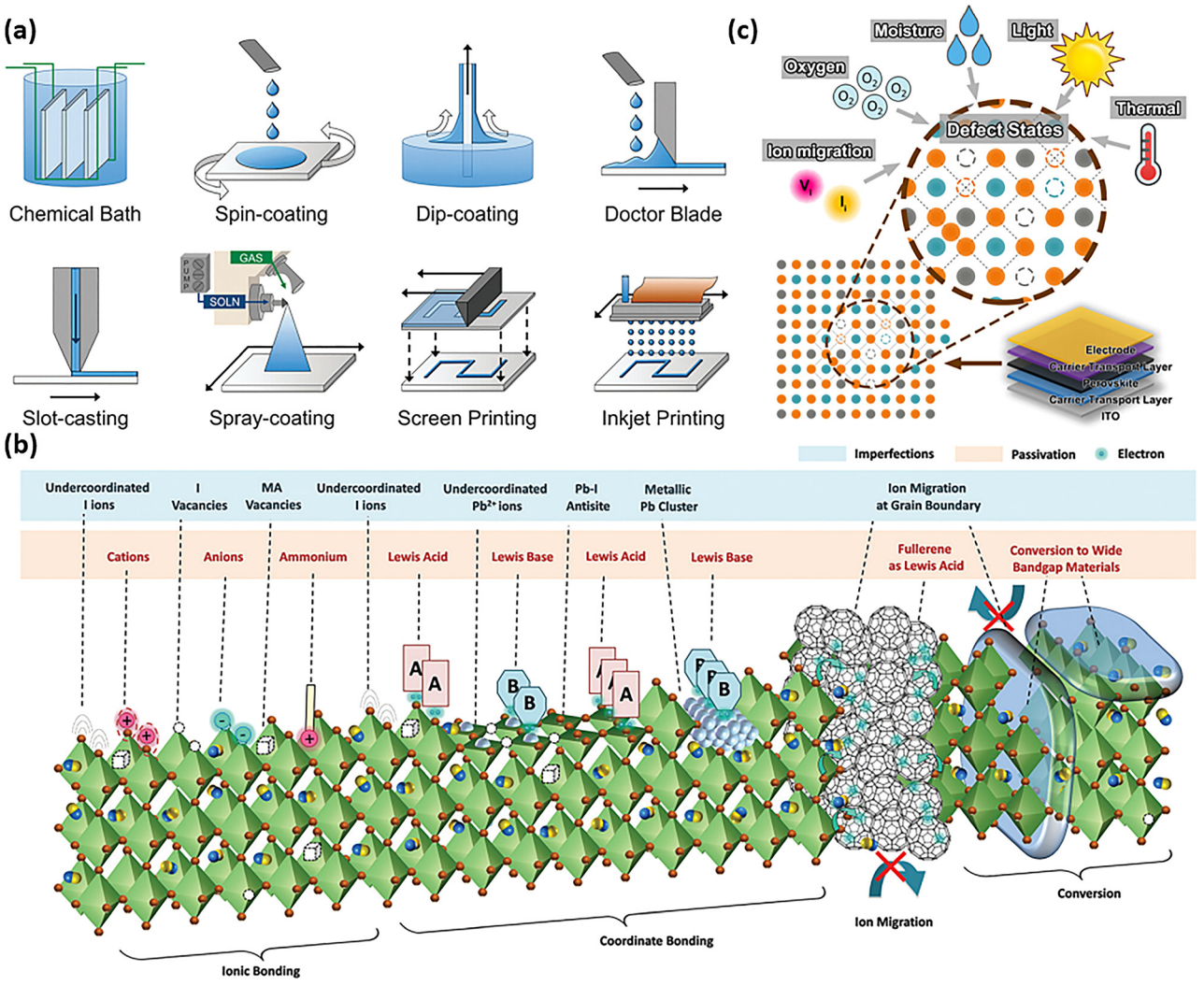

Figure 8: Schematic on the (a) various types of solution-based processing techniques with applicability to perovskites. Adapted with permission from [214]. (b) Types of defects present in perovskites and passivation routes to mediate them. Adapted with permission from [215]. (c) Mediation of perovskite degradation by crystal lattice defects. Adapted with permission from [216].

demonstrated spatial synchronicity in the fluorescence intermittency of $MAPbBr_3$ microcrystals. XRD and SEM/TEM combined with spectroscopic measurements point towards mesoscale carrier migration, aided by the presence of metastable trap states as the possible mechanism for such behaviour [227].

Aside from crystal lattice defects, poor homogeneity of perovskite morphology, can also be equally destructive. Wide variation in grain size and/or film uniformity arising from poor wetting critically affects the luminous efficacy and lifetimes across individual grains in the system, manifesting in the form of low device efficiency and unidentified loss pathways [228]. Some of these degradation routes are elucidated in Figure 9a–d.Many studies on defect tolerance properties of perovskites have shown the existence of morphological heterogeneity at sub-grain (<100 nm), grain-to-grain (100 nm–10 μm) and long-range length scales (>10 μm) (Figure 9e) [233]. Experimentally, several groups have attempted to correlate in operando and ex situ measurements via spectroscopic studies in a bid to explain the degradation processes characterizing these systems. For instance, Andaji-Garmaroudi et al. studied the degradation of $(Cs_{0.06}FA_{0.79}\ MA_{0.15})Pb(I_{0.85}Br_{0.15})_3$-based PeLEDs through simultaneous, nanoscale, cross-sectional chemical mapping (STEM-EDX and PES) using transient and steady-state spectroscopic measurements [234]. The heterogeneity at play here was found to be the accumulation of bromide ions at one interface leading to charge injection imbalance and non-radiative recombination losses. Passivation with potassium was shown to immobilize the halide and boost

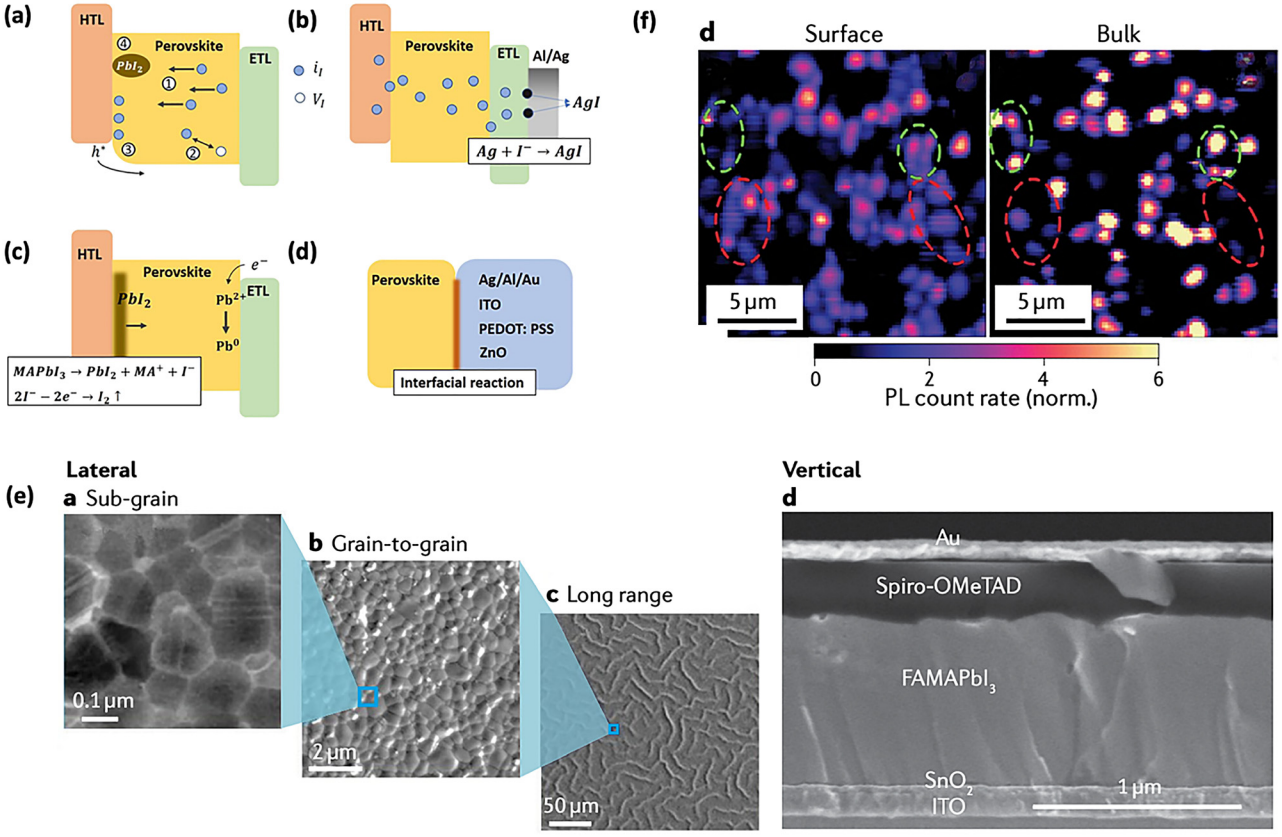

Figure 9: (a) Ion migration inside perovskite: 1) defect migration; 2) annihilation and creation of Frenkel defects; 3) modification on charge injection and 4) distortion of crystal lattice. (b) Ion migration across the interface leads to electrode corrosion. (c) Electrochemical reactions. (d) Interfacial reactions. Reproduced with permission from [229]. Heterogeneity at different length scales in halide perovskites. (e) Electron microscopy images showing sub-grain (panel a), grain-to-grain (panel b) and long-range (panel c) disorder within halide perovskites, and cross-sectional SEM image of a complete, high-performance perovskite solar cell (panel d). Vertical heterogeneity in the perovskite grain morphology is evident despite the device having an excellent power conversion efficiency of 23.32%. Reproduced with permission from [230] and [231]. (c) Single-photon (left) and two-photon (right) PL maps that probe the surface and bulk radiative recombination emission, respectively, in a $MAPbI_3$ thin film. Reproduced with permission from [232]. Published by The Royal Society of Chemistry.

device performance significantly. Again, for $MAPbI_3$-based PeLEDs, such interface defects were shown to be caused by carbon heterogeneities at the grain boundaries and surfaces [235]. Correlated imaging by grazing incidence hard X-ray diffraction (GIXRD) and X-ray photoemission electron microscopy (X-PEEM) enabled the identification of Frenkel and element vacancy defects arising out of such inhomogeneous chemical distribution, providing a detailed view of the impact that local chemistry variation has on luminescent properties.

Heterogeneity in perovskite films may also manifest in the form of crystallographic twinning as observed in pure $FAPbI_3$ and $FA_{0.875}Cs_{0.125}Pb(I_{0.666}Br_{0.333})_3$, where the increased probability of such defects occurring in the former arises from the low formation energies [236]. This has been attributed to local strain anomalies, which still requires further experimental understanding. It has been shown in the recent past that lattice strain is directly responsible for non-radiative losses in devices [217]. Time-resolved PL measurements coupled with synchrotron-based scanning X-ray diffraction by Jones et al. on $MAPbI_3$ thin films, reveal direct correlation between strained regions and charged defect density [237], where temperature-induced phase transition (from cubic to tetragonal at ~57 °C) on cooling of post-annealed films leads to the formation of spatial heterogeneities; a hub for non-radiative losses. For such cases, it is essential to turn to growth methods that prevent inhomogeneous nucleation and creation of local domains (concentration gradients), which result in long-range super-grain features and hence, show less local strain variation. In addition, regulating the contacts used as well as introducing passivation treatments can further aid performance by minimizing parasitic losses.

On a different note, with NCs gradually taking centre stage as the most promising emitters for PeLEDs, it is important to probe the heterogeneities related to this family of materials as well. NCs are surrounded by a large surface defect area instrumental in non-radiative recombination. Owing to this, external stressors such as oxygen, water, light and heat can independently or in combination, bring about an adverse impact on the luminescence properties [238, 239]. Mitigation of this obstacle through passivation methods, using core–shell structures [240], careful engineering of chemical composition [241], reducing dimensionality [242] etc. have been attempted with considerable success.

By utilizing a wide range of characterization techniques yielding details spanning morphology to optoelectronic properties, complete spatial and temporal information about perovskites' underlying defect physics can be obtained. For instance, with the goal of mapping the charge carrier transport properties of $MAPbI_3$ thin films with local variation in recombination centres, deQuilettes et al. used correlated confocal and wide-field fluorescence lifetime imaging microscopy [244]. They simulated and experimentally demonstrated heterogeneity in non-radiative losses as a function of changing excitation intensity as well as anisotropic diffusion of carriers due to differences in intergrain connectivity. For this and other studies enabled by sensitive photodetection, significantly small photon excitation intensities, have been used to image the charge carrier diffusion at low fluences. This has led to interesting revelations regarding several intrinsic phenomena such as the nature of relation between charge trapping and diffusion in $MAPbI_3$. These measurements have helped to identify trap-related non-radiative heterogeneities, and definitively link PL behaviour with low and high fluence regimes [245]. For probing further into the material system by selecting an appropriately small volume of focus, two-photon PL microscopy (2P-PL) is a viable option [246]. It affords depth-dependent studies of heterogeneity in the crystal, thus painting a complete picture of the charge and defect transport at buried depths. For $MAPbI_3$, this technique has been used in conjunction with conventional single-photon microscopy to show that perovskites exhibit morphological non-uniformity both in lateral and vertical directions that are critical to device performance. Another advanced approach employing this technique for depth-profiling of recombination kinetics was demonstrated by Stavrakas et al. for $MAPbI_3$ and $MAPbBr_3$ thin films (Figure 9f) [232]. This was done through four-dimensional imaging (dubbed 3D PL tomography) using time-resolved 2P-PL for mapping the surface-dominant and bulk-dominant luminescence inhomogeneities.

On the other hand, the ability to use low electron doses in microscopy (near to the perovskite damage threshold) have led to the discovery of interesting properties such as ferroelectricity and ferroelasticity in systems like $MAPbI_3$ [247, 248]. With doses 6000 times lower than normal, electron back-scattering diffraction (EBSD), yet another powerful tool, was used to probe grain-to-grain variation in $MAPbBr_3$ microcrystals [249]. It served to provide concrete evidence of grain boundaries expediting and being the hotbeds of recombination (and hence reduced PL lifetimes). Such complete information becomes extremely vital for device design and fabrication with a goal to achieve complete optimization. An outline of the available spectroscopic techniques and their advantages are given in Figure 10.

3.2 Carrier lattice interactions in perovskites

While crystal and morphological defects have indeed been shown to be detrimental to perovskite stability, charge carrier and lattice interactions such as in the case of polarons may also affect both electronic and optoelectronic processes that occur in these materials and in turn, the stability of the ensuing devices.

Charge carrier mobility increase with decreasing temperature suggests strong contribution of electron–phonon interactions to charge transport in perovskites [250]. Charge carrier and lattice interactions can be broadly classified into acoustic deformation potential scattering or Fröhlich type polar interactions, with the latter expected to dominate in perovskites due to the tendency for polarization of its ionic lattices, which can induce an electric field and couple to electrons. This was confirmed by studies by Wright et al., where investigations into temperature dependence of emission line broadening in formamidinium and methylammonium perovskites revealed scattering from longitudinal optical phonons via the Fröhlich interaction as the dominant source of electron–phonon coupling near room temperature [251]. Charge carrier interaction with surrounding atoms in a crystal lattice can lead to formation of localized lattice deformation that spatially localizes charge carriers and prevent their recombination due to screening effect. Munson et al. used temperature-dependent TRIR spectroscopy to investigate the origins of the exceptionally long charge recombination lifetimes of perovskite films [252]. Large polarons, which form preferentially at elevated temperatures, correlated with an increase in electron–phonon coupling, are noted from their distinct electronic transitions in the mid-IR spectral region. These processes,

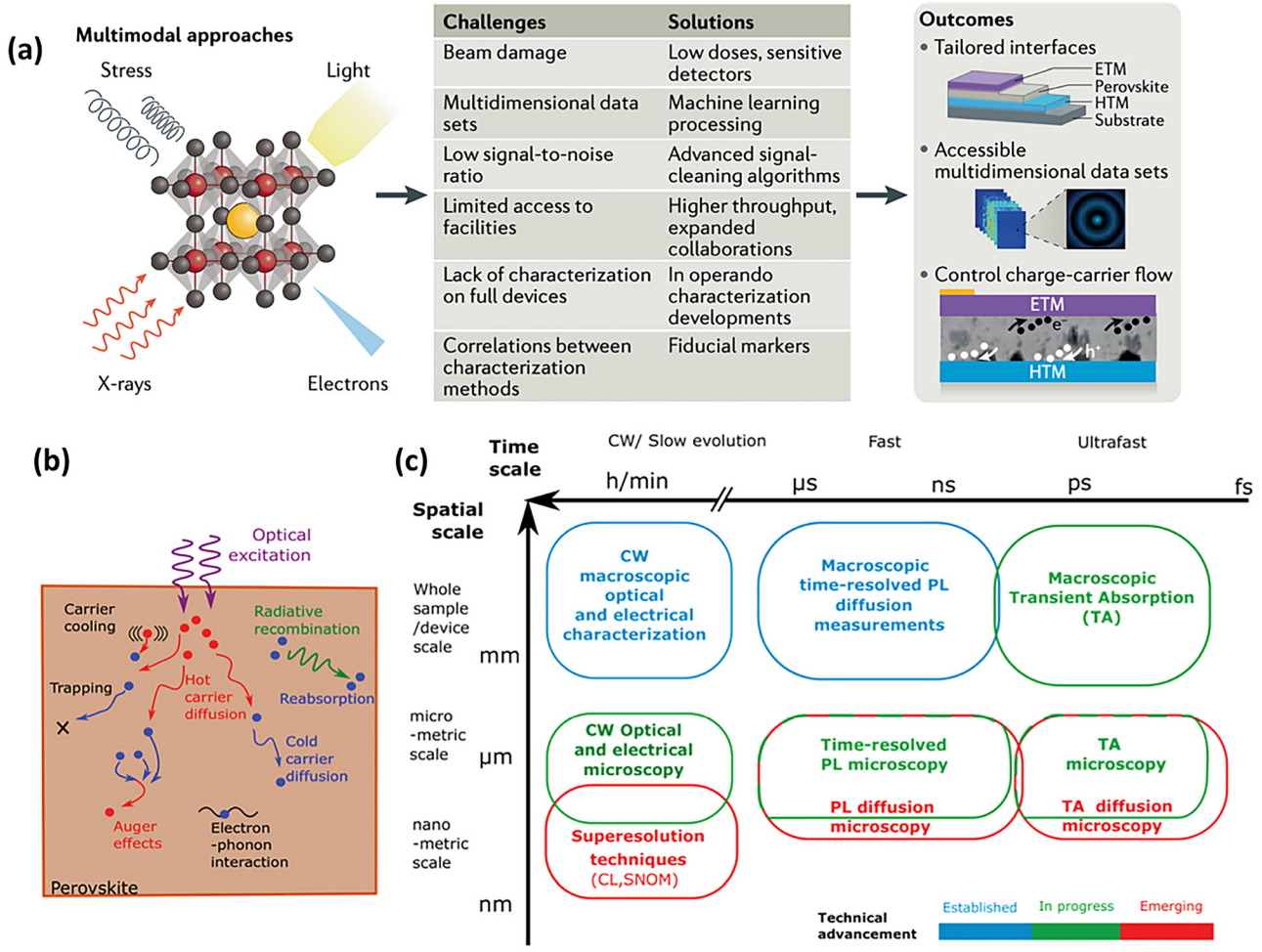

Figure 10: Information about recombination kinetics as obtained from different techniques. (a) Technique of implementing correlative microscopy to study the correlations between structural, chemical and electrical properties at the nanoscale, as well as quantify the tolerable dose limits for perovskites to external stressors (such as bias, photons, electrons and X-rays) before generation of additional defects and, hence, non-radiative loss pathways. Charge carrier processes in perovskites and the corresponding tools to study these effects. Reproduced with permission from [233]. (b) Schematic highlighting key photophysical phenomena related to carrier transport that can occur following photoexcitation of the perovskite. (c) Table summarizing the main experimental techniques that can be employed to study the recombination and diffusion of charge carriers in perovskites. These techniques are grouped according to their level of technical sophistication and relevant length and timescales accounting for typical resolution limits. CW denotes continuous wave illumination, CL is cathodoluminescence and SNOM is scanning near-field optical microscopy. Reproduced with permission from [243].

associated with an increase in dynamic disorder in the strongly anharmonic perovskite lattice are measured through the vibrational dynamics of the vibrational modes of the organic cations in the perovskite film. The inhibition of electron-hole recombination by these polarons explains the long lifetimes seen for perovskites. Studies by Nie et al. reveal presence of light-activated metastable polaronic defect states originating from intrinsic traps and ion migration, as the source of degradation in perovskites [253]. Coexistence of these charged states with photo generated charge carriers result in photo degradation in perovskite solar cells.

3.3 Degradation process in perovskites

Ionic migration facilitated by the existence of defects or structural inhomogeneity is linked as a major source for PeLED degradation. Ionic migration not only results in creation of new non-radiative recombination sites, the accumulation of defects at the interfaces also triggers higher non-radiative recombination centres at the interfaces. In 3D perovskite, both halide anions (I) and cations (organic/inorganic A-site cation and metal cation) can migrate in the presence of electric field, due to the existence of vacancies, interstitials, or antisite substitutions

[109–111]. Li et al. showed that by applying electrical switching of perovskites, photoluminescence variations can be observed in seconds. The growth of the dark region corresponds with the drift in halide vacancies, which suppresses radiative recombination, highlighting the strong correlation between interstitial and vacancy defects in determining the optoelectronic properties of perovskites [254]. This is further visualized in PL microscopy mapping studies by Phung et al., where on laser excitation, removal of ions from their crystalline lattice positions driven by light (or heat) effect, generate non-radiative recombination sites, manifesting in photoluminescence quantum yield reduction [255] (Figure 11a). While differences in ion migration energies have been reported, the results concur on the order of activation energies for the various defects, with halide related defects moving faster than A-site and lead related defects [219, 257]. Meggiolaro et al. found that perovskite film grain sizes play a crucial role in determining the ion migration process and their activation energies. It was revealed that ion migration is dominant at the surfaces and grain boundaries of perovskite films due to the surface-assisted formation of migrating defects [112]. Through current, luminance and EQE kinetics as well as pulsed voltage measurements, Cheng et al. showed two-stage degradation of $PEA_2FA_{n-1}Pb_nBr_{3n+1}$ PeLED under constant-current operation (Figure 11b). The first stage of degradation process involves the migration and accumulation of FA+ and PEA+ at the perovskite/ETL interface driven by applied bias. This results in the generation of additional built-in electric field on the injection carriers. While this results in favourable injection for both electron and holes arising from lowering of energetic barrier, the migration of the cations eventually leads to EQE decay due to loss of passivating effect. The penetration and trapping of the large number of mobile cations in the ETL, under prolonged device operation, damages the perovskite/electron transport interface and results in degradation of PeLED performance.

Aside from aiding ion migration, these defects also contribute towards facilitating degradation due to ingress of moisture and oxygen, not to mention, lowers the thermal stability. While there have been reports of moisture aiding perovskite film crystallization [258, 259], the impact of moisture on the stability of the perovskite films post-

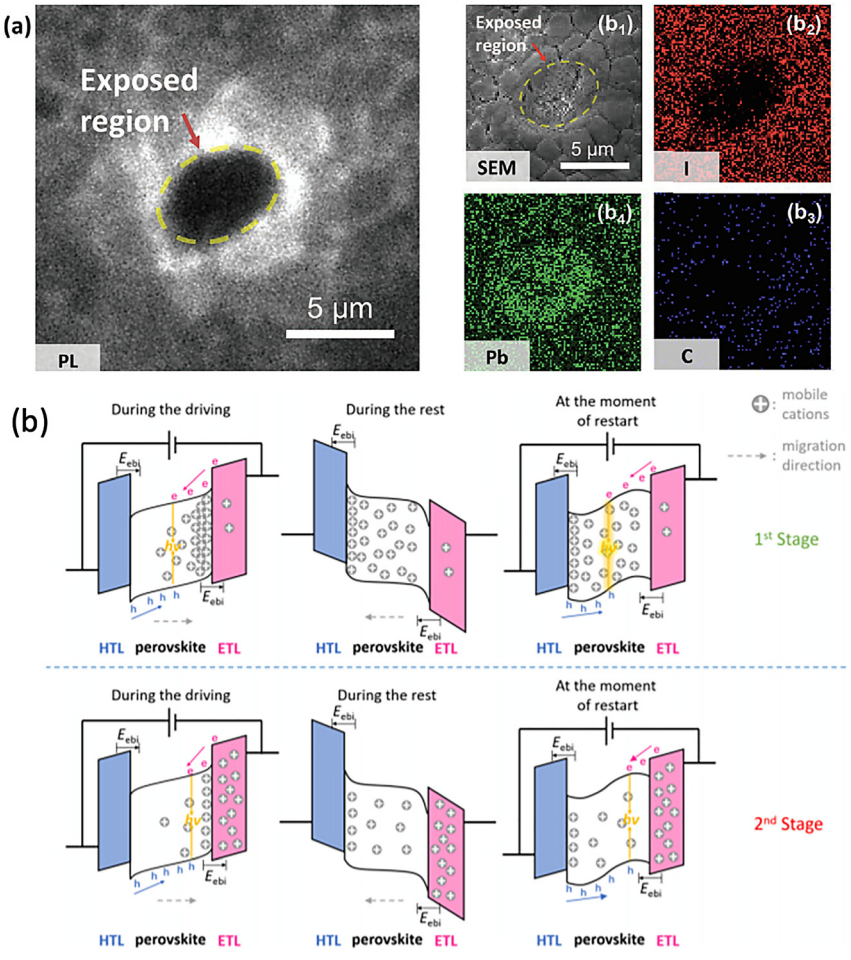

Figure 11: (a) Photoluminescence wide-field image directly after 1 min of focused laser exposure in a MAPbI3 thin film. (ii) Scanning electron microscopic (SEM) and energy dispersive X-ray (EDX) images representing elemental distribution of the elements I, C and Pb, recorded from the same film area 1 min after laser exposure. Adapted with permission from [255]. (b) Schematic showing the band energy alignment and movement of mobile cations in the first and second stages of EQE decay. Adapted with permission from [256]. Copyright (2020) American Chemical Society.

deposition cannot be ignored. The hygroscopic nature of the MA^+ cation has led to the formation of hydrated perovskite phases, which induces the chemical interactions for perovskite degradation, with the evolution of iodine gas in the reaction rendering the process irreversible. Jong et al. investigated the effect of water intercalation and hydration on decomposition and ion migration of $CH_3NH_3PbX_3$ using first-principles calculations. Thermodynamic calculations indicate that water intercalates into the perovskite, forming hydrogen bonding with PbX_6 and MA. And while the monohydrated compounds are stable with respect to decomposition, the ingress of moisture reduces the activation energies for vacancy-mediated ion migration [113]. Using infrared spectroscopy, Müller et al., demonstrated presence of O–H peaks corresponding to diffusion of moisture into the perovskite films, even at low humidity levels of 10%. The O–H stretching mode, detected only for perovskite films and not for single crystal despite exposure to similar conditions, provide further proof of the detrimental effects of grain boundaries in perovskite stability against moisture [260].

Oxygen, akin to moisture is also an initiator for the degradation process, particularly in the presence of other variables such as light, and bias, which results in auto-accelerated decomposition. This was confirmed experimentally where photo-induced formation of reactive superoxide species was found to occur in the presence of oxygen and computationally, where ab initio simulations indicate that iodide vacancies are the preferred sites for superoxide formation [261]. The rapid diffusion of oxygen into the perovskite is further mediated by the tendency for halide vacancies (Vi) to occur and coordinate with electron-donating molecules through Lewis acid–base interactions. Moreover, with the prevalence of halide defects at the surface and grain boundaries, it is almost obvious that this mode of degradation is grain boundary dependent. Electrostatic charges generated are trapped along the grain boundaries on light irradiation exacerbating the situation further through trapped charge induced crystal disruption, enabling short range interaction between electron-donating species of oxygen and/or moisture with the perovskite [262].

As mentioned, light can provide the driving force for the degradation process to occur. This is due to reduction in energetic barrier for vacancy-mediated ion migration. The influence of light becomes clearer in mixed-halide systems where separation into I-rich and Br-rich domains is hastened on exposure to light illumination. Hoke et al. exposed (MA) $Pb(Br_xI_{1-x})3$ to above-bandgap illumination which resulted in the formation of lower and higher bandgap perovskite domains with different halide composition, evidenced by presence of low energy photoluminescence feature, sub-bandgap absorption and splitting of XRD peaks; characteristics of halide segregation [263]. Nickel et al. investigated the influence of oxygen on light induced degradation and found that light-induced degradation of $CH_3NH_3PbI_3$ occurs even in the absence of oxygen, with photon of energy greater than the bandgap required to initiate the dissociation of N–H bonds [264]. In the presence of both oxygen and light, the degradation process occurs rapidly driven by the formation of superoxide species from photoexcited charge carriers.

The relatively thin PeLEDs (~hundreds of nm) coupled with high bias application result in high electric field under operating condition. The efficiency of PeLEDs are defined by the ratio of electron–hole conversion to photon generation where the excess energy will be converted to phonons (a.k.a joule heating). Hence, it is apparent that the junction temperature of inefficient PeLED will be higher due to joule heating mechanism, triggering the need to investigate the impact of thermal energy on perovskite film stability. Phase and structural stability of perovskites are not defined only by the lead halide octahedral and Goldschmidt tolerance factors, but also their resistance to thermal degradation. Despite MAPbI3's structural stability in the black perovskite phase, its thermal instability arises from the A-site cation's volatility (MA). Although early report of $CH_3NH_3I_3$ mass loss arose from sublimation of HI and CH_3NH_2 at around 250 °C [265], investigations by Conings et al. using various characterization techniques revealed that $MAPbI_3$ can undergo degradation at temperature as low as 85 °C in inert conditions [257], due to evolution of HI and CH_3NH_2, with PbI_2 and Pb^0 detected is the degraded films. Defects too influence thermal degradation process in perovskites, where $MAPbI_3$ single crystal with a low defect density of 10^9–10^{11} cm^{-3} was found to decomposes beyond 200 °C; while polycrystalline films, which naturally have higher defect densities decompose at much lower temperatures [216]. In addition, temperature also lowers the activation energy for ion/defect migration to occur.

$$MAPbI_3\,(s) \rightarrow CH_3NH_2\,(g) + HI\,(g) + PbI_2\,(s)$$

$$MAPbI_3\,(s) \rightarrow NH_3\,(g) + CH_3I\,(g) + PbI_2\,(s)$$

It has been shown that the existence of defects accelerates perovskite degradation in the presence of moisture, oxygen, light and electric field. While ingress of moisture and oxygen in PeLEDs can be suppressed by employing sophisticated encapsulation technology borrowed from OLED, stability of perovskite against light and electric field need to be addressed to enhance PeLEDs stability. Aside from emitter stability, PeLEDs efficiency can be wounded over time due to charge injection imbalance to the emitter

that shifts the emitter zone near the interfaces at high current injection [256]. Moreover, under high carrier injection, auger recombination can kick in, resulting in lower PLQY of the emitter and subsequently reduced EQE [48]. Therefore, a breakthrough in PeLEDs stability is predicted to revolve around defect management strategies spanning from materials to device, that will be discussed in the next section.

4 Managing defects

4.1 Perovskite defects

Improving stability of the perovskite requires effective management of defects both in the bulk and at the surfaces. In view that shallow defects tend to dominate at the surfaces and grain boundaries, it is almost intuitive that larger grains which result in lower grain boundary densities be sought to suppress this issue. This is compounded further by the dramatic improvement in photovoltaic stability on increasing average perovskite grain sizes [266–268]. It is thus unsurprising that this strategy has taken the front seat in efforts toward achieving high quality perovskite absorber films, where large grain boundaries not only reduce sites for non-radiative recombination but also facilitate the effective extraction of photoexcited charge carriers to the charge selective interlayers [255, 258, 262, 269].

However, in the case of light emission, where effective radiative recombination for photon generation is desired, spatial confinement of charge carriers is preferred – either through geometric [87] or electronic means [83, 270] (Figure 12a). In essence, increased probability of radiative recombination occurs on spatially and/or intrinsically confining the charge carriers within a smaller volume of space or domain. In doing so, the localized carrier density is effectively shifted to the bimolecular recombination regime (Figure 12b) where radiative recombination predominantly takes place [270, 273]. In other words, through this route, higher rates of radiative recombination can be attained without the need to increase the current density flowing through the system. This provides the basis for the shift from pure three-dimensional (3D) systems in the early stages of PeLEDs [34, 89, 274] to nanoparticles [47, 275, 276] and multi-dimensional perovskites based on the energy funnelling phenomenon [44, 72, 83, 116, 277]. Although increase in spatial and/or electronic confinement is crucial to increase photon generation for light-emitting applications, the simultaneous increase in surface area to volume ratio presents another set of problems. For multi-dimensional perovskites, this translates to large grain boundary densities rising from the various bandgap domains and for nanoparticles, as succinctly described by Brown et al., consist of surfaces made up of “essentially planes of vacancies” [278]. The nanoparticle shape is defined by the use of bifunctionalized ligands – where one side binds to the perovskite and the other functions to maintain the nanoparticles’ colloidal stability in the dispersing solvent. Needless to say, the type of ligand used to template the formation of multi-dimensional [40, 44, 279] or nanoparticle perovskites [280–282] play a pivotal role in determining the properties of the resulting perovskite and the ensuing devices. The length and functionalization of the employed ligands [280, 283, 284] contribute towards phase stability [285] and efficacy in charge conduction. Thus, extensive work has been done towards addressing defects in these systems, particularly halide anion and organic cation vacancies while, still retaining their emissive properties for efficient devices.

Despite the equimolar ratio of AX and BX_2 in the prepared precursor solutions, the stoichiometry of the resultant perovskite often deviates from the expected. This results in the presence of Pb^0 and/or under coordination of lead, both of which are detrimental to device performance due to their luminescence quenching effect and influence over stability. Dangling bonds and trap states that persists at grain boundaries not only induce non-radiative recombination [87, 286], but also facilitate ion migration, threatening perovskite’s structural stability, particularly under device operation. Cho et al. showed that a 5% excess of MABr in the perovskite precursor solution yielded significant improvement in average photoluminescence decay lifetimes that gradually increased from 12.2 to 51.0 ns, assigned to the reduction in uncoordinated metallic Pb atoms present at the grain boundaries [87]. This concurs with studies by Yuan et al. where the excess organic cation was found to suppress the non-radiative recombination in a mixed-cation-emitting perovskite. They also showed that the deprotonation of excess organic cations by the ZnO substrate, probed through IR spectroscopy, is crucial for the formation of high-quality perovskite light emitters thus enabling decent operational lifetime (T_{50}) ~ 7 h to be achieved [287]. Veldhius et al. showed that by introducing an additive, dibenzo-21-crown-7, the poor solubility of CsBr in polar solvents can be effectively addressed, thus allowing the formation of low-defect density CsPbBr3 quantum dots which are stable even at low temperatures [288]. However, improvement to film stability is not just confined to adding of excess precursors in the perovskite solution. Where early reports have included additive to spatially confine charge carriers [87, 289], more recent works have showed the use of

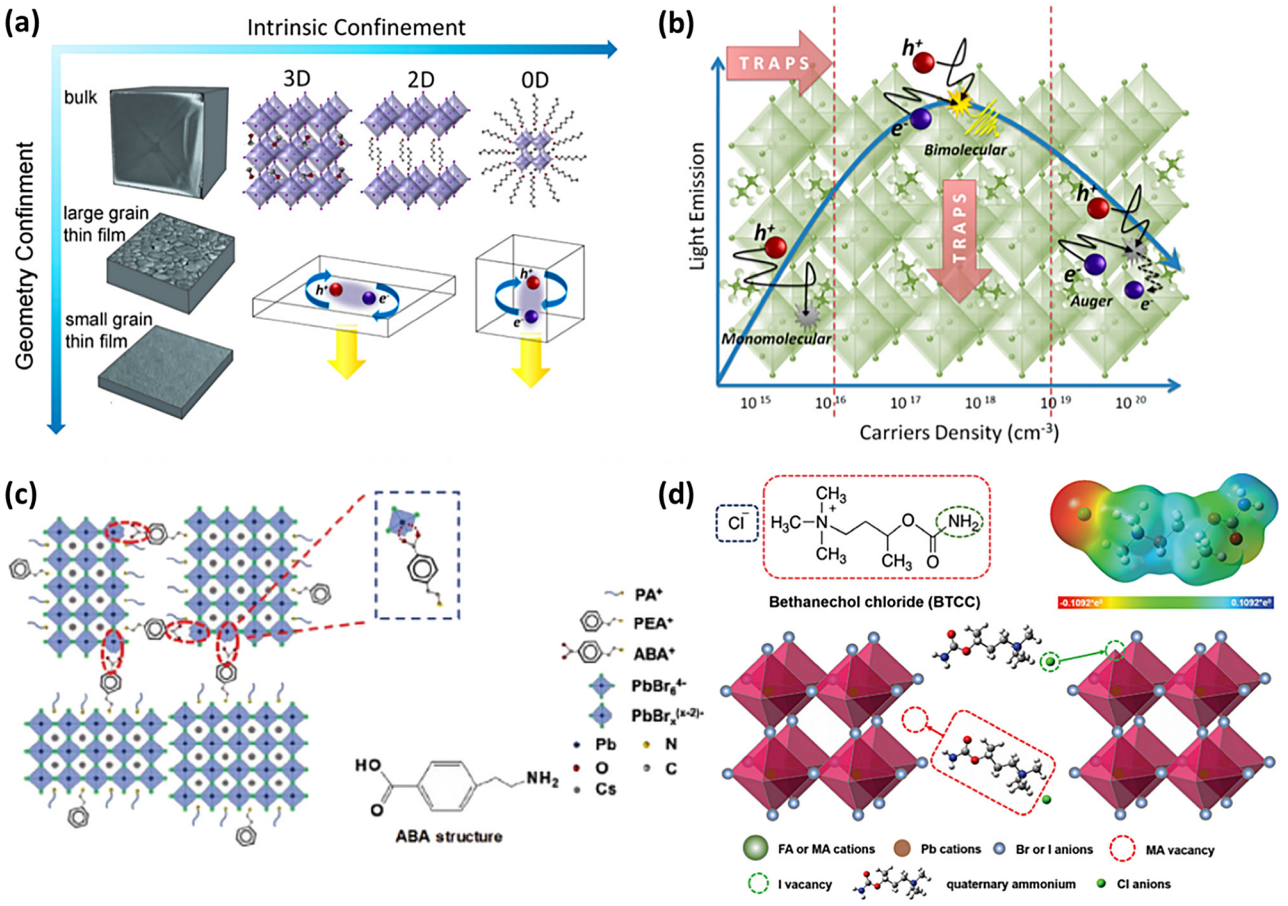

Figure 12: (a) Schematic on approaches to increase radiative recombination through exciton confinement. (b) Excited state deactivation processes at various carrier density regimes. Adapted with permission from [270]. (c) Illustration of pristine/ABA perovskite, and the interaction between neighbouring perovskite layers in pristine/ABA perovskite. Adapted with permission from [271]. (d) Depiction of zwitterion molecule consisting of both cationic and anionic moieties for passivation of both positively and negatively charged defects. Adapted with permission from [272]. Copyright (2020) The Royal Society of Chemistry.

bifunctionalized ligands to simultaneously reduce non-radiative recombination losses and improve coupling between the quasi-2D perovskite phases [123, 271] and modulate crystallization kinetics [68]. Ren and co-workers introduced a bifunctional ligand ~4-(2-aminoethyl)benzoic acid (ABA) cation into $PEA_xPA_{2-x}(CsPbBr_3)PbBr_4$ perovskite to reduce the weak van der Waals gap and promote coupling of quasi-2D perovskite layers (Fig. 12c). Not only is non-radiative recombination due to metallic Pb suppressed, the higher degree of molecular interactions between the various phases also imparts greater stability [271]. Wang et al., on the other hand, employed a dual ligand strategy of 2-phenylethanamine bromide (PEABr) and 3,3-diphenylpropylamine bromide (DPPABr) [290] to tune the quantum well distribution for photoluminescence enhancement, similar to the work by Yantara et al., where a narrower phase distribution, achieved through A-site and L cations engineering, enabled efficient and spectrally stable blue emission to be obtained [44].

Modifications to processing of nanoparticles have also evolved to include stronger binding ligands to passivate surface defects and impart greater stability through increased resilience to antisolvent purification steps. This includes the use of phosphonic acids [282, 291], sulfonic acids [281, 292] and zwitterionic [280, 293, 294] capping ligands as ligand substitutes. The presence of two hydroxyl and one phosphonyl group on the ligand head facilitates binding to an anionic surface with an anionic while retaining the ability for double hydrogen bonding, enabling the formation of inter-ligand hydrogen bonds [282, 295]. The strong binding affinity of the phosphonate grounds towards Pb^{2+} enables effective passivation of the undercoordinated lead defects and tolerance to antisolvent washing. In the case of sulfonic acid functionalization, the interaction involves the binding of the perovskite's ionic surface with that of the sulfonate group [278]. Yang et al. proposed a "Br-equivalent" ligand strategy using benzenesulfonic acid to firmly bind to the Pb^{2+} ions to form a steady binding state

and eliminate the exciton trapping probability due to bromide vacancies [281]. High photoluminescence quantum yields are achieved without need for amine-based ligands. Use of zwitterion molecules (Figure 12d) is similar to the use of bifunctionalized molecules in mixed-dimensional films, where coordination to positively and negatively charged defect sites is made possible with a single ligand, with neither the cationic nor anionic groups having any possibility of mutual neutralization [280].

Various modifications made to perovskite processing has not only enabled dramatic improvement to efficiency of radiative recombination process, but also enhanced film stability by effective management of defects. One such example is the design of energetic emitter landscape based on the energy funnelling concept. While the addition of templating ligand to three-dimensional perovskites was conceptualized to enable high radiative recombination efficiency and good charge transport properties to be reaped in bulk perovskite films, the introduction of incremental amounts of 2D cation may also template the formation of an energetic emitter landscape [295]. Numerous domains of varying bandgaps depending on the local perovskite composition results in the formation of an energetically engineered emitter which acts as a conduit for charge localization [279, 296] through effective exciton confinement [83]. On injection of charge carriers into the larger bandgap domains, the charge carriers are rapidly transferred to the energetically favoured lower bandgap regions in a process termed as energy funnelling [40, 116, 277]. This interdomain charge transfer process occurs within such short timescales that it supersedes non-radiative processes in the larger bandgap domains. As a result, the charge carriers are effectively concentrated in the smaller bandgap domains. Not only does this suppress non-radiative recombination losses but the localization of charge carriers within these emitting domains effectively shifts the recombination process to the bimolecular recombination regime. This promotes sufficiently high localized charge carrier density in these emitting domains for bimolecular recombination without the need for overall increase in charge injection density, which may give rise to Auger recombination. The release of energy, a result of third carrier excitation during this process, may induce heating which can degrade the emitter [48, 297]. Moreover, with trap filling process only required for the emitting bandgap domains, as compared to three-dimensional bulk films, high photoluminescence quantum yield and device efficiency can be achieved at lower excitation and charge carrier densities [277]. The effective modulation of radiative recombination processes occurring in the films through compositional engineering has provided the driving force for extensive work in the area of mixed-dimensional perovskites for light emission. Initial work in the area involved the simple mixing of monoammonium functionalized 2D ligand and 3D perovskites to template formation of Ruddlesden-Popper multi-dimensional perovskites for improved photon generation [33, 83, 277, 298]. More recently, attempts to push the efficiency further has been directed towards improving charge transfer processes [271], perovskite inherent stability [57, 74], charge confinement [85, 299] and managing perovskite surface defects [40, 91, 101, 300] (Table 2).

4.2 Managing electron–lattice interactions

A-site cation alloying has been garnering interest not only due to the possibility of tuning the perovskite emission properties, but also to increase the intrinsic stability of these emissive materials [319]. Ab-initio studies by Mahata et al. into the influence of chemical composition on polaron properties revealed increasing structural distortions on changing the A-site cation from FA to MA to Cs and on substituting the halide cation from I to Br. The influence of cation on polaron stability is primarily indirect, mediated by the distortion of the inorganic sub-lattice. Larger cations radiuses of MA and FA restrict the degree of inorganic shrinkage on hole injection, with the effect further compounded by the presence of hydrogen bonds [320]. The origin of greater local distortions on substituting I with Br arises from the higher degree of iconicity of the Pb–X bond, resulting in stronger localization of charges associated with higher stabilization energies. In view that the inorganic and organic A-site cations exhibit differing effect on the Pb inorganic lattice, and in turn the stability of polarons, Myung et al. propose increasing the coordination of organic cations to I to weaken the electron-phonon coupling effect and suppress polaron stability [321]. Zhou et al. found that alloying of the A-site cation enabled the delocalization of charge carriers at these lattice deformation sites, hence improving stability of the perovskite. The reduction in polaron binding energies in these alloyed systems arise from the asymmetry of the polarons, which prevents its stabilization [322]. Moreover, effective charge extraction to charge selective contacts in perovskite photovoltaics can be suppressed due to reduced charge carrier mobility [323].

4.3 Managing defects in devices

While optimization of perovskite film quality is needed for high PLQY; a metric for PeLED performance, the influence of perovskite interactions with the adjacent layers and on

Table 2: Summary of device performance and operational stability of perovskite LEDs in literature.

Ref	Device structure	Measurement condition		Operational lifetime (unless specified, it reports T_{50} in hour)	EL peak (nm)
		L_0 (cd m^{-2})	I (mA cm^{-2})		
[301]	ITO/AZO:Cs/$Cs_{10}(MA_{0.17}FA_{0.83})_{(100-x)}Pb(Br_xCl_{1-x})_3$/CuS-GaSnO/$WO_3$/Au	1000	1.42	16	475
[74]	ITO/NiOx/TFB/PVK/PBABr:FABr:$CsPbBr_3$/TPBi/LiF/Al	100		0.069	483
[85]	ITO/PEDOT: PSS/PEACl:$CsPbBr_3$:YCl_3/TPBi/LiF/Al	100		**1.67**	485
[39]	ITO/poly-TPD/BABr:$MAPbBr_3$/TPBi/LiF/Al		3	0.8	513
[302]	ITO/PEDOT: PSS/$CsPbBr_3$:CsTFA/TPBi/LiF/Al	100		250	518
[303]	ITO/NiO/$CsPbBr_3$/ZnO/Al		at 8V (RH - 20–55%)	>12 (T_{80})	519
[304]	ITO/LiF/$(Cs_{0.83}Rb_{0.17})_{0.95}K_{0.05}PbBr_3$/LiF/ZnS/ZnSe/Ag	120		**255**	519
[305]	ITO/PEDOT:PSS/$CsPb_2Br_5$/TPBi/LiF/Al		10	6	520
[306]	Au/p-MgNiO/$CsPbBr_3$ NCs/PMMA/n-MgZnO/n+-GaN		at 10 V (RH - 20–55%)	9 (T_{80})	522
[307]	ITO/SDBS-doped PEDOT: PSS/Tween 20: $CsPbBr_3$/TPBi/LiF/Al	100		6	522
[308]	ITO/PEDOT:PSS/$CsPbBr_3$/B3PYMPM/Cs_2CO_3/Al	100	66.67	>15 (L>L_0)	524
[309]	ITO/m-PEDOT: PSS/mPEG-doped $CsPbBr_3$/Bphen/LiF/Ag	100		24 (L>L_0)	~524
[310]	ITO/NiO/Benzylammonium bromide:$FAPbBr_3$/TPBi/LiF/Al	100		1.7	~525
[311]	ITO/PEDOT:PSS/$CsPbBr_3$:PEO/TPBi/LiF/Al	1000		80 (T_{80})	525
[4]	ITO/PEDOT:PSS/$CsPbBr_3$:MABr/PMMA/B3PYMPM/LiF/Al	100		46	525
[102]	ITO/ZnO/PVP/$Cs_{0.87}MA_{0.13}PbBr_3$:PVP/CBP/MoO_3/Al	65		1	526
[312]	ITO/TiO_2/$MAPbBr_3$/SPB-02T/MoO_3/Au	120		55	530
[40]	ITO/m-PEDOT:PSS/PEABr:$FAPbBr_3$/TOPO/TPBi/LiF/Al	300	0.5	1	532
[301]	ITO/AZO:Cs/$Cs_{10}(MA_{0.17}FA_{0.83})_{(100-x)}Pb(Br_xI_{1-x})_3$/CuS-GaSnO/$WO_3$/Au	1000	1.42	173	569
[104]	ITO/PEDOT:PSS/Poly-TPD/$CsPbX_3$ NCs/TPBi/Liq/Al		1.25	180	649
[301]	ITO/AZO:Cs/$Cs_{10}(MA_{0.17}FA_{0.83})_{(100-x)}Pb(Br_xI_{1-x})_3$/CuS-GaSnO/$WO_3$/Au	1000	1.42	491	650
[313]	ITO/PEDOT: PSS/Poly-TPD/PEO:BAI:CsI:PbI_2/BCP/LiF/Al		at 3.5V	4 (T_{80})	664,680
	ITO/PEDOT: PSS/Poly-TPD/$CsPbI_3$ QDs/TPBi/LiF/Al		at 6V	2	678
[314]	ITO/ZnO/PEIE/NMAI:CsCl:PbI_2/TFB/MoOx/Au		3	5	688
[315]	ITO/PEDOT:PSS/$BA_2MA_2Pb_4I_{13}$/PCBM/Al	6 (W sr^{-1})		>14	744
[39]	ITO/poly-TPD/BAI:$MAPbI_3$/TPBi/LiF/Al		3	5 (T_{70})	748
[83]	ITO/ZnO/PEIE/NMAI:$FAPbI_3$/TFB/MoOx/Au		10	1.67	763
[316]	ITO/ZnO/PEIE/$NMAFA_{0.93}Cs_{0.07}PbI_7$/TFB/MoOx/Au		10	30	783
[76]	ITO/MZO-PEIE/NMAI:$FAPbI_3$:Poly-HEMA/TFB-PFO/MoOx/Au		0.1	46	~795
[7]	ITO/ZnO-PEIE/5AVA:$FAPbI_3$/TFB/MoOx/Au		100	20	803
[317]	ITO/ZnO/PEIE/$FAPbI_3$/TFB/MoOx/Au		100	23.7	804
[318]	ITO/PVK/PEAI: CsI: SnI_2/TmPyPB/LiF/Al		10	2	~920

electrical bias has to be assessed. Introduction of additional layers such as charge selective materials can result in the formation of non-radiative recombination pathways (quenching sites) due to interfacial defects. Inappropriate selection of charge transport layers can result in imbalance of charge carrier into the perovskite, potentially leading to leakage which suppresses device efficiency [321]. Exacerbation of this phenomenon can also lead to build-up of charge carriers at the perovskite/transport layer interface and drive degradation process of functional layers [324]. Unlike the case of perovskite-based photovoltaics where the absorber layer tends to be hundreds of nm thick, in PeLEDs, the emitting layers are typically less than 100 nm. This means that the perovskite films experience high voltage drop or electric field during device operation, which provides strong impetus for ion migration to occur across the interfaces. The migration of halide and bromide, facilitated by vacancies, can initiate the perovskite degradation process [65] and simultaneously promote electrochemical reactions at the electrodes [325, 326]. Through TOF-SIMS, Lee and co-workers showed the migration of MA and Br ions in PeLEDs device after electrical biasing [327]. The forward-bias current drives the drift of MA+ ions toward the Al electrode under device operation leading to an increase in concentration of Br^- ions. Removal of the aluminium electrode post biasing also revealed changes to film morphology, where perovskite aggregates and pinholes are observed, which they correlate to dark spots on

the electrode during operation. Similarly, Prakasam et al. also observed dark spots in the EL image of biased PeLED [328]. By analysing the stripped aluminium electrode using SEM/EDX, they noted the presence of recessions consisting of Al and Pb, which they deduce to be indication of $MAPbBr_3$ decomposition due to absence of similar features in devices adopting Au electrodes. The formation of gaseous by-products increases the pressure inside the device, leading to local delamination of the cathode. Thermal instability of PeLEDs is not just confined to destruction of perovskite but can also lead to changes in distribution of m-phases governing the photo- and electroluminescence. The situation can be severe in some cases leading to spectral shifts towards longer wavelengths, and in the instance of mixed halide cases, the emergence of secondary emission profiles, although the lack of sufficient acceptor domains for monochromatic emission in these multi-dimensional systems cannot be ruled out [44, 116].

Surface modifications are extremely crucial in the effort to improve stability. Not only has introduction of additives in PEDOT:PSS been explored [40, 87], interfacial layers between the perovskite and hole-transporting material have also been inserted [33, 329], all in a bid to reduce surface defects and ensure the growth of high quality perovskite films. Doping or bilayer transport layers have been reported to improve efficiency of charge injection into the perovskite. Fakharuddin and co-workers fabricated 3D and 2D-3D PeLEDs employing undoped and Alq3 doped Bphen as ETL. It was found that in all cases, regardless of the type of emitter film used, doping of the ETL enabled more efficient and stable devices with suppression in efficiency roll-off features, compounding the need for effective modulation of charge injection into the emitter [324]. Shynkarenko et al. adopted a two-step hole injection architecture with a bilayer ETL consisting of B3PYMPM and TPBi, which can be safely assigned to efforts at balancing injection rates, despite the absence of any discussion for choice of device stack used [330]. Ion migration is hardly a new issue that needs to be addressed. Numerous reports have shown luminescence quenching due to ion migration under device operation [229, 258, 327]. Efforts to address this issue have included introduction of additives, such as Rb^+ or K^+ [304, 331], and adoption of alternative device architecture, where the $(Cs_{1-x}Rb_x)_{1-y}K_yPbBr_3$ perovskite is sandwiched between two LiF layers [304].

5 Conclusions and outlook

Perovskite LEDs have gained massive traction in the past few years due to desirable photophysical properties. While the efficiency race has reached a plateau from the materials and device engineering perspective, a breakthrough in device efficiency is predicted to come from efficient light outcoupling management. With suitable emitter and nanostructure, it is not impossible for efficiency as high as 100% to be achieved [174]. In addition, the translation of PeLED from lab to fab is hampered by its inferior stability in comparison to mature lighting technologies such as OLEDs. Therefore, a deeper understanding of both the materials and device aspects are needed to recognize and design strategies to heighten PeLED stability.

Despite that, systematic studies into these materials systems and their appropriate device configurations are only just gaining momentum. There still remains ample room for improvement and this is reflected in the rapid rate of developments in the field. The primary roadblocks to simultaneously attain desirable efficiencies and stabilities can be broadly categorized into two groups: (a) understanding and regulating intrinsic material properties for optimum performance, and (b) careful selection and seamless integration of photonic structures and interfacial layers for enhanced light outcoupling and prevention of device degradation. We anticipate the combinatory integration of these approaches to be vital for the development of future PeLEDs. The primary points of importance for these two categories are herein discussed.

5.1 Integration of photonic structure with device stack

Although largely beneficial for emission enhancement as discussed before, photonic nanostructures (both within and outside the emitter layer) carry the risk of distorting the charge carrier or exciton recombination dynamics within the perovskite system. High-temperature or ‘hard’ techniques such as e-beam evaporation, sputtering or lithography, which are used in the fabrication of these photonic nanostructures (metal oxides or other dielectrics), increases both the cost and complexity of device processing. In addition, post-treatment (e.g., annealing) conditions for the substrate and/or the perovskite layer may also be required. Perovskites are hardly suitable to be exposed to such harsh environments while fabricating the subsequent photonic structure layer, leading to instability (and quick degradation) of device. Another compelling issue is the use of appropriate solvent, which may otherwise result in perovskite decomposition within minutes on exposure to a non-orthogonal solvent. A possible solution might be to match deposition methods for subsequent steps. For example, sequential physical vapour deposition of the perovskite and

the photonic nanostructure within a reasonable temperature range might result in longer device lifetime. On the other hand, from the optical point of view, it is necessary to strike the right balance between photon recycling and extraction taking place in these nanostructures. While it is desirable to minimize non-radiative losses by repeated reabsorption for ~100% IQE, it might not be suitable for some cases. For example, in applications requiring polarized light output, too much PR is detrimental as repeated internal reflections have been shown to depolarize light and widen the angular emission profile [139]. For this, a good route to careful selection of substrate might be through computational modelling as discussed below.

5.2 Simulations for photonic enhancement

Aided by a wide range of open-source platforms, it is relatively straightforward to perform theoretical optimization of device architecture using optical simulations and finite-difference-time-domain (FDTD) methods [332]. Careful consideration of all light-extraction processes and modelling of all optical losses in the entire stack is also achievable. However, it would be a remarkable feat to be able to consider all optoelectrical events within a given material system as well as the loss pathways emanating from thermal/photo excitation and create a dynamic model for the same. This is a direction worth exploring for systematic study prior to experimental fabrication. It is also especially important for visualizing lasing systems and the effect of nanocavities on the emission properties.

5.3 Sophistication in imaging techniques

The rapid evolution of precision in spectroscopic techniques has continually brought about new waves of information regarding the previously unknown nanoscale, even in-situ. With imaging beyond the diffraction limit using super-resolution techniques [333, 334] as well as software interfaces to correlate independent data sets, many new revelations have since been uncovered. For even deeper insight into trapping mechanisms and other lesser-known phenomena, techniques such as electron paramagnetic resonance, neutron diffraction, infrared photoinduced absorption, time resolved photocurrent etc. should be thoroughly explored. This would provide the ability to correlate structural and optical properties to enable a top-down way of designing emitters suited to specific applications. In addition, further studies into local strain variations using advanced spectroscopic methods are needed to pinpoint the impact of growth and nucleation on perovskite light emission. This could possibly lead to the ability of strain engineering for novel purposes where required. As mentioned before, it has been hypothesized that large perturbations to crystal symmetry can possibly lead to heightened spin–orbit couplings and Rashba effect. This could have a non-negligible impact on the carrier dynamics. When induced in a localized manner e.g., in a perovskite/2D material heterojunction, it lends the ability to structurally fine-tune the emitter stack for maximum output.

However, the caveat to using sophisticated measurement techniques is twofold. On one hand, advanced synchrotron-based experiments with adequate spatial resolution can only be accessed at specialized facilities. Thus, using X-ray nanoprobes or powerful electron microscopy can be difficult to access for many researchers from the standpoint of geographical and economic disadvantage. In addition, the large data sets generated require automated processing with the aid of powerful software (and often machine learning) for high throughput. This often comes with steep learning curves. However, with the recent boom in the use of such techniques, open-source packages like pyXem have been made available. The other facet is the damage to sample on beam exposure. Even with fluences well below the reported damage thresholds for materials, it is often impossible to predict the spontaneous electrochemical reactions that can be set in motion by slight photo- or electrical excitation. To obtain reliable datasets, it is necessary to perform measurements on the same surface/volume earmarked at the beginning of the experimental process. This is hindered by the local instability of perovskites to continuous excitation. Having said that, with the advent of ultrasensitive detection systems coupled with smart encapsulation, it might be possible in the very near future to realize the full potential of high-resolution imaging.

5.4 Technology transfer from related domains

Partially born from the field of organic semiconductors, perovskites closely share material properties with it and several other related families of materials. These include conventional 2D materials such as graphene, transition-metal dichalcogenides (TMD), metal nanosheets etc., the counterparts to which are the Ruddlesden–Popper perovskites among others. Hence, direct extension of established ideas and techniques in domains such as OLEDs can potentially be beneficial for the improvement of PeLEDs. For instance, graphene monolayers have been heavily used

as transport layers and electrodes in planar and mesoscopic perovskite solar cells. They are also shown to improve photogating in $MAPbI_3$-based photodetectors by effective PL quenching. It could be worthwhile to explore graphene as a constituent layer of PeLEDs or as nanoconjugates with traditional perovskites. Another well-studied system is that of the interlayer excitons in monolayer TMD heterobilayers that afford long carrier lifetimes among other desirable geometric properties. When coupled with a 2D perovskite emitter, they can induce higher exciton emission without the need for post-treatments. Such heterostructures afford very strong interlayer coupling and broadband spectral response. This can be further tuned for use in valleytronics and other emerging applications. On a related note, perovskite/organic bulk heterojunctions have also been recently shown to lend better stability and efficiency to device stacks. Although much remains unknown in the defect physics of such device architectures, emission applications incorporating these materials seem extremely promising.

5.5 Spectral profile stability

Aside from maintaining EQE values, spectral profile stability is an important factor that needs to be addressed. The ability to create narrowband or broadband tunability using perovskite emitters has opened up a plethora of lighting applications. For example, white LEDs with efficiencies over 12% were very recently reported. These employ a multilayer semi-transparent electrode for efficient extraction of light through photon tunnelling and evanescent wave absorption [335]. However, even in applications demanding narrow emission, structural disorders in the perovskite framework stemming from high operational temperatures cause unwanted broadening of emission profile [336]. Ion migration accelerated by defects can also trigger emission spectral shift over time in dual or triple halide-based perovskite. Hence, it is essential to probe the origin and develop strategies to tackle this phenomenon. This can be done by combining sensitive temperature-dependent measurements of the optical and structural evolution of such systems to gain a thorough understanding of how to mitigate them. Also, it is desirable to attain complete compositional uniformity of the perovskite material for optimum colour purity in PeLEDs. The route to this is through careful optimization of synthesis methods so as to ensure maximum reduction of impurities in the system. Defect passivation strategies to curb ion migration can be employed to stop emission spectra shifts in dual or triple halide perovskite. Apart from this, certain applications require reliable orientational emission for high directionality, thus, reduction in the emitter dipole orientation isotropy through fabrication methods affording stringent control over structural ordering, should be investigated. With techniques such as Fourier-space microscopy to map the spatial and angular emission profiles, it is possible to understand and reduce losses, for instance, at the electrode interfaces through surface plasmon modes – a typical loss pathway in PeLEDs. Mostly, for such precision requirements, low-dimensional perovskites with quantum well structures have been explored. It could be worthwhile to probe the materials space in search of newer systems to maximize emission anisotropy.

5.6 Managing intrinsic and environment-related degradation

Even with steadily rising EQEs of PeLEDs, subpar operational stabilities prevent their imminent commercialization. While environmental stressors can be dealt with through appropriate encapsulation techniques, inherent electrochemical degradation needs to be addressed from a materials standpoint. Under applied bias, spontaneous interfacial reactions and decomposition of the perovskite material often occur, owing to electrically driven intragrain and interfacial ion migration [326]. In addition, photo- and thermal stability of the emitter material itself, largely impact its device performance. Although it is difficult to pinpoint the exact decomposition pathways, it is reasonable to expect initial improvement on suppression of the ion migration-related degradation. In addition, the quality of perovskite interfaces becomes an increasingly important parameter affecting PeLED efficiency and stability with reduction in emitter (perovskite) thickness (tens of nm). This underscores the importance of mitigating defects present at perovskite interfaces to minimise losses due to non-radiative recombination. Application of bias under device operation further worsens the situation due to the migration and accumulation of charge carriers at the interfaces arising from ion migration, accelerating PeLED degradation. Functional molecules offering defect passivation capability can also be employed to improve the efficiency and stability of PeLEDs [337] with ETL/HTL deposition methods also known to affect the quality of perovskite interface [338]. However, good interfacial contact is not the only factor determining device performance. Good band alignment between perovskite and ETL/HTL pairs is also needed to maximize carrier injection, balance and confinement in perovskite emitter layers for higher performing, stable devices [89, 339]. Introduction of HTL/ETL with ion blocking and hydrophobicity properties into

the PeLED device architecture can be very useful for suppression of metallic ion migration [337] and ingress of moisture to perovskite emitter [340], both of which are detrimental to PeLED stability. Hence, a multipronged approach consisting of defect management at the bulk and interfaces, as well as compositional and interfacial engineering, are all crucial towards enhancing performance and stability of PeLEDs.

5.7 Towards better blues

With plateauing of EQEs for green and red emission, blue LEDs have now taken centre stage in the PeLED community. While remarkable advancements over short time have been achieved, issues with colour stability [341], PLQY and device optimization still remain. Some of these challenges have been tackled with reduced-dimensional counterparts like quasi-2D RPPs but roadblocks like phase impurity and hence, inefficient internal energy transfer still persist in quasi-2D perovskites [342]. Chemical passivation using stabilizing ligands and/or suppression of the metallic behaviour of Pb seem to be a viable solution as reported by recent studies. Emission quenching at interfaces between the transport layers can be prevented by selecting wide bandgap ETL/HTL with negligible sub-bandgap states. It is also advisable to choose atomically thin monolayer buffer layers or thin insulating interlayers to avoid such quenching.

5.8 Pb-free and perovskite-inspired emitters

The toxicity of Pb has been under constant scrutiny for adverse environmental and human impact if applied to non-industry regulated use [343]. In addition, instability issues such as phase segregation of mobile halide ions [344], shift in emission and sub-optimal colour stabilities of Pb-containing perovskites have necessitated the pursuit of worthy replacements. Over the years, many suitable alternatives have been pitched, especially for photovoltaic applications. These approaches include substitutions of the B-site (Pb) with isovalent elements (Sn and Ge) [345, 346], adjacent kin elements of Pb (Sb, Mn, Bi) [347–349] and a combination of elements (Bi with Ag) [351] etc. With such a wide range of crystal structures afforded by such substitution, many material properties have come to light, proving their suitability for light-emitting applications as well. Simulations and experimental synthesis have led to Sn-containing perovskites being the most explored so far. For instance, 2D phenylethylammonium tin iodide (PEA_2SnI_4)-based LEDs were reported to emit at 633 nm [95]. However, plagued by spontaneous oxidation of Sn^{2+} to Sn^{4+} and non-radiative recombination due to defects, significant quenching was observed and the resultant EQE was immeasurably small. The $CsSnX_3$ family of perovskites was also studied for emission properties but yielded <1% PLQY. However, through identification and management of the oxidation pathways in Sn (as in the instance of using H_3PO_2 for reduction and prevention of SnI_4 complex formation [95]), this challenge can be tackled. Further notable studies on other material families include emission from $MA_3Bi_2Br_9$ with PLQY of 12% [351], $Cs_3Bi_2Br_9$ with PLQY of 19.4% [352] and more recently, $FA_3Bi_2Br_9$ quantum dots with PLQY of 52% [353].

Reduction of dimensionality from 3D to 2D, 1D and 0D structures (for instance, $ASnX_3$, A_2SnX_4, A_3SnX_5 and A_4SnX_6) is also a viable route to obtaining stable perovskite-inspired structures for light emission. For example, recent theoretical studies on 3D $CsSnI_3$, 2D $Cs_2SnCl_2I_2$ and 0D Cs_4SnBr_6, clearly indicated better emission properties with quantum confined structures, thus outlining the advantage of such an approach [354]. High throughput DFT computations or single-particle-diagnosis approach can help to unravel such previously unexplored material systems. A comprehensive report of many experimentally feasible Pb-free perovskite and perovskite-inspired materials can be found elsewhere to serve as a ready handbook [355].

5.9 Towards more novel applications of light emission

Perovskites, especially in lower-dimensional forms, have recently been explored for a wide range of emerging applications. Knowledge of the band-edge exciton fine structure of these perovskites along with control over composition and morphology make it possible to use them for quantum optics applications. For example, highly colour-pure $CsPbX_3$ (X = I, Br)-based single photon and entangled photon sources have been realized experimentally [356, 357]. Frequent challenges in these systems such as spectral intermittency have been probed elaborately through techniques such as fluorescence lifetime imaging (e.g., in $FAPbBr_3$) [358]. However, much remains unexplored regarding tuning NC synthesis such that dephasing rates and spectral diffusion are reduced. Blinking mechanisms are still to be investigated and the indistinguishability of emitted photons present opportunities for further enhancement. Chemically, surface passivation and post-treatment techniques are yet to be optimized. With the

advantage of high optical coherence lifetimes, extremely slow spin-flip relaxation and no band-mixing [359], highly emissive perovskite NCs stand poised to take over conventional semiconductor quantum dots for such applications.

Other emergent utilities include the fabrication of large-area [360], flexible PeLEDs for display applications. With considerable advantage over prominent commercial technologies such as colloidal chalcogenide quantum dots and organic materials (due to better colour tunability, narrow emission linewidth and relatively less toxic chemical components), perovskite emitters can find massive application in ultrahigh-definition commercial displays. The primary bottleneck is the lack of reproducibility and stability of the perovskite films. With some initial promising work in this domain [361], the primary focus is on tailoring deposition methods. Co-evaporation for more conformal and homogenous films with fine control over thickness may prove to be more suitable than solution processed techniques with regard to the resultant efficiency or reproducibility [362]. However, it may also be worthwhile to explore inkjet printing and screen printing for comparison of morphology and PL efficiency of resultant films, as indicated by relative success in previous reports.

To conclude, the detailed understanding of these underlying phenomena and mitigation of challenges aided by advancements in spectroscopy and fabrication is poised to enable rapid growth in this field. With an ongoing momentum to achieve imminent commercial deployment, this only seems to be the onset of what can be dubbed as the 'decade of perovskite optoelectronics'.

Author contributions: All the authors have accepted responsibility for the entire content of this submitted manuscript and approved submission.

Research funding: This research was supported by National Research Foundation, Prime Minister's Office, Singapore, under its Competitive Research Programme (CRP Award No. NRFCRP14-2014-03), and Intra-CREATE Collaborative Grant (NRF2018-ITC001-001), as well as Ministry of Education (MOE) under AcRF Tier 2 grants (2018-T2-1-075 and 2019-T2-2-106), and A*A*STARgs6: National Robotics Programme (W1925d0106).

Conflict of interest statement: The authors declare no conflicts of interest regarding this article.

References

[1] A. Kojima, K. Teshima, Y. Shirai, and T. Miyasaka, "Organometal halide perovskites as visible-light sensitizers for photovoltaic cells," *J. Am. Chem. Soc.*, vol. 131, no. 17, pp. 6050–6051, 2009.

[2] NREL Best Research Cell Efficiency Chart. Available at: https://www.nrel.gov/pv/cell-efficiency.html [accessed: Mar. 3, 2021].

[3] Z. K. Tan, R. S. Moghaddam, M. L. Lai, et al., "Bright light-emitting diodes based on organometal halide perovskite," *Nat. Nanotechnol.*, vol. 9, no. 9, pp. 687–692, 2014.

[4] K. Lin, J. Xing, L. N. Quan, et al., "Perovskite light-emitting diodes with external quantum efficiency exceeding 20 per cent," *Nature*, vol. 562, no. 7726, pp. 245–248, 2018.

[5] J. Song, J. Li, X. Li, L. Xu, Y. Dong, and H. Zeng, "Quantum dot light-emitting diodes based on inorganic perovskite cesium lead halides ($CsPbX_3$)," *Adv. Mater.*, vol. 27, no. 44, pp. 7162–7167, 2015.

[6] W. Cai, Z. Chen, Z. Li, et al., "Polymer-assisted in situ growth of all-inorganic perovskite nanocrystal film for efficient and stable pure-red light-emitting devices," *ACS Appl. Mater. Interfaces*, vol. 10, no. 49, pp. 42564–42572, 2018.

[7] Y. Cao, N. Wang, H. Tian, et al., "Perovskite light-emitting diodes based on spontaneously formed submicrometre-scale structures," *Nature*, vol. 562, pp. 249–253, 2018.

[8] M. Yuan, L. N. Quan, R. Comin, et al., "Perovskite energy funnels for efficient light-emitting diodes," *Nat. Nanotechnol.*, vol. 11, no. 10, pp. 872–877, 2016.

[9] K. Sim, T. Jun, J. Bang, et al., "Performance boosting strategy for perovskite light-emitting diodes," *Appl. Phys. Rev.*, vol. 6, no. 3, p. 031402, 2019.

[10] K. H. Lee, J.-H. Lee, H.-D. Kang, et al., "Over 40 cd/A efficient green quantum dot electroluminescent device comprising uniquely large-sized quantum dots," *ACS Nano*, vol. 8, no. 5, pp. 4893–4901, 2014.

[11] S. Y. Kim, W.-I. Jeong, C. Mayr, et al., "Organic light-emitting diodes with 30% external quantum efficiency based on a horizontally oriented emitter," *Adv. Funct. Mater.*, vol. 23, no. 31, pp. 3896–3900, 2013.

[12] Y. K. Chih, J.-C. Wang, R.-T. Yang, et al., "NiO_x electrode interlayer and $CH_3NH_2/CH_3NH_3PbBr_3$ interface treatment to markedly advance hybrid perovskite-based light-emitting diodes," *Adv. Mater.*, vol. 28, no. 39, pp. 8687–8694, 2016.

[13] H. Zhang, Z. Wang, L. Gao, B. Zhao, and W. Li, "Low efficiency roll-off and high color stability pure fluorescent white organic light-emitting diode based exciplex host," *RSC Adv.*, vol. 8, no. 2, pp. 954–959, 2018.

[14] J. Wang, N. Wang, Y. Jin, et al., "Interfacial control toward efficient and low-voltage perovskite light-emitting diodes," *Adv. Mater.*, vol. 27, no. 14, pp. 2311–2316, 2015.

[15] M. A. Baldo, S. Lamansky, P. E. Burrows, M. E. Thompson, and S. R. Forrest, "Very high-efficiency green organic light-emitting devices based on electrophosphorescence," *Appl. Phys. Lett.*, vol. 75, no. 1, pp. 4–6, 1999.

[16] J. W. Lee, Y. J. Choi, J.-M. Yang, et al., "In-situ formed type I nanocrystalline perovskite film for highly efficient light-emitting diode," *ACS Nano*, vol. 11, no. 3, pp. 3311–3319, 2017.

[17] R. Meerheim, S. Scholz, S. Olthof, et al., "Influence of charge balance and exciton distribution on efficiency and lifetime of phosphorescent organic light-emitting devices," *J. Appl. Phys.*, vol. 104, no. 1, p. 014510, 2008.

[18] B. Chen, X. Lin, L. Cheng, C. S. Lee, W. A. Gambling, and S. T. Lee, "Improvement of efficiency and colour purity of red-dopant organic light-emitting diodes by energy levels matching with the host materials," *J. Phys. D Appl. Phys.*, vol. 34, no. 1, pp. 30–35, 2001.

[19] D. F. O'Brien, M. A. Baldo, M. E. Thompson, and S. R. Forrest, "Improved energy transfer in electrophosphorescent devices," *Appl. Phys. Lett.*, vol. 74, no. 3, pp. 442–444, 1999.
[20] J. C. Yu, D. B. Kim, E. D. Jung, B. R. Lee, and M. H. Song, "High-performance perovskite light-emitting diodes via morphological control of perovskite films," *Nanoscale*, vol. 8, no. 13, pp. 7036–7042, 2016.
[21] Y. Seino, S. Inomata, H. Sasabe, Y. J. Pu, and J. Kido, "High-performance green OLEDs using thermally activated delayed fluorescence with a power efficiency of over 100 lm W-1," *Adv. Mater.*, vol. 28, no. 13, pp. 2638–2643, 2016.
[22] F. Yan, J. Xing, G. Xing, et al., "Highly efficient visible colloidal lead-halide perovskite nanocrystal light-emitting diodes," *Nano Lett.*, vol. 18, no. 5, pp. 3157–3164, 2018.
[23] D. H. Kim, N. S. Cho, H.-Y. Oh, et al., "Highly efficient red phosphorescent dopants in organic light-emitting devices," *Adv. Mater.*, vol. 23, no. 24, pp. 2721–2726, 2011.
[24] J. Pan, L. N. Quan, Y. Zhao, et al., "Highly efficient perovskite-quantum-dot light-emitting diodes by surface engineering," *Adv. Mater.*, vol. 28, no. 39, pp. 8718–8725, 2016.
[25] G. Li, F. W. R. Rivarola, N. J. L. K. Davis, et al., "Highly efficient perovskite nanocrystal light-emitting diodes enabled by a universal crosslinking method," *Adv. Mater.*, vol. 28, no. 18, pp. 3528–3534, 2016.
[26] S. Kumar, J. Jagielski, N. Kallikounis, et al., "Ultrapure green light-emitting diodes using two-dimensional formamidinium perovskites: achieving recommendation 2020 color coordinates," *Nano Lett.*, vol. 17, no. 9, pp. 5277–5284, 2017.
[27] Y. H. Kim, C. Wolf, Y.-T. Kim, et al., "Highly efficient light-emitting diodes of colloidal metal-halide perovskite nanocrystals beyond quantum size," *ACS Nano*, vol. 11, no. 7, pp. 6586–6593, 2017.
[28] W. Ki Bae, J. Kwak, J. W. Park, K. Char, C. Lee, and S. Lee, "Highly efficient green-light-emitting diodes based on CdSe@ZnS quantum dots with a chemical-composition gradient," *Adv. Mater.*, vol. 21, no. 17, pp. 1690–1694, 2009.
[29] H. P. Kim, J. Kim, B. S. Kim, et al., "High-efficiency, blue, green, and near-infrared light-emitting diodes based on triple cation perovskite," *Adv. Opt. Mater.*, vol. 5, no. 7, p. 1600920, 2017.
[30] J. Xing, F. Yan, Y. Zhao, et al., "High-efficiency light-emitting diodes of organometal halide perovskite amorphous nanoparticles," *ACS Nano*, vol. 10, no. 7, pp. 6623–6630, 2016.
[31] Y. Yang, Y. Zheng, W. Cao, et al., "High-efficiency light-emitting devices based on quantum dots with tailored nanostructures," *Nat. Photonics*, vol. 9, no. 4, pp. 259–265, 2015.
[32] Y. H. Kim, G.-H. Lee, Y.-T. Kim, et al., "High efficiency perovskite light-emitting diodes of ligand-engineered colloidal formamidinium lead bromide nanoparticles," *Nano Energy*, vol. 38, pp. 51–58, 2017.
[33] P. Vashishtha, M. Ng, S. B. Shivarudraiah, and J. E. Halpert, "High efficiency blue and green light-emitting diodes using ruddlesden-popper inorganic mixed halide perovskites with butylammonium interlayers," *Chem. Mater.*, vol. 31, no. 1, pp. 83–89, 2019.
[34] R. L. Z. Hoye, M. R. Chua, K. P. Musselman, et al., "Enhanced performance in fluorene-free organometal halide perovskite light-emitting diodes using tunable, low electron affinity oxide electron injectors," *Adv. Mater.*, vol. 27, no. 8, pp. 1414–1419, 2015.
[35] B. S. Kim and J. Y. Lee, "Engineering of mixed host for high external quantum efficiency above 25% in green thermally activated delayed fluorescence device," *Adv. Funct. Mater.*, vol. 24, no. 25, pp. 3970–3977, 2014.
[36] Q. Wang, J. Ren, X. F. Peng, X. X. Ji, and X. H. Yang, "Efficient sky-blue perovskite light-emitting devices based on ethylammonium bromide induced layered perovskites," *ACS Appl. Mater. Interfaces*, vol. 9, no. 35, pp. 29901–29906, 2017.
[37] C. Xie, X. Zhao, E. Woan, Y. Ong, and Z. Tan, "Transparent near-infrared perovskite light-emitting diodes," *Nat. Commun.*, vol. 11, 2020.
[38] H. Zhang, S. Chen, and X. W. Sun, "Efficient red/green/blue tandem quantum-dot light-emitting diodes with external quantum efficiency exceeding 21%," *ACS Nano*, vol. 12, no. 1, pp. 697–704, 2018.
[39] Z. Xiao, R. A. Kerner, L. Zhao, et al., "Efficient perovskite light-emitting diodes featuring nanometre-sized crystallites," *Nat. Photonics*, vol. 11, no. 2, pp. 108–115, 2017.
[40] X. Yang, X. Zhang, J. Deng, et al., "Efficient green light-emitting diodes based on quasi-two-dimensional composition and phase engineered perovskite with surface passivation," *Nat. Commun.*, vol. 9, pp. 2–9, 2018.
[41] S. Hou, M. K. Gangishetty, Q. Quan, and D. N. Congreve, "Efficient blue and white perovskite light-emitting diodes via manganese doping," *Joule*, vol. 2, no. 11, pp. 2421–2433, 2018.
[42] J. Si, Y. Liu, Z. He, et al., "Efficient and high-color-purity light-emitting diodes based on in situ grown films of CsPbX3 (X = Br, I) nanoplates with controlled thicknesses," *ACS Nano*, vol. 11, no. 11, pp. 11100–11107, 2017.
[43] G. Cheng, Y. Liu, T. Chen, et al., "Efficient all-inorganic perovskite light-emitting diodes with improved operation stability," *ACS Appl. Mater. Interfaces*, vol. 12, no. 15, pp. 18084–18090, 2020.
[44] N. Yantara, N. F. Jamaludin, B. Febriansyah, et al., "Designing the perovskite structural landscape for efficient blue emission," *ACS Energy Lett.*, vol. 5, no. 5, pp. 1593–1600, 2020.
[45] D. Y. Kondakov, "Characterization of triplet-triplet annihilation in organic light-emitting diodes based on anthracene derivatives," *J. Appl. Phys.*, vol. 102, no. 11, p. 114504, 2007.
[46] X. Zhang, C. Sun, Y. Zhang, et al., "Bright perovskite nanocrystal films for efficient light-emitting devices," *J. Phys. Chem. Lett.*, vol. 7, no. 22, pp. 4602–4610, 2016.
[47] Y. Ling, Z. Yuan, Y. Tian, et al., "Bright light-emitting diodes based on organometal halide perovskite nanoplatelets," *Adv. Mater.*, vol. 28, no. 2, pp. 305–311, 2016.
[48] C. Zou, Y. Liu, D. S. Ginger, and L. Y. Lin, "Suppressing efficiency roll-off at high current densities for ultra-bright green perovskite light-emitting diodes," *ACS Nano*, vol. 14, no. 5, pp. 6076–6086, 2020.
[49] M. Lu, J. Guo, S. Sun, et al., "Bright $CsPbI_3$ perovskite quantum dot light-emitting diodes with top-emitting structure and a low efficiency roll-off realized by applying zirconium acetylacetonate surface modification," *Nano Lett.*, vol. 20, no. 4, pp. 2829–2836, 2020.
[50] J. Kwak, W. K. Bae, D. Lee, et al., "Bright and efficient full-color colloidal quantum dot light-emitting diodes using an inverted device structure," *Nano Lett.*, vol. 12, no. 5, pp. 2362–2366, 2012.
[51] J. H. Lee, C. L. Huang, C. H. Hsiao, M. K. Leung, C. C. Yang, and C. C. Chao, "Blue phosphorescent organic light-emitting device with double emitting layer," *Appl. Phys. Lett.*, vol. 94, no. 22, pp. 23–26, 2009.

[52] C. Y. Kuei, W. L. Tsai, B. Tong, et al., "Bis-tridentate Ir(III) complexes with nearly unitary RGB phosphorescence and organic light-emitting diodes with external quantum efficiency exceeding 31%," *Adv. Mater.*, vol. 28, no. 14, pp. 2795–2800, 2016.
[53] Y. J. Cho, K. S. Yook, and J. Y. Lee, "A universal host material for high external quantum efficiency close to 25% and long lifetime in green fluorescent and phosphorescent OLEDs," *Adv. Mater.*, vol. 26, no. 24, pp. 4050–4055, 2014.
[54] Z. Yan, Y. Wang, J. Wang, Y. Wang, J. Ding, and L. Wang, "A novel furo[3,2-: C] pyridine-based iridium complex for high-performance organic light-emitting diodes with over 30% external quantum efficiency," *J. Mater. Chem. C*, vol. 5, no. 39, pp. 10122–10125, 2017.
[55] H. H. Chou and C. H. Cheng, "A highly efficient universal bipolar host for blue, green, and red phosphorescent OLEDs," *Adv. Mater.*, vol. 22, no. 22, pp. 2468–2471, 2010.
[56] C. H. Shih, P. Rajamalli, C. A. Wu, M. J. Chiu, L. K. Chu, and C. H. Cheng, "A high triplet energy, high thermal stability oxadiazole derivative as the electron transporter for highly efficient red, green and blue phosphorescent OLEDs," *J. Mater. Chem. C*, vol. 3, no. 7, pp. 1491–1496, 2015.
[57] F. Yuan, C. Ran, L. Zhang, et al., "A cocktail of multiple cations in inorganic halide perovskite toward efficient and highly stable blue light-emitting diodes," *ACS Energy Lett.*, vol. 5, no. 4, pp. 1062–1069, 2020.
[58] J. Li, L. Xu, T. Wang, et al., "50-Fold EQE improvement up to 6.27% of solution-processed all-inorganic perovskite CsPbBr3 QLEDs via surface ligand density control," *Adv. Mater.*, vol. 29, no. 5, p. 1603885, 2017.
[59] M. Ban, Y. Zou, J. P. H. Rivett, et al., "Solution-processed perovskite light emitting diodes with efficiency exceeding 15% through additive-controlled nanostructure tailoring," *Nat. Commun.*, vol. 9, pp. 1–10, 2018.
[60] M. K. Leung, C.-C. Chang, M.-H. Wu, et al., "6-N,N-diphenylaminobenzofuran-derived pyran containing fluorescent dyes: A new class of high-brightness red-light-emitting dopants for OLED," *Org. Lett.*, vol. 8, no. 12, pp. 2623–2626, 2006.
[61] S. G. R. Bade, J. Li, X. Shan, et al., "Fully printed halide perovskite light-emitting diodes with silver nanowire electrodes," *ACS Nano*, vol. 10, no. 2, pp. 1795–1801, 2016.
[62] Z. Chen, C. Zhang, X.-F. Jiang, et al., "High-performance color-tunable perovskite light emitting devices through structural modulation from bulk to layered film," *Adv. Mater.*, vol. 29, no. 8, pp. 1–8, 2017.
[63] A. Perumal, S. Shendre, M. Li, et al., "High brightness formamidinium lead bromide perovskite nanocrystal light emitting devices," *Sci. Rep.*, vol. 6, pp. 1–10, 2016.
[64] L. Meng, E.-P. Yao, Z. Hong, et al., "Pure formamidinium-based perovskite light-emitting diodes with high efficiency and low driving voltage," *Adv. Mater.*, vol. 29, no. 4, p. 1603826, 2017.
[65] L. Zhao, J. Gao, Y. L. Lin, et al., "Electrical stress influences the efficiency of CH3NH3PbI3 perovskite light emitting devices," *Adv. Mater.*, vol. 29, no. 24, pp. 1–6, 2017.
[66] H. Uoyama, K. Goushi, K. Shizu, H. Nomura, and C. Adachi, "Highly efficient organic light-emitting diodes from delayed fluorescence," *Nature*, vol. 492, no. 7428, pp. 234–238, 2012.
[67] H. Hu, T. Salim, B. Chen, and Y. M. Lam, "Molecularly engineered organic-inorganic hybrid perovskite with multiple quantum well structure for multicolored light-emitting diodes," *Sci. Rep.*, vol. 6, pp. 1–8, 2016.
[68] Z. Fang, W. Chen, Y. Shi, et al., "Dual passivation of perovskite defects for light-emitting diodes with external quantum efficiency exceeding 20%," *Adv. Funct. Mater.*, vol. 30, no. 12, pp. 1–9, 2020.
[69] X. Y. Chin, A. Perumal, A. Bruno, et al., "Self-assembled hierarchical nanostructured perovskites enable highly efficient LEDs: via an energy cascade," *Energy Environ. Sci.*, vol. 11, no. 7, pp. 1770–1778, 2018.
[70] Y. Shen, L. P. Cheng, Y. Q. Li, et al., "High-efficiency perovskite light-emitting diodes with synergetic outcoupling enhancement," *Adv. Mater.*, vol. 31, no. 24, pp. 1–8, 2019.
[71] W. Deng, X. Xu, X. Zhang, et al., "Organometal halide perovskite quantum dot light-emitting diodes," *Adv. Funct. Mater.*, vol. 26, no. 26, pp. 4797–4802, 2016.
[72] J. Xing, Y. Zhao, M. Askerka, et al., "Color-stable highly luminescent sky-blue perovskite light-emitting diodes," *Nat. Commun.*, vol. 9, no. 1, pp. 1–8, 2018.
[73] J. Chang, S. Zhang, N. Wang, et al., "Enhanced performance of red perovskite light-emitting diodes through the dimensional tailoring of perovskite multiple quantum wells," *J. Phys. Chem. Lett.*, vol. 9, no. 4, pp. 881–886, 2018.
[74] Y. Liu, J. Cui, K. Du, et al., "Efficient blue light-emitting diodes based on quantum-confined bromide perovskite nanostructures," *Nat. Photonics*, vol. 13, no. 11, pp. 760–764, 2019.
[75] P. Vashishtha and J. E. Halpert, "Field-driven ion migration and color instability in red-emitting mixed halide perovskite nanocrystal light-emitting diodes," *Chem. Mater.*, vol. 29, no. 14, pp. 5965–5973, 2017.
[76] B. Zhao, S. Bai, V. Kim, et al., "High-efficiency perovskite–polymer bulk heterostructure light-emitting diodes," *Nat. Photonics*, vol. 12, pp. 783–789, 2018.
[77] S. Zhang, C. Yi, N. Wang, et al., "Efficient red perovskite light-emitting diodes based on solution-processed multiple quantum wells," *Adv. Mater.*, vol. 29, no. 22, pp. 1–6, 2017.
[78] J. R. Manders, L. Qian, A. Titov, et al., "High efficiency and ultra-wide color gamut quantum dot LEDs for next generation displays," *J. Soc. Inf. Disp.*, vol. 23, no. 11, pp. 523–528, 2015.
[79] Z. Xiao, L. Zhao, N. L. Tran, et al., "Mixed-halide perovskites with stabilized bandgaps," *Nano Lett.*, vol. 17, no. 11, pp. 6863–6869, 2017.
[80] Y. Hamada, H. Kanno, T. Tsujioka, H. Takahashi, and T. Usuki, "Red organic light-emitting diodes using an emitting assist dopant," *Appl. Phys. Lett.*, vol. 75, no. 12, pp. 1682–1684, 1999.
[81] Y. L. Chang, Z. B. Wang, M. G. Helander, J. Qiu, D. P. Puzzo, and Z. H. Lu, "Enhancing the efficiency of simplified red phosphorescent organic light emitting diodes by exciton harvesting," *Org. Electron.*, vol. 13, no. 5, pp. 925–931, 2012.
[82] S. Jeon, S. Lee, K.-H. Han, et al., "High-quality white OLEDs with comparable efficiencies to LEDs," *Adv. Opt. Mater.*, vol. 6, no. 8, pp. 1–8, 2018.
[83] N. Wang, L. Cheng, R. Ge, et al., "Perovskite light-emitting diodes based on solution-processed self-organized multiple quantum wells," *Nat. Photonics*, vol. 10, no. 11, pp. 699–704, 2016.
[84] D. Ma, P. Todorović, S. Meshkat, et al., "Chloride insertion-immobilization enables bright, narrowband, and stable blue-emitting perovskite diodes," *J. Am. Chem. Soc.*, vol. 142, no. 11, pp. 5126–5134, 2020.

[85] Q. Wang, X. Wang, Z. Yang, et al., "Efficient sky-blue perovskite light-emitting diodes via photoluminescence enhancement," *Nat. Commun.*, vol. 10, 2019.
[86] T. Tsuzuki and S. Tokito, "Highly efficient, low-voltage phosphorescent organic light-emitting diodes using an iridium complex as the host material," *Adv. Mater.*, vol. 19, no. 2, pp. 276–280, 2007.
[87] H. Cho, S.-H. Jeong, M.-H. Park, et al., "Overcoming the electroluminescence efficiency limitations of perovskite light-emitting diodes," *Science*, vol. 350, no. 6265, pp. 1222–1225, 2015.
[88] Y. Ling, Y. Tian, X. Wang, et al., "Enhanced optical and electrical properties of polymer-assisted all-inorganic perovskites for light-emitting diodes," *Adv. Mater.*, vol. 28, no. 40, pp. 8983–8989, 2016.
[89] Y. H. Kim, H. Cho, J. H. Heo, et al., "Multicolored organic/inorganic hybrid perovskite light-emitting diodes," *Adv. Mater.*, vol. 27, no. 7, pp. 1248–1254, 2015.
[90] Z. B. Wang, M. G. Helander, J. Qiu, et al., "Unlocking the full potential of organic light-emitting diodes on flexible plastic," *Nat. Photonics*, vol. 5, no. 12, pp. 753–757, 2011.
[91] W. Xu, Q. Hu, S. Bai, et al., "Rational molecular passivation for high-performance perovskite light-emitting diodes," *Nat. Photonics*, vol. 13, no. 6, pp. 418–424, 2019.
[92] J. Li, X. Shan, S. G. R. Bade, et al., "Single-layer halide perovskite light-emitting diodes with sub-band gap turn-on voltage and high brightness," *J. Phys. Chem. Lett.*, vol. 7, no. 20, pp. 4059–4066, 2016.
[93] H. Kim, C.-R. Lee, J.-H. Im, et al., "Lead iodide perovskite sensitized all-solid-state submicron thin film mesoscopic solar cell with efficiency exceeding 9%," *Sci. Rep.*, vol. 2, no. 591, pp. 1–7, 2012.
[94] J. Kang and L. Wang, "High defect tolerance in lead halide perovskite $CsPbBr_3$," *J. Phys. Chem. Lett.*, vol. 8, no. 2, pp. 489–493, 2017.
[95] H. Liang, F. Yuan, A. Johnston, et al., "High color purity lead-free perovskite light-emitting diodes via Sn stabilization," *Adv. Sci.*, vol. 7, no. 8, p. 1903213, 2020.
[96] C. W. Tang, S. A. Vanslyke, and C. H. Chen, "Electroluminescence of doped organic thin films," *J. Appl. Phys.*, vol. 65, no. 9, pp. 3610–3616, 1989.
[97] M. A. Baldo, D. F. O'Brien, Y. You, A. Shoustikov, S. Sibley, M. E. Thompson, and S. R. Forrest, "Highly efficient phosphorescent emission from organic electroluminescent devices," *Nature*, vol. 395, pp. 151–154, 1998.
[98] D. R. Lee, B. S. Kim, C. W Lee, et al., "Above 30% external quantum efficiency in green delayed fluorescent organic light-emitting diodes," *ACS Appl. Mater. Interfaces*, vol. 7, no. 18, pp. 9625–9629, 2015.
[99] T. Watabe, R. Yamaoka, N. Ohsawa, and A. Tomida, "Extremely high-efficient OLED achieving external quantum efficiency over 40 % by carrier injection layer with super-low refractive index," *Dig. Tech. Pap.*, pp. 332–335, 2018.
[100] S. A. Veldhuis, P. P. Boix, N. Yantara, et al., "Perovskite materials for light-emitting diodes and lasers," *Adv. Mater.*, vol. 28, no. 32, pp. 6804–6834, 2016.
[101] Y. Jiang, C. Qin, M. Cui, et al., "Spectra stable blue perovskite light-emitting diodes," *Nat. Commun.*, vol. 10, pp. 1–9, 2019.
[102] L. Zhang, X. Yang, Q. Jiang, et al., "Ultra-bright and highly efficient inorganic based perovskite light-emitting diodes," *Nat. Commun.*, vol. 8, no. 1, p. 15640, 2017.
[103] Y. Kim, S. Kim, A. Kakekhani, et al., "Comprehensive defect suppression in perovskite nanocrystals for high-efficiency light-emitting diodes," *Nat. Photonics*, vol. 15, pp. 148–155, 2021.
[104] T. Chiba, Y. Hayashi, H. Ebe, et al., "Anion-exchange red perovskite quantum dots with ammonium iodine salts for highly efficient light-emitting devices," *Nat. Photonics*, vol. 12, pp. 681–687, 2018.
[105] Y. Cao, N. Wang, H. Tian, et al., "Perovskite light-emitting diodes based on spontaneously formed submicrometre-scale structures," *Nature*, vol. 562, pp. 249–253, 2018.
[106] X. Zhao and Z. Tan, "Large-area near-infrared perovskite light-emitting diodes," *Nat. Photonics*, vol. 14, pp. 215–218, 2020.
[107] D. Liu, C. Yang, M. Bates, and R. R. Lunt, "Room temperature processing of inorganic perovskite films to enable flexible solar cells," *Science*, vol. 6, pp. 272–279, 2018.
[108] J. Kim, C. H. Chung, and K. H. Hong, "Understanding of the formation of shallow level defects from the intrinsic defects of lead tri-halide perovskites," *Phys. Chem. Chem. Phys.*, vol. 18, no. 39, pp. 27143–27147, 2016.
[109] L. Qiao, W. H. Fang, R. Long, and O. V. Prezhdo, "Extending carrier lifetimes in lead halide perovskites with alkali metals by passivating and eliminating halide interstitial defects," *Angew. Chem. Int. Ed.*, vol. 59, no. 12, pp. 4684–4690, 2020.
[110] J. M. Azpiroz, E. Mosconi, J. Bisquert, and F. De Angelis, "Defect migration in methylammonium lead iodide and its role in perovskite solar cell operation," *Energy Environ. Sci.*, vol. 8, no. 7, pp. 2118–2127, 2015.
[111] C. Eames, J. M. Frost, P. R. F. Barnes, B. C. O'Regan, A. Walsh, and M. S. Islam, "Ionic transport in hybrid lead iodide perovskite solar cells," *Nat. Commun.*, vol. 6, pp. 2–9, 2015.
[112] D. Meggiolaro, E. Mosconi, and F. De Angelis, "Formation of surface defects dominates ion migration in lead-halide perovskites," *ACS Energy Lett.*, vol. 4, no. 3, pp. 779–785, 2019.
[113] U. G. Jong, C.-J. Yu, G.-C. Ri, et al., "Influence of water intercalation and hydration on chemical decomposition and ion transport in methylammonium lead halide perovskites," *J. Mater. Chem. A*, vol. 6, no. 3, pp. 1067–1074, 2018.
[114] Y. Zhou, Y. Yin, X. Zuo, et al., "Enhancing chemical stability and suppressing ion migration in $CH_3NH_3PbI_3$ perovskite solar cells via direct backbone attachment of polyesters on grain boundaries," *Chem. Mater.*, vol. 32, no. 12, pp. 5104–5117, 2020.
[115] G. Xing, B. Wu, X. Wu, et al., "Transcending the slow bimolecular recombination in lead-halide perovskites for electroluminescence," *Nat. Commun.*, vol. 8, 2017.
[116] N. Yantara, A. Bruno, A. Iqbal, et al., "Designing efficient energy funneling kinetics in Ruddlesden–Popper perovskites for high-performance light-emitting diodes," *Adv. Mater.*, vol. 30, no. 33, p. 1800818, 2018.
[117] L. N. Quan, Y. Zhao, F. P. García de Arquer, et al., "Tailoring the energy landscape in quasi-2D halide perovskites enables efficient green-light emission," *Nano Lett.*, vol. 17, no. 6, pp. 3701–3709, 2017.
[118] J. Shamsi, A. S. Urban, M. Imran, L. De Trizio, and L. Manna, "Metal halide perovskite nanocrystals: synthesis, post-

synthesis modifications, and their optical properties," *Chem. Rev.*, vol. 119, no. 5, pp. 3296–3348, 2019.
[119] G. S. Kumar, R. R. Sumukam, and B. Murali, "Quasi-2D perovskite emitters: A boon for efficient blue light-emitting diodes," *J. Mater. Chem. C*, vol. 8, no. 41, pp. 14334–14347, 2020.
[120] M. Kim, T. K. Lee, I. W. Choi, et al., "Effects of cation size and concentration of cationic chlorides on the properties of formamidinium lead iodide based perovskite solar cells," *Sustain. Energy Fuels*, vol. 4, no. 7, pp. 3753–3763, 2020.
[121] R. A. Kerner, L. Zhao, Z. Xiao, and B. P. Rand, "Ultrasmooth metal halide perovskite thin films: via sol-gel processing," *J. Mater. Chem. A*, vol. 4, no. 21, pp. 8308–8315, 2016.
[122] L. Mao, W. Ke, L. Pedesseau, et al., "Hybrid Dion-Jacobson 2D lead iodide perovskites," *J. Am. Chem. Soc.*, vol. 140, no. 10, pp. 3775–3783, 2018.
[123] Y. Shang, Y. Liao, Q. Wei, et al., "Highly stable hybrid perovskite light-emitting diodes based on Dion-Jacobson structure," *Sci. Adv.*, vol. 5, no. 8, p. eaaw8072, 2019.
[124] S. Yuan, Z. K. Wang, L. X. Xiao, et al., "Optimization of low-dimensional components of quasi-2D perovskite films for deep-blue light-emitting diodes," *Adv. Mater.*, vol. 31, no. 44, pp. 1–9, 2019.
[125] C. H. Chen, Z. Li, Q. Xue, et al., "Engineering of perovskite light-emitting diodes based on quasi-2D perovskites formed by diamine cations," *Org. Electron.*, vol. 75, p. 105400, 2019.
[126] C. M. M. Soe, C. C. Stoumpos, M. Kepenekian, et al., "New type of 2D perovskites with alternating cations in the interlayer space, $(C(NH_2)_3)(CH_3NH_3)_nPb_nI_{3n+1}$: structure, properties, and photovoltaic performance," *J. Am. Chem. Soc.*, vol. 139, no. 45, pp. 16297–16309, 2017.
[127] Y. H. Kim, J. S. Kim, and T. W. Lee, "Strategies to improve luminescence efficiency of metal-halide perovskites and light-emitting diodes," *Adv. Mater.*, vol. 31, no. 47, pp. 1–28, 2019.
[128] Y. Zou, Z. Yuan, S. Bai, F. Gao, and B. Sun, "Recent progress toward perovskite light-emitting diodes with enhanced spectral and operational stability," *Mater. Today Nano*, vol. 5, p. 100028, 2019.
[129] T. Xuan and R. J. Xie, "Recent processes on light-emitting lead-free metal halide perovskites," *Chem. Eng. J.*, vol. 393, p. 124757, 2020.
[130] X. K. Liu, W. Xu, S. Bai, et al., "Metal halide perovskites for light-emitting diodes," *Nat. Mater.*, vol. 20, pp. 10–21, 2021.
[131] R. L. Z. Hoye, A. Fakharuddin, D. N. Congreve, J. Wang, and L. Schmidt-Mende, "Light emission from perovskite materials," *APL Mater.*, vol. 8, no. 7, pp. 10–13, 2020.
[132] Y. Zhang, C.-K. Lim, Z. Dai, et al., "Photonics and optoelectronics using nano-structured hybrid perovskite media and their optical cavities," *Phys. Rep.*, vol. 795, pp. 1–51, 2019.
[133] S. A. Kulkarni, N. Yantara, K. Seng, N. Mathews, and S. G. Mhaisalkar, "Perovskite nanostructures: leveraging quantum effects to challenge optoelectronic limits," *Mater. Today*, vol. 33, pp. 122–140, 2020.
[134] Q. Zhang, D. Zhang, Y. Fu, et al., "Light out-coupling management in perovskite LEDs — What can we learn from the past?," *Adv. Funct. Mater.*, vol. 30, no. 38, pp. 1–22, 2020.
[135] X. Zheng, Y. Hou, H. T. Sun, O. F. Mohammed, E. H. Sargent, and O. M. Bakr, "Reducing defects in halide perovskite nanocrystals for light-emitting applications," *J. Phys. Chem. Lett.*, vol. 10, no. 10, pp. 2629–2640, 2019.
[136] S. Jung, J. H. Kim, J. W. Choi, et al., "Enhancement of photoluminescence quantum yield and stability in CsPbBr3 perovskite quantum dots by trivalent doping," *Nanomaterials*, vol. 10, no. 4, p. 710, 2020.
[137] G. D. Cody, "Urbach edge of crystalline and amorphous silicon: A personal review," *J. Non. Cryst. Solids*, vol. 141, pp. 3–15, 1992.
[138] C. W. Greeff and H. R. Glyde, "Anomalous Urbach tail in GaAs," *Phys. Rev. B*, vol. 51, no. 3, pp. 1778–1783, 1995.
[139] S. D. Stranks, R. L. Z. Hoye, D. Di, R. H. Friend, and F. Deschler, "The physics of light emission in halide perovskite devices," *Adv. Mater.*, vol. 31, no. 47, p. 1803336, 2019.
[140] S. Adjokatse, H. Fang, and M. A. Loi, "Broadly tunable metal halide perovskites for solid-state light-emission applications," *Biochem. Pharmacol.*, vol. 20, no. 8, pp. 413–424, 2017.
[141] M. B. Johnston and L. M. Herz, "Hybrid perovskites for photovoltaics: charge-carrier recombination, diffusion, and radiative efficiencies," *Acc. Chem. Res.*, vol. 49, no. 1, pp. 146–154, 2016.
[142] C. Wehrenfennig, G. E. Eperon, M. B. Johnston, H. J. Snaith, and L. M. Herz, "High charge carrier mobilities and lifetimes in organolead trihalide perovskites," *Adv. Mater.*, vol. 26, no. 10, pp. 1584–1589, 2014.
[143] F. Zheng, L. Z. Tan, S. Liu, and A. M. Rappe, "Rashba spin-orbit coupling enhanced carrier lifetime in $CH_3NH_3PbI_3$," *Nano Lett.*, vol. 15, no. 12, pp. 7794–7800, 2015.
[144] E. M. Hutter, M. C. Gélvez-Rueda, A. Osherov, et al., "Direct-indirect character of the bandgap in methylammonium lead iodide perovskite," *Nat. Mater.*, vol. 16, no. 1, pp. 115–120, 2017.
[145] P. Azarhoosh, "Relativistic origin of slow electron-hole recombination in hybrid halide perovskite solar cells," *APL Mater.*, vol. 4, no. 9, p. 091501, 2016.
[146] T. C. Sum, M. Righetto, and S. S. Lim, "Quo vadis, perovskite emitters?," *J. Chem. Phys.*, vol. 152, no. 13, p. 091501, 2020.
[147] M. A. Becker, R. Vaxenburg, G. Nedelcu, et al., "Bright triplet excitons in caesium lead halide perovskites," *Nature*, vol. 553, pp. 189–193, 2018.
[148] C. Qin, T. Matsushima, W. J. Potscavage, et al., "Triplet management for efficient perovskite light-emitting diodes," *Nat. Photonics*, vol. 14, pp. 70–75, 2020.
[149] Y. Jiang, M. Cui, S. Li, et al., "Reducing the impact of Auger recombination in quasi-2D perovskite light-emitting diodes," *Nat. Commun.*, vol. 12, pp. 1–10, 2021.
[150] X. Gao, X. Shen, D. Xue, et al., "Dual-color emitting Mn^{2+} ion doped $(PEA)_2PbBr_4$ perovskite towards white light-emitting diodes," *Mater. Chem. Front.*, vol. 5, no. 2, pp. 937–943, 2021.
[151] Y. Shang, G. Li, W. Liu, and Z. Ning, "Quasi-2D inorganic $CsPbBr_3$ perovskite for efficient and stable light-emitting diodes," *Adv. Funct. Mater.*, vol. 28, no. 22, pp. 2–9, 2018.
[152] Z. Yuan, C. Zhou, Y. Tian, et al., "One-dimensional organic lead halide perovskites with efficient bluish white-light emission," *Nat. Commun.*, vol. 8, 2017.
[153] F. Zhang, Z. Zhao, B. Chen, et al., "Strongly emissive lead-free 0D $Cs_3Cu_2I_5$ perovskites synthesized by a room temperature solvent evaporation crystallization for down-conversion light-emitting devices and fluorescent inks," *Adv. Opt. Mater.*, vol. 8, no. 8, pp. 1–8, 2020.
[154] C. Deng, G. Zhou, D. Chen, J. Zhao, Y. Wang, and Q. Liu, "Broadband photoluminescence in 2D organic–inorganic

hybrid perovskites: $(C_7H_{18}N_2)PbBr_4$ and $(C_9H_{22}N_2)PbBr_4$," *J. Phys. Chem. Lett.*, vol. 11, no. 8, pp. 2934–2940, 2020.
[155] D. Cortecchia, J. Yin, A. Petrozza, and C. Soci, "White light emission in low-dimensional perovskites," *J. Mater. Chem. C*, vol. 7, no. 17, pp. 4956–4969, 2019.
[156] M. You, H. Wang, F. Cao, et al., "Improving efficiency and stability in quasi-2D perovskite light- emitting diodes by a multifunctional LiF interlayer," *ACS Appl. Mater. Interfaces*, vol. 12, no. 38, pp. 43018–43023, 2020.
[157] Y. Yang, F. Gao, S. Gao, and S.-H. Wei, "Origin of the stability of two-dimensional perovskites: A first-principles study," *J. Mater. Chem. A*, vol. 6, no. 30, pp. 14949–14955, 2018.
[158] S. Soumitra, N. K. Tailor, M. Abdi-jalebi, V. Gupta, and H. Hu, "Recent progress in morphology optimization in perovskite solar cell," *J. Mater. Chem. A*, vol. 8, no. 41, pp. 21356–21386, 2020.
[159] B. Roose, K. Dey, Y. H. Chiang, R. H. Friend, and S. D. Stranks, "Critical assessment of the use of excess lead iodide in lead halide perovskite solar cells," *J. Phys. Chem. Lett.*, vol. 11, no. 16, pp. 6505–6512, 2020.
[160] G. H. Ahmed, J. Yin, O. M. Bakr, and O. F. Mohammed, "Near-unity photoluminescence quantum yield in inorganic perovskite nanocrystals by metal-ion doping," *J. Chem. Phys.*, vol. 152, no. 2, p. 020902, 2020.
[161] Y. Sun, L. Zhang, N. Wang, et al., "The formation of perovskite multiple quantum well structures for high performance light-emitting diodes," *npj Flex. Electron.*, vol. 2, no. 1, pp. 1–5, 2018.
[162] T. Morgenstern, C. Lampe, T. Naujoks, et al., "Elucidating the performance limits of perovskite nanocrystal light emitting diodes," *J. Lumin.*, vol. 220, p. 116939, 2020.
[163] M. Lehnhardt, T. Riedl, T. Weimann, and W. Kowalsky, "Impact of triplet absorption and triplet-singlet annihilation on the dynamics of optically pumped organic solid-state lasers," *Phys. Rev. B Condens. Matter.*, vol. 81, no. 16, pp. 1–5, 2010.
[164] M. A. Baldo, R. J. Holmes, and S. R. Forrest, "Prospects for electrically pumped organic lasers," *Phys. Rev. B Condens. Matter*, vol. 66, no. 3, pp. 353211–353216, 2002.
[165] C. Qin, A. S. D. Sandanayaka, C. Zhao, et al., "Stable room-temperature continuous-wave lasing in quasi-2D perovskite films," *Nature*, vol. 585, pp. 53–57, 2020.
[166] A. S. D. Sandanayaka, T. Matsushima, F. Bencheikh, et al., "Indication of current-injection lasing from an organic semiconductor," *Appl. Phys. Express*, vol. 12, no. 6, 2019.
[167] R. K. Ahrenkiel, B. M. Keyes, G. B. Lush, M. R. Melloch, M. S. Lundstrom, and H. F. MacMillan, "Minority-carrier lifetime and photon recycling in n-GaAs," *J. Vac. Sci. Technol. A*, vol. 10, no. 4, pp. 990–995, 1992.
[168] L. M. Pazos-Outón, M. Szumilo, R. Lamboll, et al., "Photon recycling in lead iodide perovskite solar cells," *Science*, vol. 351, no. 6280, pp. 1430–1433, 2016.
[169] S. De Wolf, J. Holovsky, S.-J. Moon, et al., "Organometallic halide perovskites: Sharp optical absorption edge and its relation to photovoltaic performance," *J. Phys. Chem. Lett.*, vol. 5, no. 6, pp. 1035–1039, 2014.
[170] T. Chen, W.-L. Chen, B. J. Foley, et al., "Origin of long lifetime of band-edge charge carriers in organic–inorganic lead iodide perovskites," *Proc. Natl. Acad. Sci. U.S.A.*, vol. 114, no. 29, pp. 7519–7524, 2017.
[171] T. S. Sherkar, C. Momblona, L. Gil-Escrig, et al., "Recombination in perovskite solar cells: significance of grain boundaries, interface traps, and defect ions," *ACS Energy Lett.*, vol. 2, no. 5, pp. 1214–1222, 2017.
[172] A. R. Bowman, M. Anaya, N. C. Greenham, and S. D. Stranks, "Quantifying photon recycling in solar cells and light-emitting diodes: absorption and emission are always key," *Phys. Rev. Lett.*, vol. 125, no. 6, pp. 1–6, 2020.
[173] J. M. Richter, M. Abdi-Jalebi, A. Sadhanala, et al., "Enhancing photoluminescence yields in lead halide perovskites by photon recycling and light out-coupling," *Nat. Commun.*, vol. 7, 2016.
[174] C. Cho, B. Zhao, G. D. Tainter, et al., "The role of photon recycling in perovskite light-emitting diodes," *Nat. Commun.*, vol. 11, pp. 1–8, 2020.
[175] P. Fassl, V. Lami, F. J. Berger, et al., "Revealing the internal luminescence quantum efficiency of perovskite films via accurate quantification of photon recycling," *Matter*, pp. 1–83, 2021.
[176] F. Staub, T. Kirchartz, K. Bittkau, and U. Rau, "Manipulating the net radiative recombination rate in lead halide perovskite films by modification of light outcoupling," *J. Phys. Chem. Lett.*, vol. 8, no. 20, pp. 5084–5090, 2017.
[177] S. Lin, T.-M. Shih, W. Yan, et al., "Maximum limits on external quantum efficiencies in bare LEDs," *IEEE Trans. Electron. Dev.*, vol. 64, no. 4, pp. 1597–1601, 2017.
[178] T. Yamada, Y. Yamada, and Y. Kanemitsu, "Photon recycling in perovskite CH3NH3PbX3 (X = I, Br, Cl) bulk single crystals and polycrystalline films," *J. Lumin.*, vol. 220, p. 116987, 2020.
[179] E. Oksenberg, A. Merdasa, L. Houben, et al., "Large lattice distortions and size-dependent bandgap modulation in epitaxial halide perovskite nanowires," *Nat. Commun.*, vol. 11, pp. 1–11, 2020.
[180] I. Schnitzer and E. Yablonovitch, "30 % external quantum efficiency from surface textured, thin-film light-emitting diodes," *Appl. Phys. Lett.*, vol. 63, no. 16, p. 2174, 1993.
[181] S. S. Meng, Y. Q. Li, and J. X. Tang, "Theoretical perspective to light outcoupling and management in perovskite light-emitting diodes," *Org. Electron.*, vol. 61, pp. 351–358, 2018.
[182] S. W. Baek, P. Molet, M. J. Choi, et al., "Nanostructured back reflectors for efficient colloidal quantum-dot infrared optoelectronics," *Adv. Mater.*, vol. 31, no. 33, pp. 1–7, 2019.
[183] A. Peer, R. Biswas, J.-M. Park, R. Shinar, and J. Shinar, "Light management in perovskite solar cells and organic LEDs with microlens arrays," *Opt. Express*, vol. 25, no. 9, p. 10704, 2017.
[184] I. L. Braly, D. W. deQuilettes, L. M. Pazos-Outon, et al., "Hybrid perovskite films approaching the radiative limit with over 90% photoluminescence quantum efficiency," *Nat. Photonics*, vol. 12, no. 6, pp. 355–361, 2018.
[185] I. Dursun, Y. Zheng, T. Guo, et al., "Efficient photon recycling and radiation trapping in cesium lead halide perovskite waveguides," *ACS Energy Lett.*, vol. 3, no. 7, pp. 1492–1498, 2018.
[186] X. Shi, Y. Liu, Z. Yuan, et al., "Optical energy losses in organic–inorganic hybrid perovskite light-emitting diodes," *Adv. Opt. Mater.*, vol. 6, no. 17, pp. 1–7, 2018.
[187] D. Zhu, "Prospects of III-nitride optoelectronics grown on Si," *Rep. Prog. Phys.*, vol. 76, no. 10, p. 106501, 2013.
[188] M. S. Alias, J. A. Holguin-lerma, R. C. Subedi, and B. S. Ooi, "Review of nanophotonics approaches using nanostructures and nanofabrication for III-nitrides ultraviolet-photonic devices," *J. Nanophotonics*, vol. 12, no. 4, p. 043508, 2018.

[189] D. Zhang, L. Gu, Q. Zhang, et al., "Increasing photoluminescence quantum yield by nanophotonic design of quantum-confined halide perovskite nanowire arrays," *Nano Lett.*, vol. 19, no. 5, pp. 2850–2857, 2019.
[190] S. Makarov, A. Furasova, E. Tiguntseva, et al., "Halide-perovskite resonant nanophotonics," *Adv. Opt. Mater.*, vol. 7, no. 1, pp. 1–19, 2019.
[191] L. Gu, K. Wen, Q. Peng, W. Huang, and J. Wang, "Surface-plasmon-enhanced perovskite light-emitting diodes," *Small*, vol. 16, no. 30, pp. 1–12, 2020.
[192] R. Shwetharani, V. Nayak, M. S. Jyothi, and R. G. Balakrishna, "Review on recent advances of core-shell structured lead halide perovskites quantum dots," *J. Alloys Compd.*, vol. 834, p. 155246, 2020.
[193] Q. Luo, C. Zhang, X. Deng, et al., "Plasmonic effects of metallic nanoparticles on enhancing performance of perovskite solar cells," *ACS Appl. Mater. Interfaces*, vol. 9, no. 40, pp. 34821–34832, 2017.
[194] X. Zhang, B. Xu, W. Wang, S. Liu, Y. Zheng, and S. Chen, "Plasmonic perovskite light-emitting diodes based on the Ag – $CsPbBr_3$ system," *ACS Appl. Mater. Interfaces*, vol. 9, no. 5, pp. 4926–4931, 2017.
[195] T. P. Nguyen, A. Ozturk, J. Park, et al., "Facile synthesis of CsPbBr 3/PbSe composite clusters," *Sci. Technol. Adv. Mater.*, vol. 19, no. 1, pp. 1–8, 2018.
[196] S. Wang, C. Bi, J. Yuan, L. Zhang, and J. Tian, "Original core – shell structure of cubic quantum dots with a high blue," *ACS Energy Lett.*, vol. 3, no. 1, pp. 245–251, 2018.
[197] W. Chen, J. Hao, W. Hu, Z. Zang, X. Tang, and L. Fang, "Enhanced stability and tunable photoluminescence in perovskite $CsPbX_3$/ZnS quantum dot heterostructure," *Small*, vol. 13, no. 21, p. 1604085, 2017.
[198] A. Pan, X. Ma, S. Huang, et al., "$CsPbBr_3$ perovskite nanocrystal grown on MXene nanosheets for enhanced photoelectric detection and photocatalytic CO_2 reduction," *J. Phys. Chem. Lett.*, vol. 10, no. 21, pp. 6590–6597, 2019.
[199] P. Lova, D. Cortecchia, H. N. S. Krishnamoorthy, et al., "Engineering the emission of broadband 2D perovskites by polymer distributed Bragg reflectors," *ACS Photonics*, vol. 5, no. 3, pp. 867–874, 2018.
[200] Q. Zhang, M. M. Tavakoli, L. Gu, et al., "Efficient metal halide perovskite light-emitting diodes with significantly improved light extraction on nanophotonic substrates," *Nat. Commun.*, vol. 10, no. 1, pp. 1–9, 2019.
[201] S. Jeon, L. Zhao, Y.-J. Jung, et al., "Perovskite light-emitting diodes with improved outcoupling using a high-index contrast nanoarray," *Small*, vol. 15, no. 8, pp. 1–7, 2019.
[202] D. Geng, E. Cabello-Olmo, G. Lozano, and H. Míguez, "Tamm plasmons directionally enhance rare-earth nanophosphor emission," *ACS Photonics*, vol. 6, no. 3, pp. 634–641, 2019.
[203] S. Chen and A. Nurmikko, "Stable green perovskite vertical-cavity surface-emitting lasers on rigid and flexible substrates," *ACS Photonics*, vol. 4, no. 10, pp. 2486–2494, 2017.
[204] A. S. Berestennikov, P. M. Voroshilov, S. V. Makarov, and Y. S. Kivshar, "Active meta-optics and nanophotonics with halide perovskites," *Appl. Phys. Rev.*, vol. 6, no. 3, p. 031307, 2019.
[205] A. I. Kuznetsov, A. E. Miroshnichenko, M. L. Brongersma, Y. S. Kivshar, and B. Luk'yanchuk, "Optically resonant dielectric nanostructures," *Science*, vol. 354, no. 6314, p. aag2472, 2016.
[206] S. Yakunin, L. Protesescu, F. Krieg, et al., "Low-threshold amplified spontaneous emission and lasing from colloidal nanocrystals of caesium lead halide perovskites," *Nat. Commun.*, vol. 6, p. 8056, 2015.
[207] Q. Zhang, Q. Shang, R. Su, T. T. H. Do, and Q. Xiong, "Halide perovskite semiconductor lasers: materials, cavity design, and low threshold," *Nano Lett.*, vol. 21, no. 5, pp. 1903–1914, 2021.
[208] J. T. Hugall, A. Singh, and N. F. Van Hulst, "Plasmonic cavity coupling," *ACS Photonics*, vol. 5, no. 1, pp. 43–53, 2018.
[209] M. M. Stylianakis, T. Maksudov, A. Panagiotopoulos, G. Kakavelakis, and K. Petridis, "Inorganic and hybrid perovskite based laser devices: A review," *Materials*, vol. 16, no. 6, pp. 1–28, 2019.
[210] Z. Liu, Z. Hu, T. Shi, et al., "Stable and enhanced frequency up-converted lasing from $CsPbBr_3$ quantum dots embedded in silica sphere," *Opt. Express*, vol. 27, no. 7, p. 9459, 2019.
[211] W. B. Gunnarsson and B. P. Rand, "Electrically driven lasing in metal halide perovskites: Challenges and outlook," *APL Mater.*, vol. 8, no. 3, p. 030902, 2020.
[212] J. Qin, X. K. Liu, C. Yin, and F. Gao, "Carrier dynamics and evaluation of lasing actions in halide perovskites," *Trends Chem.*, vol. 3, no. 1, pp. 34–46, 2021.
[213] Z. Zhou, Z. Wang, Y. Zhou, et al., "Methylamine-gas-induced defect-healing behavior of $CH_3NH_3PbI_3$ thin films for perovskite solar cells," *Angew. Chem. Int. Ed.*, vol. 54, no. 33, pp. 9705–9709, 2015.
[214] R. M. Pasquarelli, D. S. Ginley, and R. O'hayre, "Solution processing of transparent conductors: from flask to film," *Chem. Soc. Rev.*, vol. 40, no. 11, pp. 5406–5441, 2011.
[215] B. Chen, P. N. Rudd, S. Yang, Y. Yuan, and J. Huang, "Imperfections and their passivation in halide perovskite solar cells," *Chem. Soc. Rev.*, vol. 48, no. 14, pp. 3842–3867, 2019.
[216] Y. Chen and H. Zhou, "Defects chemistry in high-efficiency and stable perovskite solar cells," *J. Appl. Phys.*, vol. 128, no. 6, p. 060903, 2020.
[217] K. X. Steirer, P. Schulz, G. Teeter, et al., "Defect tolerance in methylammonium lead triiodide perovskite," *ACS Energy Lett.*, vol. 1, no. 2, pp. 360–366, 2016.
[218] A. Walsh, D. O. Scanlon, S. Chen, X. G. Gong, and S. H. Wei, "Self-regulation mechanism for charged point defects in hybrid halide perovskites," *Angew. Chem. Int. Ed.*, vol. 54, no. 6, pp. 1791–1794, 2015.
[219] D. Meggiolaro and F. De Angelis, "First-principles modeling of defects in lead halide perovskites: Best practices and open issues," *ACS Energy Lett.*, vol. 3, no. 9, pp. 2206–2222, 2018.
[220] A. F. Akbulatov, L. A. Frolova, S. A. Tsarev, et al., "Film deposition techniques impact the defect density and photostability of $MAPbI_3$ Perovskite films," *J. Phys. Chem. C*, vol. 124, no. 39, pp. 21378–21385, 2020.
[221] X. Chen, S. Cheng, L. Xiao, and H. Sun, "Identifying, understanding and controlling defects and traps in halide perovskites for optoelectronic devices: A review," *J. Phys. D Appl. Phys.*, vol. 53, no. 37, p. 373001, 2020.
[222] S. Seth, T. Ahmed, and A. Samanta, "Photoluminescence flickering and blinking of single $CsPbBr_3$ perovskite nanocrystals: Revealing explicit carrier recombination dynamics," *J. Phys. Chem. Lett.*, vol. 9, no. 24, pp. 7007–7014, 2018.
[223] A. L. Efros and D. J. Nesbitt, "Origin and control of blinking in quantum dots," *Nat. Nanotechnol.*, vol. 11, no. 8, pp. 661–671, 2016.

[224] Z. Shangguan, X. Zheng, J. Zhang, et al., "The stability of metal halide perovskite nanocrystals—A key issue for the application on quantum-dot-based micro light-emitting diodes display," *Nanomaterials*, vol. 10, no. 7, pp. 1–33, 2020.
[225] N. Mishra, N. J. Orfield, F. Wang, et al., "Using shape to turn off blinking for two-colour multiexciton emission in CdSe/CdS tetrapods," *Nat. Commun.*, vol. 8, pp. 1–9, 2017.
[226] J. Wang, Q. Shi, E.-M. Shih, et al., "Diffusivity reveals three distinct phases of interlayer excitons in $MoSe_2/WSe_2$ heterobilayers," *Phys. Rev. Lett.*, vol. 126, p. 106804, 2021.
[227] N. Pathoor, A. Halder, A. Mukherjee, J. Mahato, S. K. Sarkar, and A. Chowdhury, "Fluorescence blinking beyond nanoconfinement: spatially synchronous intermittency of entire perovskite microcrystals," *Angew. Chem. Int. Ed.*, vol. 57, no. 36, pp. 11603–11607, 2018.
[228] T. A. S. Doherty, A. J. Winchester, S. Macpherson, et al., "Performance-limiting nanoscale trap clusters at grain junctions in halide perovskites," *Nature*, vol. 580, no. 7803, pp. 360–366, 2020.
[229] Q. Dong, L. Lei, J. Mendes, and F. So, "Operational stability of perovskite light emitting diodes," *J. Phys. Mater.*, vol. 3, no. 1, p. 012002, 2020.
[230] A. Bercegol, F. J. Ramos, A. Rebai, et al., "Spatial inhomogeneity analysis of cesium-rich wrinkles in triple- cation perovskite," *J. Phys. Chem. C*, vol. 122, no. 41, pp. 23345–23351, 2018.
[231] Q. Jiang, Y. Zhao, X. Zhang, et al., "Surface passivation of perovskite film for efficient solar cells," *Nat. Photonics*, vol. 13, pp. 460–466, 2019.
[232] C. Stavrakas, A. A. Zhumekenov, R. Brenes, et al., "Probing buried recombination pathways in perovskite structures using 3D photoluminescence tomography," *Energy Environ. Sci.*, vol. 11, no. 10, pp. 2846–2852, 2018.
[233] E. M. Tennyson, T. A. S. Doherty, and S. D. Stranks, "Heterogeneity at multiple length scales in halide perovskite semiconductors," *Nat. Rev. Mater.*, vol. 4, no. 9, pp. 573–587, 2019.
[234] Z. Andaji-Garmaroudi, M. Abdi-Jalebi, F. U. Kosasih, et al., "Elucidating and mitigating degradation processes in perovskite light-emitting diodes," *Adv. Energy Mater.*, vol. 10, no. 48, pp. 1–10, 2020.
[235] Y. Li, Q. Hu, P. Wang, et al., "Surface and grain boundary carbon heterogeneity in $CH_3NH_3PbI_3$ perovskites and its impact on optoelectronic properties," *Appl. Phys. Rev.*, vol. 7, no. 4, p. 041412, 2020.
[236] K. P. McKenna, "Electronic properties of {111} twin boundaries in a mixed-ion lead halide perovskite solar absorber," *ACS Energy Lett.*, vol. 3, no. 11, pp. 2663–2668, 2018.
[237] T. W. Jones, A. Osherov, M. Alsari, et al., "Lattice strain causes non-radiative losses in halide perovskites," *Energy Environ. Sci.*, vol. 12, no. 2, pp. 596–606, 2019.
[238] Y. Zhou and Y. Zhao, "Chemical stability and instability of inorganic halide perovskites," *Energy Environ. Sci.*, vol. 12, no. 5, pp. 1495–1511, 2019.
[239] X. Li, F. Cao, D. Yu, et al., "All inorganic halide perovskites nanosystem: synthesis, structural features, optical properties and optoelectronic applications," *Small*, vol. 13, no. 9, pp. 1–24, 2017.
[240] S. Wang, C. Bi, J. Yuan, L. Zhang, and J. Tian, "Original core-shell structure of cubic $CsPbBr_3$@Amorphous CsPbBrx perovskite quantum dots with a high blue photoluminescence quantum yield of over 80%," *ACS Energy Lett.*, vol. 3, no. 1, pp. 245–251, 2018.
[241] S. Thapa, K. Bhardwaj, S. Basel, et al., "Long-term ambient air-stable cubic $CsPbBr_3$ perovskite quantum dots using molecular bromine," *Nanoscale Adv.*, vol. 1, no. 9, pp. 3388–3391, 2019.
[242] L. Martínez-Sarti, S. H. Jo, Y.-H. Kim, et al., "Low-dimensional iodide perovskite nanocrystals enable efficient red emission," *Nanoscale*, vol. 11, no. 27, pp. 12793–12797, 2019.
[243] G. Delport, S. Macpherson, and S. D. Stranks, "Imaging carrier transport properties in halide perovskites using time-resolved optical microscopy," *Adv. Energy Mater.*, vol. 10, no. 26, pp. 1–13, 2020.
[244] D. W. DeQuilettes, W. Zhang, V. M. Burlakov, et al., "Photo-induced halide redistribution in organic-inorganic perovskite films," *Nat. Commun.*, vol. 7, 2016.
[245] M. U. Rothmann, W. Li, Y. Zhu, et al., "Structural and chemical changes to $CH_3NH_3PbI_3$ induced by electron and gallium ion beams," *Adv. Mater.*, vol. 30, no. 25, pp. 1–7, 2018.
[246] E. S. Barnard, B. Ursprung, E. Colegrove, et al., "3D lifetime tomography reveals how $CdCl_2$ improves recombination throughout CdTe solar cells," *Adv. Mater.*, vol. 29, no. 3, p. 1603801, 2017.
[247] E. Strelcov, Q. Dong, T. Li, et al., "$CH_3NH_3PbI_3$ perovskites: ferroelasticity revealed (supplementary materials)," *Sci. Adv.*, vol. 3, no. 4, p. e1602165, 2017.
[248] Y. Rakita, O. Bar-Elli, E. Meirzadeh, et al., "Tetragonal $CH_3NH_3PbI_3$ is ferroelectric," *Proc. Natl. Acad. Sci. U.S.A*, vol. 114, no. 28, pp. E5504–E5512, 2017.
[249] G. W. P. Adhyaksa, S. Brittman, H. Āboliņš, et al., "Understanding detrimental and beneficial grain boundary effects in halide perovskites," *Adv. Mater.*, vol. 30, no. 52, p. 1804792, 2018.
[250] R. L. Milot, G. E. Eperon, H. J. Snaith, M. B. Johnston, and L. M. Herz, "Temperature-dependent charge-carrier dynamics in $CH_3NH_3PbI_3$ perovskite thin films," *Adv. Funct. Mater.*, vol. 25, no. 39, pp. 6218–6227, 2015.
[251] A. D. Wright, C. Verdi, R. L. Milot, et al., "Electron-phonon coupling in hybrid lead halide perovskites," *Nat. Commun.*, vol. 7, 2016.
[252] K. T. Munson, E. R. Kennehan, G. S. Doucette, and J. B. Asbury, "Dynamic disorder dominates delocalization, transport, and recombination in halide perovskites," *Chem*, vol. 4, no. 12, pp. 2826–2843, 2018.
[253] W. Nie, J.-C. Blancon, A. J. Neukirch, et al., "Light-activated photocurrent degradation and self-healing in perovskite solar cells," *Nat. Commun.*, vol. 7, pp. 1–9, 2016.
[254] C. Li, A. Guerrero, S. Huettner, and J. Bisquert, "Unravelling the role of vacancies in lead halide perovskite through electrical switching of photoluminescence," *Nat. Commun.*, vol. 9, 2018.
[255] N. Phung, A. Al-Ashouri, S. Meloni, et al., "The role of grain boundaries on ionic defect migration in metal halide perovskites," *Adv. Energy Mater.*, vol. 10, no. 20, p. 1903735, 2020.
[256] T. Cheng, G. Tumen-ulzii, D. Klotz, S. Watanabe, T. Matsushima, and C. Adachi, "Ion migration-induced degradation and efficiency roll-o ff in quasi-2D perovskite light-emitting diodes," *ACS Appl. Mater. Interfaces*, vol. 12, no. 29, pp. 33004–33013, 2020.
[257] B. Conings, J. Drijkoningen, N. Gauquelin, et al., "Intrinsic thermal instability of methylammonium lead trihalide perovskite," *Adv. Energy Mater.*, vol. 5, no. 15, pp. 1–8, 2015.

[258] M. N. F. Hoque, R. He, J. Warzywoda, and Z. Fan, "Effects of moisture-based grain boundary passivation on cell performance and ionic migration in organic-inorganic halide perovskite solar cells," *ACS Appl. Mater. Interfaces*, vol. 10, no. 36, pp. 30322–30329, 2018.

[259] L. Ling, S. Yuan, P. Wang, et al., "Precisely controlled hydration water for performance improvement of organic–inorganic perovskite solar cells," *Adv. Funct. Mater.*, vol. 26, no. 28, pp. 5028–5034, 2016.

[260] C. Müller, T. Glaser, M. Plogmeyer, et al., "Water infiltration in methylammonium lead iodide perovskite: fast and inconspicuous," *Chem. Mater.*, vol. 27, no. 22, pp. 7835–7841, 2015.

[261] N. Aristidou, C. Eames, I. Sanchez-Molina, et al., "Fast oxygen diffusion and iodide defects mediate oxygen-induced degradation of perovskite solar cells," *Nat. Commun.*, vol. 8, pp. 1–10, 2017.

[262] K. Kwak, E. Lim, N. Ahn, et al., "An atomistic mechanism for the degradation of perovskite solar cells by trapped charge," *Nanoscale*, vol. 11, no. 23, pp. 11369–11378, 2019.

[263] E. T. Hoke, D. J. Slotcavage, E. R. Dohner, A. R. Bowring, H. I. Karunadasa, and M. D. McGehee, "Reversible photo-induced trap formation in mixed-halide hybrid perovskites for photovoltaics," *Chem. Sci.*, vol. 6, no. 1, pp. 613–617, 2015.

[264] N. H. Nickel, F. Lang, V. V. Brus, O. Shargaieva, and J. Rappich, "Unraveling the light-induced degradation mechanisms of $CH_3NH_3PbI_3$ perovskite films," *Adv. Electron. Mater.*, vol. 3, no. 12, pp. 1–9, 2017.

[265] A. Dualeh, N. Tétreault, T. Moehl, P. Gao, M. K. Nazeeruddin, and M. Grätzel, "Effect of annealing temperature on film morphology of organic-inorganic hybrid pervoskite solid-state solar cells," *Adv. Funct. Mater.*, vol. 24, no. 21, pp. 3250–3258, 2014.

[266] J. Choi, S. Song, M. T. Hörantner, H. J. Snaith, and T. Park, "Well-defined nanostructured, single-crystalline TiO_2 electron transport layer for efficient planar perovskite solar cells," *ACS Nano*, vol. 10, no. 6, pp. 6029–6036, 2016.

[267] J. Wu, J. Shi, Y. Li, et al., "Quantifying the interface defect for the stability origin of perovskite solar cells," *Adv. Energy Mater.*, vol. 9, no. 37, pp. 1–9, 2019.

[268] Y. Yang, J. Wu, X. Wang, et al., "Suppressing vacancy defects and grain boundaries via Ostwald ripening for high-performance and stable perovskite solar cells," *Adv. Mater.*, vol. 32, no. 7, pp. 1–7, 2020.

[269] C. Park, H. Ko, D. H. Sin, K. C. Song, and K. Cho, "Organometal halide perovskite solar cells with improved thermal stability via grain boundary passivation using a molecular additive," *Adv. Funct. Mater.*, vol. 27, no. 42, pp. 1–8, 2017.

[270] S. Colella, M. Mazzeo, A. Rizzo, G. Gigli, and A. Listorti, "The bright side of perovskites," *J. Phys. Chem. Lett.*, vol. 7, no. 21, pp. 4322–4334, 2016.

[271] Z. Ren, J. Yu, Z. Qin, et al., "High-performance blue perovskite light-emitting diodes enabled by efficient energy transfer between coupled quasi-2D perovskite layers," *Adv. Mater.*, vol. 33, no. 1, pp. 1–10, 2021.

[272] D. Wang, L. Huang, Q. Chen, et al., "A dual function-enabled novel zwitterion to stabilize a Pb-I framework and passivate defects for highly efficient inverted planar perovskite solar cells," *Chem. Commun.*, vol. 56, no. 51, pp. 6929–6932, 2020.

[273] N. Yantara, N. F. Jamaludin, B. Febriansyah, et al., "Regulating vertical domain distribution in Ruddlesden-Popper perovskites for electroluminescence devices," *J. Phys. Chem. Lett.*, vol. 10, no. 24, pp. 7949–7955, 2019.

[274] N. Yantara, S. Bhaumik, F. Yan, et al., "Inorganic halide perovskites for efficient light-emitting diodes," *J. Phys. Chem. Lett.*, vol. 6, no. 21, pp. 4360–4364, 2015.

[275] E. P. Yao, Z. Yang, L. Meng, et al., "High-brightness blue and white LEDs based on inorganic perovskite nanocrystals and their composites," *Adv. Mater.*, vol. 29, no. 23, pp. 1–7, 2017.

[276] D. M. Jang, K. Park, D. H. Kim, et al., "Reversible halide exchange reaction of organometal trihalide perovskite colloidal nanocrystals for full-range band gap tuning," *Nano Lett.*, vol. 15, no. 8, pp. 5191–5199, 2015.

[277] Y. F. Ng, S. A. Kulkarni, S. Parida, et al., "Highly efficient Cs-based perovskite light-emitting diodes enabled by energy funnelling," *Chem. Commun.*, vol. 53, no. 88, pp. 12004–12007, 2017.

[278] A. A. M. Brown, B. Damodaran, L. Jiang, et al., "Lead halide perovskite nanocrystals: Room temperature syntheses toward commercial viability," *Adv. Energy Mater.*, vol. 10, no. 34, pp. 1–19, 2020.

[279] M. Yu, C. Yi, N. Wang, et al., "Control of barrier width in perovskite multiple quantum wells for high performance green light–emitting diodes," *Adv. Opt. Mater.*, vol. 7, no. 3, pp. 1–6, 2019.

[280] F. Krieg, S. T. Ochsenbein, S. Yakunin, et al., "Colloidal $CsPbX_3$ (X = Cl, Br, I) nanocrystals 2.0: zwitterionic capping ligands for improved durability and stability," *ACS Energy Lett.*, vol. 3, no. 3, pp. 641–646, 2018.

[281] D. Yang, X. Li, W. Zhou, et al., "$CsPbBr_3$ quantum dots 2.0: benzenesulfonic acid equivalent ligand awakens complete purification," *Adv. Mater.*, vol. 31, no. 30, pp. 1–8, 2019.

[282] A. A. M. Brown, T. J. N. Hooper, S. A. Veldhuis, et al., "Self-assembly of a robust hydrogen-bonded octylphosphonate network on cesium lead bromide perovskite nanocrystals for light-emitting diodes," *Nanoscale*, vol. 11, no. 25, pp. 12370–12380, 2019.

[283] Q. A. Akkerman, M. Gandini, F. Di Stasio, et al., "Strongly emissive perovskite nanocrystal inks for high-voltage solar cells," *Nat. Energy*, vol. 2, pp. 1–7, 2017.

[284] E. Moyen, H. Jun, H. Kim, and J. Jang, "Surface engineering of room temperature-grown inorganic perovskite quantum dots for highly efficient inverted light-emitting diodes," *ACS Appl. Mater. Interfaces*, vol. 10, no. 49, pp. 42647–42656, 2018.

[285] S. Bhaumik, S. A. Veldhuis, Y. F. Ng, et al., "Highly stable, luminescent core–shell type methylammonium–octylammonium lead bromide layered perovskite nanoparticles," *Chem. Commun.*, vol. 52, no. 7, pp. 7118–7121, 2016.

[286] Y. Ye, Y. Li, Y. Tian, et al., "Surface-induced phase engineering and defect passivation of perovskite nanograins for efficient red light-emitting diodes," *Nanoscale*, vol. 13, no. 1, pp. 340–348, 2021.

[287] Z. Yuan, Y. Miao, J. Wang, W. Xu, and C. Kuang, "Unveiling the synergistic effect of precursor stoichiometry and interfacial reactions for perovskite light-emitting diodes," *Nat. Commun.*, vol. 10, pp. 1–9, 2019.

[288] S. A. Veldhuis, Y. F. Ng, R. Ahmad, et al., "Crown ethers enable room-temperature," *ACS Energy Lett.*, vol. 3, no. 3, pp. 526–531, 2018.
[289] N. F. Jamaludin, N. Yantara, Y. F. Ng, et al., "Perovskite templating via a bathophenanthroline additive for efficient light-emitting devices," *J. Mater. Chem. C*, vol. 6, no. 9, pp. 2295–2302, 2018.
[290] X. Zhang, S. Chang, K. Wu, and H. Zhong, "Dimension control of in situ fabricated $CsPbClBr_2$ nanocrystal fi lms toward efficient blue light-emitting diodes," *Nat. Commun.*, vol. 11, no. 6428, pp. 2–9, 2020.
[291] Y. Tan, Y. Zou, L. Wu, et al., "Highly luminescent and stable perovskite nanocrystals with octylphosphonic acid as a ligand for efficient light-emitting diodes," *ACS Appl. Mater. Interfaces*, vol. 10, no. 4, pp. 3784–3792, 2018.
[292] X. Kong, F. Xu, W. Wang, et al., "Ligand induced anomalous emission shift of size-controlled $CsPbBr_3$ nanocrystals," *Appl. Phys. Lett.*, vol. 115, no. 15, p. 153104, 2019.
[293] H. Kim, N. Hight-Huf, J. H. Kang, et al., "Polymer zwitterions for stabilization of $CsPbBr_3$ perovskite nanoparticles and nanocomposite films," *Angew. Chem.*, vol. 59, no. 27, pp. 10802–10806, 2020.
[294] S. Wang, L. Du, Z. Jin, Y. Xin, and H. Mattoussi, "Enhanced stabilization and easy phase transfer of $CsPbBr_3$ perovskite quantum dots promoted by high-affinity polyzwitterionic ligands," *J. Am. Chem. Soc.*, vol. 142, no. 29, pp. 12669–12680, 2020.
[295] B. Zhang, L. Goldoni, J. Zito, et al., "Alkyl phosphonic acids deliver $CsPbBr_3$ nanocrystals with high photoluminescence quantum yield and truncated octahedron shape," *Chem. Mater.*, vol. 31, no. 21, pp. 9140–9147, 2019.
[296] S. Silver, Q. Dai, H. Li, J. L. Brédas, and A. Kahn, "Quantum well energetics of an n = 2 ruddlesden–popper phase perovskite," *Adv. Energy Mater.*, vol. 9, no. 25, pp. 1–7, 2019.
[297] W. Wu, Y. Zhang, T. Liang, and J. Fan, "Carrier accumulation enhanced Auger recombination and inner self-heating- induced spectrum fluctuation in $CsPbBr_3$ perovskite nanocrystal light-emitting devices," *Appl. Phys. Lett.*, vol. 115, no. 24, p. 243503, https://doi.org/10.1063/1.5124617.
[298] J. Byun, H. Cho, C. Wolf, et al., "Efficient visible quasi-2D perovskite light-emitting diodes," *Adv. Mater.*, vol. 28, no. 34, pp. 7515–7520, 2016.
[299] P. Pang, G. Jin, C. Liang, et al., "Rearranging low-dimensional phase distribution of quasi-2D perovskites for efficient sky-blue perovskite light-emitting diodes," *ACS Nano*, vol. 14, no. 9, pp. 11420–11430, 2020.
[300] L. Song, X. Guo, Y. Hu, et al., "Improved performance of $CsPbBr_3$ perovskite light-emitting devices by both boundary and interface defects passivation," *Nanoscale*, vol. 10, pp. 18315–18322, 2018.
[301] A. Perumal, H. Faber, N. Yaacobi-Gross, et al., "High-efficiency, solution-processed, multilayer phosphorescent organic light-emitting diodes with a copper thiocyanate hole-injection/hole-transport layer," *Adv. Mater.*, vol. 27, no. 1, pp. 93–100, 2015.
[302] H. Wang, X. Zhang, Q. Wu, et al., "Trifluoroacetate induced small-grained $CsPbBr_3$ perovskite films result in efficient and stable light-emitting devices," *Nat. Commun.*, vol. 10, p. 665, 2019.
[303] Z. Shi, S. Li, Y. Li, et al., "Strategy of solution-processed all-inorganic heterostructure for humidity/temperature-stable perovskite quantum dot light-emitting diodes," *ACS Nano*, vol. 12, no. 2, pp. 1462–1472, 2018.
[304] L. Zhang, F. Yuan, J. Xi, et al., "Suppressing ion migration enables stable perovskite light-emitting diodes with all-inorganic strategy," *Adv. Funct. Mater.*, vol. 30, no. 40, pp. 1–8, 2020.
[305] C. Qin, T. Matsushima, A. S. D. Sandanayaka, Y. Tsuchiya, and C. Adachi, "Centrifugal-coated quasi-two-dimensional perovskite $CsPb_2Br_5$ films for efficient and stable light-emitting diodes," *J. Phys. Chem. Lett.*, vol. 8, no. 21, pp. 5415–5421, 2017.
[306] Z. Shi, Y. Li, Y. Zhang, et al., "High-efficiency and air-stable perovskite quantum dots light-emitting diodes with an all-inorganic heterostructure," *Nano Lett.*, vol. 17, no. 1, pp. 313–321, 2017.
[307] X. Liu, X. Guo, Y. Lv, et al., "High brightness and enhanced stability of $CsPbBr_3$-based perovskite light-emitting diodes by morphology and interface engineering," *Adv. Opt. Mater.*, vol. 6, no. 24, p. 1801245, 2018.
[308] Z. Wei, A. Perumal, R. Su, et al., "Solution-processed highly bright and durable cesium lead halide perovskite light-emitting diodes," *Nanoscale*, vol. 8, pp. 18021–18026, 2016.
[309] S. Wu, S. Zhao, Z. Xu, et al., "Highly bright and stable all-inorganic perovskite light-emitting diodes with methoxypolyethylene glycols modified $CsPbBr_3$ emission layer," *Appl. Phys. Lett.*, vol. 113, p. 213501, 2018.
[310] S. Lee, D. B. Kim, I. Hamilton, et al., "Control of interface defects for efficient and stable quasi-2D perovskite light-emitting diodes using nickel oxide hole injection layer," *Adv. Sci.*, vol. 5, no. 11, p. 1801350, 2018.
[311] C. Wu, Y. Zou, T. Wu, et al., "Improved performance and stability of all-inorganic perovskite light-emitting diodes by antisolvent vapor treatment," *Adv. Funct. Mater.*, vol. 27, no. 28, p. 1700338, 2017.
[312] J. C. Yu, D. B. Kim, G. Baek, et al., "High-performance planar perovskite optoelectronic devices: A morphological and interfacial control by polar solvent treatment," *Adv. Mater.*, vol. 27, no. 23, pp. 3492–500, 2015.
[313] Y. Tian, C. Zhou, M. Worku, et al., "Highly efficient spectrally stable red perovskite light-emitting diodes," *Adv. Mater.*, vol. 30, no. 20, p. 1707093, 2018.
[314] S. Zhang, C. Yi, N. Wang, et al., "Efficient red perovskite light-emitting diodes based on solution-processed multiple quantum wells," vol. 29, no. 22, p.1606600.
[315] H. Tsai, W. Nie, J.-C. Blancon, et al., "Stable light-emitting diodes using phase-pure Ruddlesden-Popper layered perovskites," *Adv. Mater.*, vol. 30, no. 6, p. 1704217, 2018.
[316] M. Yang, N. Wang, S. Zhang, et al., "Reduced efficiency roll-off and enhanced stability in perovskite light-emitting diodes with multiple quantum wells," *J. Phys. Chem. Lett.*, vol. 9, no. 8, pp. 2038–2042, 2018.
[317] Y. Miao, Y. Ke, N. Wang, et al., "Stable and bright formamidinium-based perovskite light-emitting diodes with high energy conversion efficiency," *Nat. Commun.*, vol. 10, no. 3624, 2019.
[318] Y. Wang, R. Zou, J. Chang, et al., "Tin-based multiple quantum well perovskites for light-emitting diodes with improved stability," *J. Phys. Chem. Lett.*, vol. 10, no. 3, pp. 453–459, 2019.
[319] D. Meggiolaro, F. Ambrosio, E. Mosconi, A. Mahata, and F. De Angelis, "Polarons in metal halide perovskites," *Adv. Energy Mater.*, vol. 10, no. 13, pp. 1–15, 2020.

[320] A. Mahata, D. Meggiolaro, and F. De Angelis, "From large to small polarons in lead, tin, and mixed lead-tin halide perovskites," *J. Phys. Chem. Lett.*, vol. 10, no. 8, pp. 1790–1798, 2019.
[321] C. W. Myung, J. Yun, G. Lee, and K. S. Kim, "A new perspective on the role of A-site cations in perovskite solar cells," *Adv. Energy Mater.*, vol. 8, no. 14, pp. 1–7, 2018.
[322] L. Zhou, C. Katan, W. Nie, et al., "Cation alloying delocalizes polarons in lead halide perovskites," *J. Phys. Chem. Lett.*, vol. 10, no. 13, pp. 3516–3524, 2019.
[323] L. M. Herz, "Charge-carrier mobilities in metal halide perovskites: fundamental mechanisms and limits," *ACS Energy Lett.*, vol. 2, no. 7, pp. 1539–1548, 2017.
[324] A. Fakharuddin, W. Qiu, G. Croes, et al., "Reduced efficiency roll-off and improved stability of mixed 2D/3D perovskite light emitting diodes by balancing charge injection," *Adv. Funct. Mater.*, vol. 29, no. 37, pp. 1–12, 2019.
[325] L. Zhao, R. A. Kerner, Z. Xiao, et al., "Redox chemistry dominates the degradation and decomposition of metal halide perovskite optoelectronic devices," *ACS Energy Lett.*, vol. 1, no. 3, pp. 595–602, 2016.
[326] Q. Dong, L. Lei, J. Mendes, and F. So, "Operational stability of perovskite light emitting diodes operational stability of perovskite light emitting diodes," *J. Phys. Mater.*, vol. 3, no. 1, p. 012002, 2020.
[327] H. Lee, D. Ko, and C. Lee, "Direct evidence of ion-migration-induced degradation of ultrabright perovskite light-emitting diodes," *ACS Appl. Mater. Interfaces*, vol. 11, no. 12, pp. 11667–11673, 2019.
[328] V. Prakasam, D. Tordera, H. J. Bolink, and G. Gelinck, "Degradation mechanisms in organic lead halide perovskite light-emitting diodes," *Adv. Opt. Mater.*, vol. 7, no. 22, pp. 1–7, 2019.
[329] B. Zhao, Y. Lian, L. Cui, et al., "Efficient light-emitting diodes from mixed-dimensional perovskites on a fluoride interface," *Nat. Electron.*, vol. 3, pp. 704–710, 2020.
[330] Y. Shynkarenko, M. I. Bodnarchuk, C. Bernasconi, et al., "Direct synthesis of quaternary alkylammonium-capped perovskite nanocrystals for efficient blue and green light-emitting diodes," *ACS Energy Lett.*, vol. 4, no. 11, pp. 2703–2711, 2019.
[331] A. Kanwat, N. Yantara, Y. F. Ng, et al., "Stabilizing the electroluminescence of halide perovskites with potassium passivation," *ACS Energy Lett.*, vol. 5, no. 6, pp. 1804–1813, 2020.
[332] G. Walters, L. Haeberlé, R. Quintero-Bermudez, J. Brodeur, S. Kéna-Cohen, and E. H. Sargent, "Directional light emission from layered metal halide perovskite crystals," *J. Phys. Chem. Lett.*, vol. 11, no. 9, pp. 3458–3465, 2020.
[333] A. Merdasa, Y. Tian, R. Camacho, et al., "'Super-Trap' at work: extremely efficient non-radiative recombination channels in $MAPbI_3$ perovskites revealed by luminescence super-resolution imaging and spectroscopy," *ACS Nano*, vol. 11, no. 6, pp. 5391–5404, 2017.
[334] K. Song, L. Liu, D. Zhang, M. P. Hautzinger, S. Jin, and Y. Han, "Atomic-resolution imaging of halide perovskites using electron microscopy," *Adv. Energy Mater.*, vol. 10, no. 26, pp. 1–15, 2020.
[335] Z. Chen, Z. Li, Z. Chen, et al., "Utilization of trapped optical modes for white perovskite light-emitting diodes with efficiency over 12 %," *Joule*, vol. 5, no. 2, pp. 456–466, 2021.
[336] J. H. Heo, J. K. Park, and S. H. Im, "Full-color spectrum coverage by high-color- purity perovskite nanocrystal light-emitting diodes full-color spectrum coverage by high-color-purity perovskite nanocrystal light-emitting diodes," *Cell Rep. Phys. Sci.*, vol. 1, no. 9, p. 100177, 2020.
[337] H. D. Pham, L. Xianqiang, W. Li, S. Manzhos, A. K. K. Kyaw, and P. Sonar, "Organic interfacial materials for perovskite-based optoelectronic devices," *Energy Environ. Sci.*, vol. 12, pp. 1177–1209, 2019.
[338] S. Wang, A. Cabreros, Y. Yang, et al., "Impacts of the hole transport layer deposition process on buried interfaces in perovskite solar cells," *Cell Rep. Phys. Sci.*, vol. 1, no. 7, p. 100103, 2020.
[339] N. Ahn, K. Kwak, M. S. Jang, et al., "Trapped charge-driven degradation of perovskite solar cells," *Nat. Commun.*, vol. 7, no. 13422, pp. 1–9, 2016.
[340] T. Leijtens, T. Giovenzana, S. N. Habisreutinger, et al., "Hydrophobic organic hole transporters for improved moisture resistance in metal halide perovskite solar cells," *ACS Appl. Mater. Interfaces*, vol. 8, no. 9, pp. 5981–5989, 2016.
[341] M. Karlsson, Z. Yi, S. Reichert, et al., "Mixed halide perovskites for spectrally stable and high-efficiency blue light-emitting diodes," *Nat. Commun.*, vol. 12, 2021.
[342] H. Chen, J. Lin, J. Kang, et al., "Structural and spectral dynamics of single-crystalline Ruddlesden-Popper phase halide perovskite blue light-emitting diodes," *Sci. Adv.*, vol. 6, no. 4, pp. 1–9, 2020.
[343] Q. Zhang, F. Hao, J. Li, Y. Zhou, Y. Wei, and H. Lin, "Perovskite solar cells: must lead be replaced–and can it be done?," *Sci. Technol. Adv. Mater.*, vol. 19, no. 1, pp. 425–442, 2018.
[344] L. Cheng, C. Yi, Y. Tong, et al., "Halide homogenization for high-performance blue perovskite electroluminescence," *Research*, vol. 2020, 2020.
[345] T. M. Koh, T. Krishnamoorthy, N. Yantara, et al., "Formamidinium tin-based perovskite with low Eg for photovoltaic applications," *J. Mater. Chem. A*, vol. 3, no. 29, pp. 14996–15000, 2015.
[346] I. Kopacic, B. Friesenbichler, S. F. Hoefler, et al., "Enhanced performance of germanium halide perovskite solar cells through compositional engineering," *ACS Appl. Energy Mater.*, vol. 1, no. 2, pp. 343–347, 2018.
[347] Y. Yang, H. Peng, C. Liu, et al., "Bi-functional additive engineering for high-performance perovskite solar cells with reduced trap density," *J. Mater. Chem. A*, vol. 7, no. 11, pp. 6450–6458, 2019.
[348] K. Xu, E. T. Vickers, B. Luo, et al., "First synthesis of Mn-doped cesium lead bromide perovskite magic sized clusters at room temperature," *J. Phys. Chem. Lett.*, vol. 11, no. 3, pp. 1162–1169, 2020.
[349] K. Ahmad and S. M. Mobin, "Recent progress and challenges in $A_3Sb_2X_9$-based perovskite solar cells," *ACS Omega*, vol. 5, no. 44, pp. 28404–28412, 2020.
[350] L. Schade, A. D. Wright, R. D. Johnson, et al., "Structural and optical properties of $Cs_2AgBiBr_6$ double perovskite," *ACS Energy Lett.*, vol. 4, no. 1, pp. 299–305, 2019.
[351] M. Leng, Z. Chen, Y. Yang, et al., "Lead-free, blue emitting bismuth halide perovskite quantum dots," *Angew. Chem. Int. Ed.*, vol. 55, no. 48, pp. 15012–15016, 2016.

[352] M. Gao, C. Zhang, L. Lian, et al., "Controlled synthesis and photostability of blue emitting $Cs_3Bi_2Br_9$ perovskite nanocrystals by employing weak polar solvents at room temperature," *J. Mater. Chem. C*, vol. 7, no. 12, pp. 3688–3695, 2019.
[353] Y. Shen, J Yin, B Cai, et al., "Lead-free, stable, high-efficiency (52%) blue luminescent $FA_3Bi_2Br_9$ perovskite quantum dots," *Nanoscale Horiz.*, vol. 5, no. 3, pp. 580–585, 2020.
[354] R. Chiara, Y. O. Ciftci, V. I. E. Queloz, M. K. Nazeeruddin, G. Grancini, and L. Malavasi, "Green-emitting lead-free Cs_4SnBr_6 zero-dimensional perovskite nanocrystals with improved air stability," *J. Phys. Chem. Lett.*, vol. 11, no. 3, pp. 618–623, 2020.
[355] M. Roknuzzaman, K. K. Ostrikov, H. Wang, A. Du, and T. Tesfamichael, "Towards lead-free perovskite photovoltaics and optoelectronics by ab-initio simulations," *Sci. Rep.*, vol. 7, no. 1, pp. 1–8, 2017.
[356] J. Chen, Q. Zhang, J. Shi, et al., "Room temperature continuous – wave excited biexciton emission in perovskite nanoplatelets via plasmonic nonlinear fano resonance," *Commun. Phys.,* vol. 2, 2019.
[357] H. Utzat, W. Sun, A. E. K. Kaplan, et al., "Coherent single-photon emission from colloidal lead halide perovskite quantum dots," *Science*, vol. 363, no. 6431, pp. 1068–1072, 2019.
[358] V. C. Nair, C. Muthu, A. L. Rogach, R. Kohara, and V. Biju, "Channeling exciton migration into electron transfer in formamidinium lead bromide perovskite nanocrystal/fullerene composites," *Angew. Chem.*, vol. 129, no. 5, pp. 1234–1238, 2017.
[359] P. Tamarat, L. Hou, J.-B. Trebbia, et al., "The dark exciton ground state promotes photon-pair emission in individual perovskite nanocrystals," *Nat. Commun.*, vol. 11, no. 6001, pp. 1–8, 2020.
[360] S. Chu, W. Chen, Z. Fang, et al., "Large-area and efficient perovskite light-emitting diodes via low-temperature blade-coating," *Nat. Commun.*, vol. 12, 2021.
[361] G. Li, K. Chen, Y. Cui, et al., "Stability of perovskite light sources: status and challenges," *Adv. Opt. Mater.*, vol. 8, no. 6, pp. 1–15, 2020.
[362] V. Bulović, "All-vacuum-deposited inorganic cesium lead halide perovskite light-emitting diodes," *APL Mater.*, vol. 8, no. 5, p. 051113, 2020.